High Capacity VCSEL Array Based Optical Wireless Links

Yi Liu

Department of Engineering

University of Cambridge

"This dissertation is submitted for the degree of Doctor of Philosophy"

Fitzwilliam College December 2023

Declaration

I hereby declare that except where specific reference is made to the work of others, the contents of this dissertation are original and have not been submitted in whole or in part for consideration for any other degree or qualification in this, or any other University. This dissertation is the result of my own work and includes nothing which is the outcome of work done in collaboration, except where specifically indicated in the text. This dissertation contains less than 65,000 words including appendices, bibliography, footnotes, tables and equations and has less than 150 figures.

Yi Liu
December 2023

Abstract

The development of new high-speed wireless data transmission applications, such as high-definition video streaming, virtual reality, and the Internet of Things, increases the future demand for mobile data traffic capacity. However, the limited RF spectrum is not sufficient to meet this demand.

Optical wireless communication (OWC) systems have the potential to overcome the rapidly increasing demand for indoor data traffic. Compared to Radio frequency (RF) wireless systems, OWC systems offer several advantages, including a larger unlicensed bandwidth, immunity against electrical interference and freedom from fading. However, they are affected by background noise caused by natural and artificial light sources and the risk of the laser beam being hazardous to the skin and eyes. The need for high-precision link alignment between the laser transmitter and user receiver limits the user mobility.

Within this thesis, Vertical-Cavity Surface-Emitting Lasers (VCSEL) are employed in laser-based OWC systems due to their compatible eye-safe working wavelengths within the near-infrared range, lower cost, and easy large-scale two-dimensional chip fabrication compared to other laser sources.

The main contributions of the research are as follows:

A novel 5 × 5 VCSEL array based OWC transmitter is proposed and designed. A microlens array homogeniser is the first time employed in OWC to generate the uniform optical power distribution in each atto-cell and to minimise the interference between adjacent cells. Each VCSEL generates >80% beam uniformity across a 20 cm × 20 cm square atto-cell where the receiver power in the square area is 5 mW m^{-2}.

Data transmission of single VCSEL - OWC links using the homogeniser is experimentally demonstrated. A single VCSEL achieves 8 Gbps data transmission using On-Off Keying (OOK) modulation and Decision Feedback Equalization (DFE) over a 3 m link, using a Silicon Photomultiplier (SiPM) receiver.

The novel multibeam VCSEL array based-OWC transmitter is demonstrated to enhance the channel capacity Three 20 cm × 20 cm square cells are shown on the receiver surface with low interference to adjacent cells. A 9.2 Gbps data

transmission is achieved for each OW channel using a VCSEL array, Avalanche Photodiode (APD) receiver and Orthogonal Frequency-Division Multiplexing (OFDM) modulation scheme.

A VCSEL-array-based free space optical (FSO) fronthaul link with easy alignment for next-generation radio access network is demonstrated for the first time.

Together these demonstrate the attractiveness of VCSEL array-based transmitters for use in optical wireless communication systems.

Acknowledgements

I am profoundly grateful for the invaluable guidance and unwavering support I have received throughout my academic journey, and I extend my heartfelt thanks to the individuals who have played pivotal roles in my success.

First and foremost, my deepest appreciation goes to my supervisor, Prof Richard Penty, whose unwavering support and guidance have been the cornerstone of my academic journey. Prof. Richard Penty's mentorship, insightful feedback, and dedication to my success have been invaluable. I am truly fortunate to have had such an inspiring mentor. Additionally, I am grateful to my academic adviser, Prof. Michael Crisp, for his valuable insights and guidance that have enriched my academic experience.

My heartfelt thanks extend to Dr. Wajahat Ali, Dr. Rui Chen and Dr Tongyun Li, our postdoctoral researcher, whose expertise and encouragement have enriched my research experience. Their collaborative spirit and willingness to share their knowledge have been instrumental in shaping the direction of my work. I am grateful for the stimulating discussions and collaborative efforts that have expanded my understanding of the field.

No words can adequately convey my appreciation for the endless support and encouragement I have received from my parents. Their sacrifices, belief in my abilities, and unconditional love have driven my academic achievements. My accomplishments are a reflection of their unwavering dedication, and for that, I am eternally thankful.

In addition to my academic mentors, my friends have been a constant source of motivation and joy throughout this journey. Their encouragement, understanding, and shared moments of success and challenge have made this experience memorable. To my close circle of friends— Dr Zheng Liu, Dr Shichen Yu, Dr Fan Yang, Dr Zhe Fu, Dr Han Ding, Dr Zehao Ji, Dr Zhuotong Sun, Dr Jiakai Guo, Dr Yiyi He, Dr Fang Zhang, Dr Liyi Dong, Dr Qianyue Zhang, Dr Geyunjian Zhu, Prof Boyang Shen —thank you for being my pillars of strength.

I would also like to extend my gratitude to the friends who supported me through the highs and lows of this academic pursuit. To Dr Yibo Gao, Dr Jiaqi Chen,

Dr Ye Ma, Dr Shijie Zhan, Ms. Duzhiyun Zheng, Dr Shuyu Liu, Ms Jiayue Yang, Dr Benxun Li, Dr Rui Ma, Dr Yue Yin, Dr Xin Li, Dr Tianwei Zhang, Ms Yichun Xu, Dr Xinran Gao, Dr Jialin Dou, Dr Xiaohan Pan, Ms Yin Lin, Dr Qin Guo, Dr Yuwan - Lin, Prof. Kuang Shen, Dr Xiaozheng Jin, Dr Xiaozheng Jin, Dr Sicheng Yu, Prof. Nan Chi, Dr Shengjun Ren, Dr Junfei Xia, Dr Han Qin, Dr Xinke Tang, Ms Ziyi Zhong, Dr Qianyu Lu, Ms Yi Hu.

Your encouragement and camaraderie made the challenging moments more bearable and the triumphs more meaningful. In particular, the late-night study sessions, the laughter during breaks, and the shared triumphs have created lasting memories that I will cherish.

Lastly, my heartfelt thanks go to my extended family for their unwavering support and belief in my potential. Their encouragement and understanding during the intense periods of research and writing were crucial to my perseverance.

In conclusion, completing this academic journey has been a collective effort. I am deeply grateful to all who have played a role, big or small, in this significant achievement. Each person mentioned has left an indelible mark on my academic and personal growth; I am forever thankful for that.

List of publications:

1. Y. Liu, W. Ali, R. Chen, N. Bamiedakis, M. Crisp, I. White, and R. Penty, “High-capacity optical wireless VCSEL ARRAY transmitter with uniform coverage,” Free-Space Laser Communications XXXV, vol. 12413, pp. 144-150, March 15, 2023.

2. T. Li, W. Ali, R. Chen, Y. Liu, M. Crisp, and R. Penty, “Next Generation Wireless Fronthaul using VCSEL-based Free Space Optics,” 2023 Optical Fiber Communications Conference and Exhibition (OFC), May 19, 2023.

3. Y. Liu, W. Ali, R. Chen, N. Bamiedakis, M. Crisp, I. White, and R. Penty, “High-capacity multichannel VCSEL array-based OWC transmitter,” Journal of Lightwave Technology, (In preview)

4. Chen, R., Ali, W., Liu, Y., Crisp, M., & Penty, R. (2023). “High Speed Optical Wireless Receiver with Wide Field of View using Commercial Components”. Apollo - University of Cambridge Repository.

5. M. D. Soltani et al., "Terabit Indoor Laser-Based Wireless Communications: Li-Fi 2.0 For 6G," in IEEE Wireless Communications, vol. 30, no. 5, pp. 36-43, October 2023

6. Q.D. Ahmad et al,” Indoor Laser-Based Wireless Communications” from book: “Free Space Optics Technologies in B5G and 6G Era - Recent Advances, New Perspectives and Applications”, Intech open, 2024

List of Figures:

List of Tables:

List of Abbreviations

ADC	Analog-To-Digital Converter
AEL	Admitted Exposure Limit
AFE	Analog Front End
APD	Avalanche Photodiode
AWG	Arbitrary Waveform Generator
AWGN	Additive White Gaussian Noise
AWGR	Waveguide Grating Router
BBU	Baseband Unit
BER	Bit Error Ratio
BPSK	Binary Phase Shift Keying
CDMA	Code-Division Multiple Access
CLB	Configurable Logic Blocks
COTS	Commercial-Off-The-Shelf
CPC	Compound Parabolic Concentrator
CPRI	Common Public Radio Interface
CPU	Central Processing Unit
DAC	Digital-To-Analog Converter
DBR	Distributed Bragg Reflector
DDC	Digital Downconverter
DFE	Decision Feedback Equalization
DOE	Diffractive Optical Elements
eCPRI	Evolved Common Public Radio Interface
EDFA	Erbium-Doped Fibre Amplifiers

EEL	Edge Emitting Laser
ESA	European Space Agency
EVM	Error Vector Magnitude
FDMA	Frequency-Division Multiple Access
FFT	Fast Fourier Transform
FPGA	FPGA Based Digital Signal Processing
FSO	Free-Space Optics
FWHM	Full Width At Half Maximum
GaAs	Gallium Arsenide
GCPW	Grounded Coplanar Waveguide
GeoLITE	Geosynchronous Lightweight Technology Experiment
GOLD	Global-Scale Observations Of The Limb And
IEC	International Electrotechnical Commission
IF	Intermediate Frequency
IFFT	Inverse Fast Fourier Transform
InGaN	Indium Gallium Nitride
InP	Indium Phosphide
ISI	Inter-Symbol Interference
LD	Laser Diodes
LED	Light-Emitting Diodes
LMS	Least Mean Squares
LOS	Line-Of-Sight
LSMS	Line Strip Multibeam System
MHP	Most Hazardous Position

MIMO	Multiple Input And Multiple Output
MLA	Microlens Array
mmW	Millimetre Wave
MPE	Maximum Permissible Exposure
NASA	National Aeronautics And Space Administration
ND	Neutral Density
NIR	Near-Infrared
NLOS	Non-Line-Of-Sight
NRZ	Non-Return To Zero
OFDM	Orthogonal Frequency-Division Multiplexing
OLED	Organic Led
OMA	Orthogonal Multiple Access
OOK	On-Off-Keying
OWC	Optical Wireless Communication
P/S	Parallel-To-Serial
PAPR	Peak-To-Average Power Ratio
PC-LED	Phosphor Converted Led
PCV	Plano-Concave Lenses
PCX	Plano-Convex Lens
PD	Photodetector
PSK	Phase Shift Keying
PtP	Point-To-Point
QAM	Quadrature Amplitude Modulation
RAN	Radio Access Network

RE	Radio Equipment
REC	Radio Equipment Control
RF	Radio Frequency
RU	Remote Units
RZ	Return To Zero
S/P	Serial-To-Parallel
SDMA	Space Division Multiple Access
SFP	Small Form-Factor Pluggable
SILEX	Semiconductor Inter-Satellite Link Experiment
SiPM	Silicon Photomultipliers
SLM	Spatial Light Modulator
SNIR	Signal To Noise And Interference Ratio
SNR	Signal-To-Noise Ratio
SPAD	Single-Photon Avalanche Diodes
TDM	Time-Division Multiplexing
TDMA	TIME Division Multiple Access
THz	Terahertz
TIA	Trans-Impedance Amplifier
VCSEL	Vertical-Cavity Surface-Emitting Laser
VLC	Visible Light Communication
VSA	Vector Signal Generator
WDM	Wavelength Division Multiplexing
Wi-Fi	Wireless Fidelity
YAG	Yttrium Aluminum Garnet

List of Symbols

E_C	Conduction band
E_v	Valence band
h	Planck's constant
v	Light speed.
E_g	Bandgap
m_1	Lambert's mode number
ϕ	Angle of irradiance
$\Phi_{1/2}$	Semi-angle at half-power
$I(\varphi)$	Angular intensity distribution
φ	Angle of light emission
P_t	Total radiated optical power
$E_{(r)}$	Electric field
I(r)	Intensity of laser
E_0	Electric field at the centre of the beam
ω	Beam waist
I_0	The intensity of light at the beam centre
λ	Wavelength of light
Z_R	Rayleigh range
ω0	Beam waist at laser source
$U_{l,m}$	Optical intensity of the mode
L_m^l	Generalized laguerre polynomials
$A_{l,m}$	Normalized mode coefficient
I_p	Photocurrent
R	Responsivity of the photodetector
$\sigma^2_{Theraml}$	Thermal noise
R_L	Load resister
F_n	Amplifiers noise figure
Δf	Effective noise bandwidth

I_d	Dark current
T	Period time
M	Avalanche gain
p_{in}	Input optical power
'R'	Radius
f	Focal length of the lens
n	Refractive index of the lens material
R_1	Radius of curvature of the lens surface closer to the light source
R_2	The radius of curvature of the lens surface farther from the light source
t_{ex}	Exposure duration
D_s	Size of light source
z	The distance of the apparent source from the considered position in space
H_d	DC gain
Apd	Active area of PD
Ts(Ψ)	Optical band-pass filter of transmission
g(Ψ)	Optical gain
Ψ_c	Width of the field of vision at a receiver
$\delta(0)$	The Dirac function
Wd	The beam waist of laser at the distance 'd'.
S	Electrical power signal component
γ	Responsivity (A/W)
$P_{r\ Signal}$	Received signal power
T_{sp}	Sampling period
T_0	The time taken when the first signal arrives at the receiver.
p_t	Average transmitted optical power
q	Electronic charge
B	Equivalent noise bandwidth
I_{bg}	Background current

k	Boltzmann’s constant
T_k	Absolute temperature
G	The open-loop voltage gain
η	The fixed capacitance of photo detector per unit area
Γ	The FET channel noise factor
gm	The FET transconductance.
ρ	Reflection coefficient
dA	Detector area
Z_{MPH}	Distance of the Most Hazardous Position
D_{FT}	Diameter of the flat-top beam profile
P_{LA}	Pitch of the microlens array
fLA2	Focal lengths of the microlens array2
f_{LA3}	Focal lengths of the microlens array3
F_{FL}	Focal length of the Fourier lens
a_{23}	Spacing between the microlens array2 and microlens array3
N	Noise
σ^2_{Shot}	Shot noise
$P_{r\ ISI}$	Received ISI power

Contents

Chapter 1 Introduction

1.1 Introduction of Optical wireless communication

With the rapid increase in mobile data traffic, an exponential increase in mobile data traffic is anticipated (5,016 EB per month in 2030) [1][2]. The proliferation of data-intensive applications demands a revolution of the current high-speed indoor wireless communication technologies. Wireless user access is dominated mainly by radio frequency (RF) technologies like Bluetooth, ZigBee, Post-5G, MM-Wave and Wi-Fi6 technologies, which support more spectrum resources and data capacity. However, these RF methods face limitations, notably the overcrowded RF spectrum that hampers the potential for faster communication speeds [2]. Therefore, optical wireless communication (OWC) has emerged as a promising high-speed wireless communication technology that uses light as a medium to transmit signals wirelessly through free space.

Optical wireless technologies have been used for signal transmission for thousands of years—initially, significant applications involved mirrors, fire beacons, and smoke signals to communicate over extended distances. In modern times, the experiment demonstrated by Alexander Bell in 1880 stands as a landmark in the evolution of OWC [3]. This experiment encompassed the transmission of voice signals through free space over 200 meters, where voice signals were transmitted via free space over 200 m. The voice signal caused the vibration of a mirror at the transmitter side. The change of sunlight was synchronously transported at the received side, and the light signal was recovered into the original voice.

Despite the development of OWC technologies and the demonstration of numerous systems throughout the 20th century, the outcomes yielded by OWC still needed improvement. The main limitations of OWC development are as follows:

1. OWC systems suffer from severe atmospheric effects, leading to system performance degradations such as beam scintillation and requiring accurate alignment between the transmitter and receiver.
2. OWC reliability is unstable due to optical path blockages and the impact of weather conditions such as fog, rain, and snow.
3. General interests have shifted to optical fibre transmission systems since the key technological breakthroughs, including developing low-loss single-mode fibres, erbium-doped fibre amplifiers (EDFAs), and wavelength division multiplexing (WDM).

However, OWC technology still attracted substantial attention in space applications; OWC takes advantage of easy deployment, security, flexibility, and large-capacity features. On the space application side, the National Aeronautics and Space Administration (NASA) investigated the near-Earth OWC systems in the Geosynchronous Lightweight Technology Experiment (GeoLITE) and the Global-Scale Observations of the Limb and Disk (GOLD) programs [4][5], while the European Space Agency (ESA) investigated similar systems in the Semiconductor Inter-Satellite Link Experiment (SILEX). Such near-Earth OWC technologies have continued to develop in the past decade, with up to 10 Gbps inter-satellite links have been demonstrated.

Thanks to the development of high-performance and low-cost optoelectronic devices, OWC has become a hot topic again. This trend is further accelerated by the ever-growing bandwidth requirement of end users and the high-speed real-time connectivity required by emerging services. The renewed interest in OWC focuses on indoor short-range environments. One studied system in recent years is Li-Fi technology, which can provide high-speed wireless connections to users in personal working and living spaces. The IEEE 802.15.7 standard for OWC/ visible light communication (VLC) systems was proposed in 2011[6], which made detailed specifications in terms of VLC modulation mode, networking architecture, and physical layer design. Last updated new standard for Li-Fi technology is IEEE 802.11 bb. IEEE 802.11bb standardizes the application of light in the near-infrared spectrum, specifically within the 800 to 1000 nm range, for achieving data transmission rates ranging from 10 Mbps to 9.6 Gbps [7].

OWC leverages light propagation, usually laser or light-emitting-diode (LED) beams, to establish high-speed data transmission links between communication

devices. LED-based-OWC systems have been studied and developed over decades as they offer an opportunity to transmit optical signals and provide indoor illumination at the same time [8][9]. Moreover, LEDs suffer from fewer eye-safety restrictions on indoor OWC transmitter design. However, the low modulation bandwidth of LED remains one of the main challenges for achieving high-speed data transmission [10]. To further increase the aggerated data rate (>tens of Gbps), high density LED arrays, and high-resolution modulation technologies have been employed to increase the aggerated data rate [11]. In the last decade, laser diodes have attracted research interest for indoor OWC due to their higher modulation bandwidth (>GHz) [12].

1.2 Comparison of OWC / RF wireless communication

The RF communication technology can provide comprehensive coverage at lower carrier frequencies. This is because of the RF waves' diffraction and scattering and the RF receiver's sensitivity. RF systems are also robust to blocking and shadowing and can provide full coverage between rooms. However, at higher carrier frequencies, the RF channels become more line of sight and problems encountered are similar to those using light. Moreover, the RF components are expensive, and the key advantages of RF technology (i.e., mobility, coverage, and receiver sensitivity) become less clear compared to OW technology.

The RF band, which lies between 3 kHz and 300 GHz of the electromagnetic spectrum and the use of this band is strictly regulated by local and international authorities. The available light band (300GHz -30PHz) is potentially offering 10,000 times more bandwidth capacity than the RF based technologies, and all of them are license free. The electromagnetic spectrum is shown in Figure 1.1.

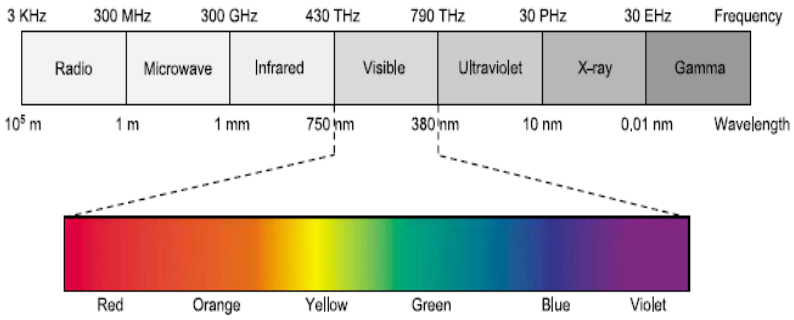

Figure 1.1 The electromagnetic spectrum [13]

Moreover, OWC is a suitable solution in indoor environments due to its multiple user-size cellular, minimum interference between adjacent cellular, and

carrier reuse capabilities beam its intrinsically abrupt cell boundaries. OWC systems are also immune to electromagnetic interference. Therefore, they can be deployed in RF-sensitive environments such as hospitals or complicated RF environments [14]. Furthermore, since the optical beam is naturally confined to a certain area and cannot penetrate opaque objects, it is difficult to intercept the optical signal, providing inherent security in the physical layer [15].

1.3 Applications of optical wireless communication

OWC's development gained momentum in the late 20th century as researchers explored its potential applications in various domains, including telecommunications, indoor networking, interrail satellite communication and underwater communication [16][17]. B5G/6G's is proposed to extend the architecture beyond current wireless communication, creating an integrated space-ground-underwater network, as shown in Figure 1.2. [1]

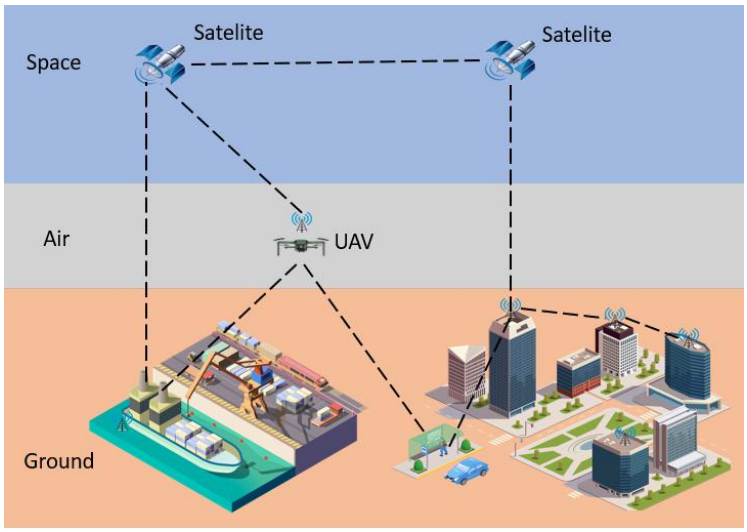

Figure 1.2 integrated space-air-ground wireless network

- **Free space optical communication (FSO)**

OWC technology is widely applied in free space communications, including satellite-to-satellite, satellite-to-ground and lunar communications scenarios, where communication distances are exceptionally long [18][19][20][21]. One reason of using OW for such applications is that the size of antenna can be much smaller than RF systems. The directional propagation property of light is other key reasons of

using OWC in space communications. For example, the NASA's lunar laser communication demonstration in 2013. The data rate of 622 Mbps is achieved with an ultra-long transmission distance of 384,600 km to send data between Moon and Earth.

- **Outdoor OWC application**

One attractive outdoor application of OWC system is providing the fronthauling of the future mobile wireless networks. Although RF and optical fibre-based systems have been used to satisfy current data traffic demand, optical fibre-based backhaul networks require the deployment of fibre, which is costly especially in high-density urbans, and the microwave-based solution faces the limited data rates, licensed spectrum and electromagnetic interference (EMI) issues. To overcome these problems, the OWC principle can be used, where a pair of optical transmitter and receiver directly establishes a wireless link between base stations or between the base station and the core network.

Up to 200 m wireless range has been demonstrated, and a reliability of 99.9% is achieved even considering diverse weather conditions such as rainfall, snow and fog [22]. High data rate has also been achieved using the OWC technology, where up to 200 Gbps has been demonstrated combining the WDM technology [23]. In 2021, the Taara project leaded by Alphabet demonstrated a 20 Gbps Free Space Optical Communications (FSOC) system over 4.8 km. This work on bridging the connectivity gap between Brazzaville in the Republic of the Congo and Kinshasa in the Democratic Republic of Congo [24].

- **Indoor OWC application**

OWC technologies has also been applied in indoor environment to provide high-speed wireless data transmissions. Both the VLC and near-infrared optical wireless technology have been studied in indoor OWC applications [25]. In VLC systems, since multiple LEDs available to provide a satisfying illumination level, these LEDs can be used for data transmissions simultaneously. The Multiple input and multiple output (MIMO) are implemented to further increase the system data rate and capacity. With a small-scale 2 × 2 LEDs MIMO system, over 6 Gbps VLC has been realized [29].

In near-infrared indoor OWC systems, lasers are used as light sources. Compared to LED, the key advantage of lasers is the much larger modulation

bandwidth. In this case, high-speed wireless connections can be achieved even without advanced modulation format, signal equalization or WDM technologies. For example, with just simple OOK modulation format, up to 12.5 Gbps communication data rate has been experimentally demonstrated[30]. Recently, Vertical-cavity surface-emitting laser (VCSEL) has attract great attention as a cost-effective near-infrared laser source[31]. VCSEL is a sophisticated optical source applied in optical modulator, optical fibre communications and Lidar scanning since their narrow divergence, high bandwidth, and invisible working wavelength [32-35].

1.4 Research motivation

This research is motivated by the increasing demand for data traffic driven by high-definition video streaming, virtual reality, and the Internet of Things. Existing wireless technologies like cellular networks and Wi-Fi are nearing capacity limitations due to the limited and crowded RF spectrum.

To address this challenge, there is a growing interest in developing high-speed, cost-effective, and eye-safe laser-based OWC systems. VCSEL has attracted research interest in OWC systems due to their eye-safe operation in the near-infrared range and the ease of large-scale, two-dimensional chip fabrication, making them comparable to other types of lasers.[36]

In previous research, VCSEL-based OWC systems have been focused on single-channel communication with point-to-point wireless links offering high data rates over relatively long communication distances but do not address the issue of indoor atto-cell coverage and user mobility. Moreover, available VCSEL arrays developed for data communications are multimode devices, which provide a doughnut-shaped beam profile. This means that if they are used with a simple lens arrangement or direct emission, the illumination at a receiver plane can form a no-signal zone at the centre of the atto-cell area. In addition, adjacent cells can interfere with each other since the VCSEL arrays are densely deployed with a pitch distance of 250 μm.

Therefore, this work aims to develop a high-capacity optical wireless system using arrays of VCSEL array transmitters. A VCSEL array transmitter optic is designed to provide relatively wide coverage and ensure uniform signal-to-noise ratio (SNR) distribution for each atto-cellular unit, enabling regular deployment without optical irradiance overlapping. Careful consideration has been given to adhering to standard

laser safety regulations for free-space optical transmission transmitters to ensure the design complies with eye safety standards.

1.5 Organisation of the thesis

This thesis is organised as follows:

Chapter two reviews the fundamentals of indoor optical wireless communication systems and optical components (i.e. LED/Laser transmitters, PIN/APD/SiPM receivers and simple optical lenses). Advanced modulation schemes employed for indoor OWC systems are described in the literature. The challenge of indoor OWC transmitter eye-safety limitations has also been discussed.

Chapter three presents the channel model simulation of indoor VCSEL based-OWC system. A 5 m × 5 m × 3 m indoor room environment has been simulation to evaluate the Signal-Noise-Ratio distribution and data transmission. In simulation, a VCSEL array is assumed to be a gaussian beam for low complexity programming.

Chapter four presents an over Tbps high-capacity optical wireless VCSEL array system. A novel transmits optics design involving a plano-concave lens, microlens arrays and a large-scale plano-convex is proposed. The transit optics for a 5 × 5 square deployed VCSEL array transmitter is verified in Zemax.

Chapter five shows the demonstration of the proposed transmitter using the Off-the-shelf component. To build the transmit optics, a 3D printing holder is designed to mount the lenses. A single element from the VCSEL array OWC link with the SiPM receiver is demonstrated.

Chapter Six demonstrates a 1×3 symmetrical multibeam VCSEL array-based-OWC system using the transmit optics presented in Chapter Four. The interference among the optical wireless channels is investigated. A higher modulation bandwidth APD receiver is employed to improve the data receiver performance.

In Chapter Seven, a VCSEL-array-based FSO fronthaul link with easy alignment for next-generation radio access network (RAN) is first time demonstrated. With a lens system, a 20 cm x 20 cm area coverage is created at a 3m distance.

Chapter eight concludes and summarises this thesis. The outlook for future work related to the proposed approaches and applications for future improvements is also discussed.

Chapter 2: Indoor optical wireless communications: components, modulation schemes and systems.

2.1 Introduction

The Optical Wireless Communication system comprises a transmitter, a free space channel, and an optical receiver, as illustrated in Figure 2.1. On the transmitter side, the optical source, typically light-emitting diodes (LED) or laser diodes (LD), initially converts the electrical signal containing the transmitted information into an optical beam. This optical beam then traverses the transmitter optics, where beam properties are adjusted. The modulation scheme employed at the transmitter governs the intensity and frequency of the optical signal, transforming them into data transmission coefficients. Moreover, the light source's compliance with laser safety standards and eye safety is ensured.

At the receiver end, the optics module captures the optical signal, directing it to a photodetector (PD). The PD converts the optical signal back into the electrical domain, recovering the transmitted data. In Optical Wireless Communication systems, P-I-N and avalanche photodiodes (APDs) are commonly used as PDs. Notably, Single-Photon Avalanche Diodes (SPADs) are increasingly integrated as optical receivers in laser-based OWC systems due to their high sensitivity.

In light propagation, optical lens is used to transfer the optical beam path and beam characteristics. Transmit optics are commonly used to collimate and align light beam into the receiver direction. At receiver side, a lens is used to collect more light onto receiver.

Modulation schemes convert electrical signals into optical bit streams. Non-return-to-zero (NRZ) modulation is a prevalent choice for illustrating optical wireless

communication, primarily due to its ease of implementation and compatibility with straightforward clock recovery circuits. In response to the demand for higher transmission data rates at multi-gigabit levels, advanced modulation schemes with elevated spectral efficiency have been extensively explored to bolster capacity.

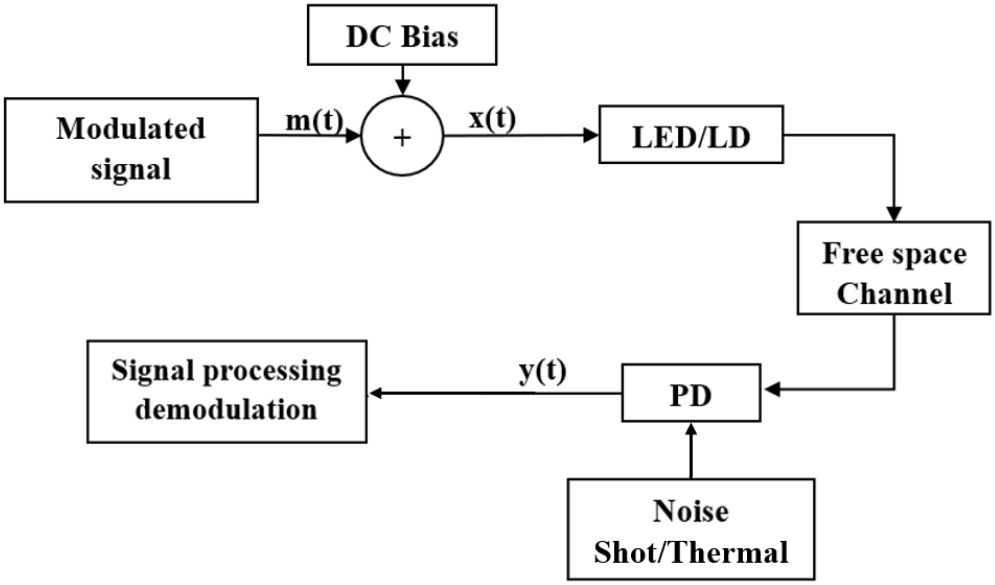

Figure 2.1 The basic structure of indoor OWC system

The remainder of this chapter is organized as follows. The different optical transmitters, optical receivers, and optical lenses are illustrated in section 2.2. The basic modulation schemes for the OWC links are reviewed in section 2.3. Indoor LED/LD-based OWC systems are reviewed in section 2.4. The international standards for laser-safety regulation and research for OWC transmitter eye-safety consideration are discussed in section 2.5.

2.2 Optical transmitter

2.2.1 LED

LEDs emit incoherent light through spontaneous emission when subjected to electronic excitation as shown in Figure 2.2. The electronic excitation is achieved by applying a forward bias voltage across the p-n junction. An electron spontaneously falls from conduction band E_c to the Valence band E_v emitting a photon with the energy of hv, where h is the Planck's constant and v is the light frequency.

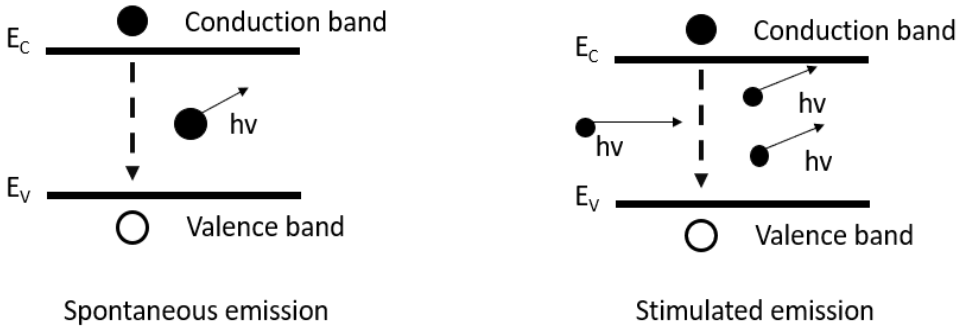

(a) (b)

Figure 2.2 Schematic illustrations of (a) spontaneous emission and (b) stimulated emission.

The wavelength of light is determined by the bandgap E_g between the conduction band and the valence band, which can be expressed as

$$\lambda = \frac{hc}{E_g(eV)}\ \mu m \tag{2.1}$$

In generally, it is assumed that the angular distribution of the radiation intensity pattern is modelled using a generalized Lambertian radiant intensity. The distribution can be represented as:

$$R_0(\phi) = \begin{cases} \frac{(m_1+1)}{2\pi}\cos^{m_1}(\phi), & for\ \phi \in [-\pi/2, \pi/2] \\ 0, & for\ |\phi| \geq \pi/2 \end{cases} \tag{2.2}$$

Where m_1 is the Lambert's mode number expressing directivity of the source beam. The Maximum radiated power is achieved when the angle of irradiance ϕ equally to 0 degree. The angle of irradiance is from 0 to $\pi/2$, thus, the celling will not reflection surface are only the walls in the room to the celling from the LEDs. The order of Lambertian emission m_1 is given by the LED semi-angle at half-power $\Phi_{1/2}$, which is given by

$$m_1 = \frac{-\ln 2}{\ln(\cos \Phi_{1/2})} \tag{2.3}$$

The angular intensity distribution $I(\varphi)$of the radiation pattern can be modelled using.

$$I(\varphi) = \frac{m_1+1}{2\pi} \times P_t \times \cos^{m_1}(\varphi) \tag{2.4}$$

Where φ is the angle of light emission with respect to the LED's surface normal, P_t is the total radiated optical power. The different types of LED are investigated for OWC system and summary below:

a) Organic LED (OLED):

OLED is a LED in which the emissive electroluminescent layer is a film of organic compound that emits light in response to an electric current. It is widely used is display equipment. The typical modulation bandwidth of OLEDs is around hundreds of kHz, which makes them less capable as optical transmitters for high-speed communication [37].

b) Phosphor Converted-LEDs (PC-LED):

A PC-LED employs a single blue Indium Gallium Nitride (InGaN) LED chip to pump an Yttrium Aluminum Garnet (YAG) phosphor coating. The phosphor converts part of the blue light to green, yellow, and red portions of the spectrum while the other part of the blue light leaks out, a mixture that produces white [38].

However, the absorption rate of phosphor is high, which makes them less output light power for long distances transmission.

c) Micro LEDs:

Compared to the other LEDs, Micro-LEDs can provide a relatively wide modulation bandwidth (> 100 MHz). In addition, the development of transfer print technology allows the fabrication of a dense micro-LED array. The 2-dimensional array micro-LED can support multiple input multiple output (MIMO) technology since it can be used either to increase the overall data rate or to improve the reliability of transmission [39].

2.2.2 Laser

The principle of the laser relies on the stimulated emission process as shown in Figure 2.2. A photon with energy 'hv' strikes an excited state, where the energy difference between the conduction band and the valence band results in the emission of another photon. More importantly, this photon generated is identical to the photon that triggers this process, which means the two photons have the same phase and frequency. Therefore, the photons emitted through the stimulated emission process are coherent. This stimulated emission continues, where the generated photon further triggers the emission of more photons in the coherent way, forming the working

principle of the laser. Due to the coherence of all photons, the laser generally has a much narrower wavelength spectral width than that of the LED.

The light emitted by lasers are normally modelled as the single-mode Gaussian profile (TEM_{00}). The electric field distribution of a Gaussian beam on the cross section can be expressed by

$$E(r) = E_0 exp\left(-\frac{r^2}{\omega_0^2}\right) \tag{2.5}$$

So that, the intensity of laser can be expressed as:

$$I(r) = I_0 exp\left(-\frac{2r^2}{\omega_0^2}\right) \tag{2.6}$$

Where r is the distance from the centre of the beam, E_0 is the electric field at the centre of the beam and ω is called the beam waist. I_0 is the intensity of light at the beam centre.

The Gaussian beam propagation property can be described by three parameters: beam width at the distance z from the laser source, the Rayleigh range and beam divergence.

$$\omega(Z) = \omega_0 \left[1 + \left(\frac{\lambda Z}{\pi \omega_0^2}\right)^2\right]^{\frac{1}{2}} \tag{2.7}$$

$$Z_R = \frac{\pi \omega_0^2}{\lambda}$$

$$\Theta = \frac{\lambda}{\pi \omega_0}$$

where λ is the wavelength of light. The Rayleigh range is the distance from the laser at which the beam width is $2\omega_0$ (it is also called the f parameter of the Gaussian beam), and the beam divergence is far field.

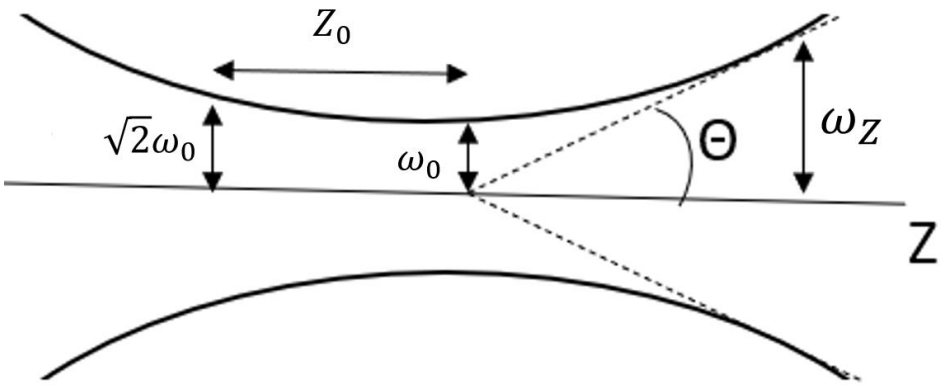

Figure 2.3 The cross-section of the ideal gaussian beam profile.

Depending on the direction of laser beam output from the chip's substance, the laser can catalogue as Edge emitting laser (i.e. the laser beam parallels to the substance) and Vertical cavity surface emitting laser (i.e. the laser beam perpendicular to the substance). The detailed of them are introduced as below:

- **Edge Emitting Laser (EEL)**

In an edge-emitting laser, light is emitted from the edge of the substrate. A solid-state laser is grown within a semiconductor wafer, with the optical cavity parallel to the surface of the wafer. The wafer is cleaved at both ends and coated with a mirror to create the laser. A type of semiconductor laser where the active region is confined in a thin strip along the edge of the wafer.

The basic structure of an EEL consists of a substrate, a cladding layer, an active layer, and a contact layer, as shown in Figure 2.4. The substrate is usually made of gallium arsenide (GaAs) or indium phosphide (InP) and provides a platform for the other layers to grow on. The cladding layers are made of a material with a lower refractive index than the active layer, which helps confine the light within the waveguide. The active layer is the region where the light is generated and typically consists of multiple quantum wells. The contact layer is used to provide electrical contact to the device and is typically made of a heavily doped material such as n+ GaAs.

When a current is applied to the device, electrons and holes recombine in the active layer, producing photons through the process of stimulated emission. The photons travel along the waveguide and are emitted out of the edge of the device. The emission wavelength is determined by the bandgap energy of the active layer

material.

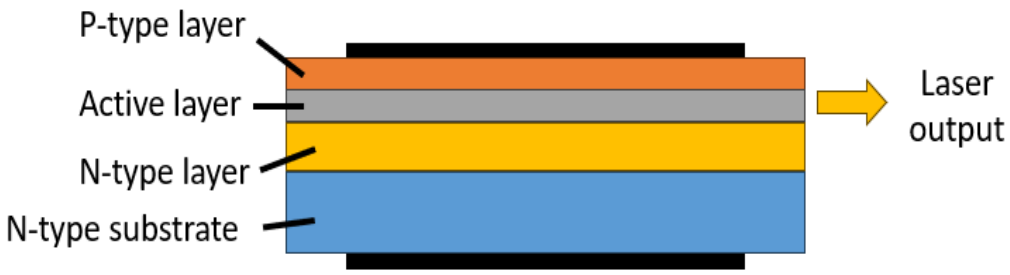

Figure 2.4 The basic structure of Edge Emitting Laser

- **Vertical Cavity Surface Emitting Laser (VCSEL)**

VCSEL is one of commercial infrared optical source for data communication and senser. It has been widely applied in the optical interconnect for data base and distance senser. The most special characteristics of the VCSEL is that its output beam is perpendicular to the substance surface due to the vertical resonant cavity. Additionally, the circular symmetric VCSEL beam is easily to beam shaping (e.g., collimate, re-forces, coupling) by the optics rather than eclipse beam of EEL.

Figure 2.5 illustrates a cross-section of the fundamental structure of a Vertical-Cavity Surface-Emitting Laser. The layer composition, from top to bottom, comprises: (i) the P contact layer, (ii) the p-type Distributed Bragg Reflector (DBR), (iii) the oxidation layer, (iv) the quantum well gain region (active region), (v) the n-type DBR, (vi) the N-type substrate, and (vii) the N contact layer. Above and below the active layer, vertically, narrowband mirror layers are situated. These mirrors consist of alternating high/low-refractive index layers, each designed to a quarter wavelength of the laser's operational wavelength.

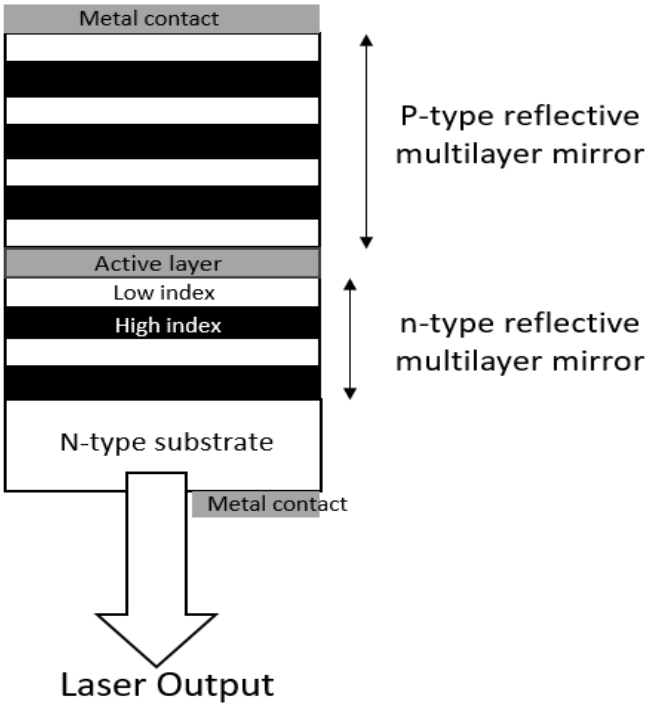

Figure 2.5 The common structure of VCSEL [40]

The VCSEL beam presents a doughnut-shape spot which has a low optical irradiance area at the centre as show in Figure 2.6(b). Commonly, the multimode beam profile can be expressed as the incoherent superposition of transverse modes. The total optical intensity of the beam can be expressed as:

$$I = \sum_{l=0}^{L_{max}} \sum_{m=0}^{M_{max}} C_{l,m} \left| U_{l,m} \right|^2 \tag{2.8}$$

Where $\left|U_{l,m}\right|^2$ is the optical intensity of the mode (l,m), C is the mode power coefficient. The Laguerre-Gaussian mode is one of the well know transverse modes, which represents the circularly or cylindrically symmetric beams. The irradiance of Laguerre-gaussian mode (m,l) in the cylindrical coordinate system at the distance z is represented as:

$$\left|U_{l,m}(r,\phi,z)\right|^2 = \left| A_{l.m} \left[\frac{w_o}{W(z)}\right] \cdot \left(\frac{\sqrt{2}r}{W(z)}\right)^l \cdot L_m^l \left(\frac{2r^2}{W^2(z)}\right) \cdot e^{\left(-\frac{r^2}{W^2(z)}\right)} \right|^2 \tag{2.9}$$

Where L_m^l is the generalized Laguerre polynomials, which can be expressed as:

$$L_m^l(x) = (m+l)! \sum_{i=0}^{m} \frac{(-x)^i}{i!(m-i)!(l+i)!} \tag{2.10}$$

$A_{l,m}$ is the normalized mode coefficient which is used to ensure that the total power of each mode is equal to 1 and is expressed as:

$$A_{l,m} = \sqrt{\frac{2m!}{\pi(m+l)!}} \tag{2.11}$$

Figure 2.6 shows some examples of beam profile of difference Laguerre-Gaussian modes. In fact, the beam profile of single-mode VCSEL is gaussian distribution which is Figure 2.6 (a). However, the most commercially available VCSELs are multi-mode TEM and their beam profiles are illustrate as a doughnut-shape showing in Figure 2.6(b). There are relatively low power at the centre of beam.

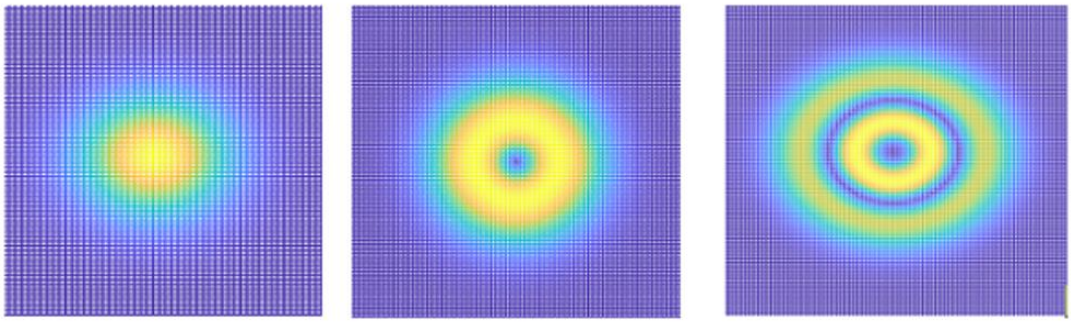

(a) (b) (c)

Figure 2.6 The beam profile of (a) TEM (0,0), (b) TEM (0,1) and (c) TEM (1,2) using Laguerre-Gaussian modes.

2.3 Optical Receivers

Optical receivers convert the received optical signal into the electrical domain and recover the transmitted data. The receiver sensitivity typically characterizes the performance of an optical receiver. The minimum magnitude of the input optical signal required to produce a specified output signal with a specified bit error rate (BER). In OWC, the other crucial characteristics of the optical receiver are the Field of view, noise performance and 3 dB bandwidth.

In optical communication systems, the modulated light signal is typically detected by a PD, which converts the optical signal into the electrical domain for recovering the transmitted data. PIN/APD based- OWC systems have been widely investigated [41][42]. Recently, The SPAD/SiPM has been proposed as a suitable optical receiver for the OWC system. It offers a highly attractive alternative that extremely increases the detection sensitivity of photo-electronic transition while

providing all the benefits of PD [66]. The optical output irradiance in the free space is relatively lower than the laser safety consideration.

2.3.1 PIN photodetector

The PIN PD consists of one additional intrinsic region in addition to the normal PN junction, as shown in Figure 2.7. The intrinsic region is much wider than both P and N regions. Most photons are absorbed in the intrinsic region to create electron and hole pairs. When a reverse bias is applied to the PIN PD, a very large electric field appears across the wide intrinsic region, and hence, the photon generated electrons and holes can be drifted out with high velocity. Due to the wide intrinsic region, the drifting process dominates, and the diffusion time of carriers is significantly reduced. Therefore, the operation speed and bandwidth supported by PIN are usually high, where 10 GHz and higher can be easily achieved.

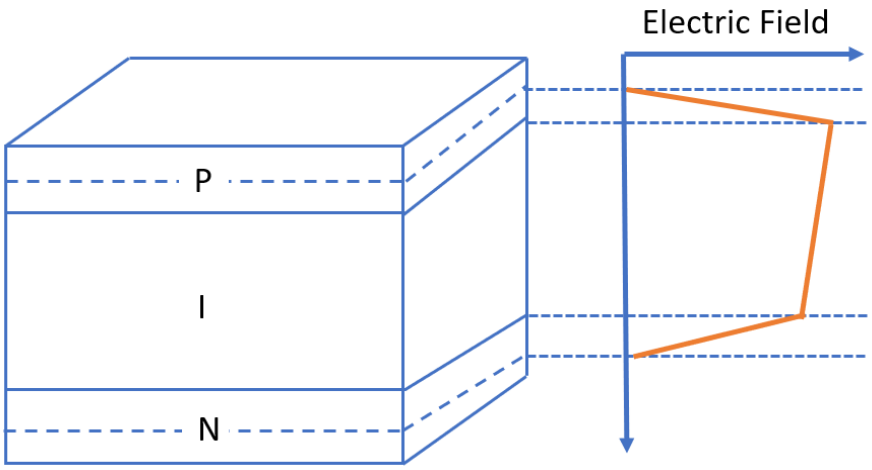

Figure 2.7 The basic structure of PIN photodetector with electric field distribution under reverse bias

The photocurrent I_p is directly proportional to the input optical power P_{in}:

$$I_p = R \times P_{in} \tag{2.12}$$

Where R is the responsivity of the photodetector (A/W), which depends on the quantum efficiency of the device.

- Noise performance

The shot noise and thermal noise are the two fundamental noise mechanisms exits in the optical receiver. The thermal noise is caused by the random thermal

motion of electrons in a resistor which result into a fluctuation in the current even in the absence of an applied voltage. The thermal noise can be expressed as:

$$\sigma_{Theraml}^2 = 4\left(\frac{k_B T}{R_L}\right) F_n \Delta f \tag{2.13}$$

Where the R_L is the load resister; F_n is the amplifiers noise figure and Δf is effective noise bandwidth which is relative to the bandwidth of the receiver.

The shot noise current is generated since the collection of random pulsed corresponding to the electron hold pairs created by the photons. The dark current is another shot noise source, therefore, the total shot noise can be present as

$$\sigma_{shot}^2 = 2q(I_p + I_d)\Delta f \tag{2.14}$$

Where is I_d is the dark current.

Consequently, the total noise can be obtained by the sum up the two noises:

$$\sigma_{Total}^2 = \sigma_{Theraml}^2 + \sigma_{shot}^2 = 2q\left(I_p + I_d\right)\Delta f + 4\left(\frac{k_B T}{R_L}\right) F_n \Delta f \tag{2.15}$$

2.3.2 Avalanche photodetector (APD)

An APD is designed to be a highly sensitive semiconductor-based photodetector and the basic structure of APD is illustrated in Figure 2.8. Compared to the PIN structure, the APD has an added internal gain region which is capable to improves responsivity.

The working principle of the APD is relies on the avalanche multiplication. The APD is operated by a high reverse voltage in resulting a very high electric field created in the gain region, therefore, the carriers generated by the absorbed photons in the intrinsic region are accelerated. Those carries undergo ionizing collision with lattice atoms creating secondary carries. This process can continues build up more carries, thus, it provides an avalanche gain (M) to the photocurrent. This avalanche gain depends on the value of the electric field applied across the gain region. So that, the higher reverse bias voltage can improve to the avalanche gain. The current generated by a APD with an input optical power can be written as:

$$I_{APD} = M \times R \times P_{in} \tag{2.16}$$

where I_{out} is the total current at the output of APD and I_p is the primary photocurrent before multiplication. The typical internal gain, M, of APD is in the range of 50–300. Since it takes time for the avalanche multiplication process to build up, normally the speed and bandwidth of APD are lower than that of PIN.

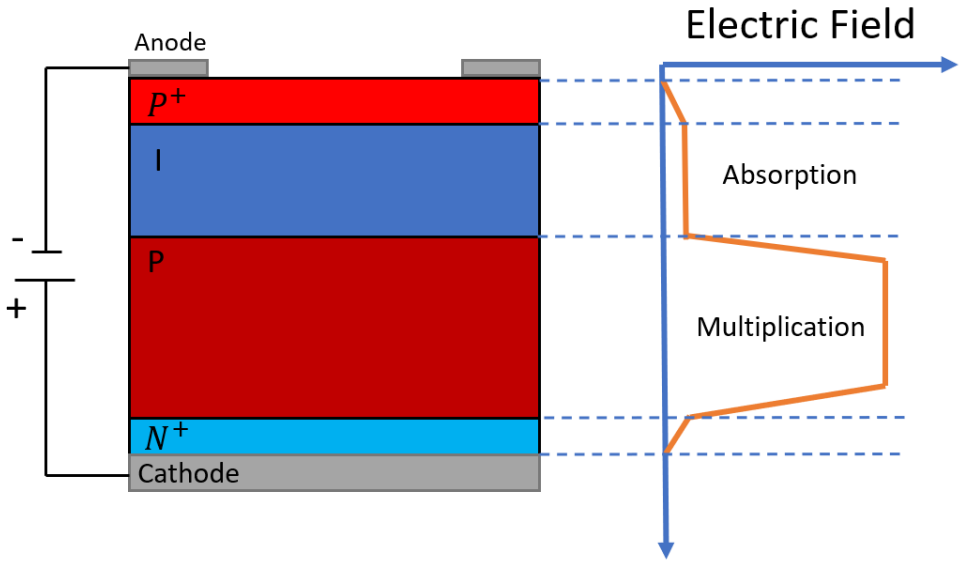

Figure 2. 8The basic structure of APD photodetector with electric field distribution under reverse bias

- Noise performance

The shot noise and thermal noise also existed in an APD receiver. The thermal noise of the APD is the same as in PIN detectors since it caused by electrical circuit. However, the shot noise of APD is affected by the multiplication process. The ionization of each individual carrier is random, and the avalanche gain M represent the average multiplication level. Meanwhile, the dark current is amplified by the avalanche multiplication process. As a result, the shot noise of APD can be represented as:

$$\sigma_s^2 = 2qM^2F_A(RP_{in} + I_d)\Delta f \tag{2.17}$$

The total noise performance of the APD receiver can be represented as:

$$\sigma_{APD}^2 = \sigma_{Theraml}^2 + \sigma_{Shot}^2 = 4\left(\frac{k_BT}{R_L}\right)F_n\Delta f + 2qM^2F_A(RP_{in} + I_d)\Delta f \tag{2.18}$$

2.3.3 Silicon photomultiplier (SiPM)

SiPM is a dense array of independent single photon avalanche diodes (SPADs), each with its own quench resistor. The operation unit of SiPM is called as microcell. The basis of the microcells is a reach-through avalanche structure[43]. Figure 2.9 (a) illustrated the simple electric circuit of a 2×4 array SiPM. On top of the avalanche microstructure is placed a semi-transparent electrode, which can have an antireflection coating. The depletion region is represented by a thin 'n' area and 'p' area, of total thickness. The SiPM output signal is a sum of the signals from a number of microcells.

SPAD is a special APD which generate the secondary carriers though the impact ionization. A single absorbed photon can trigger a self- perpetuating ionization cascade. The silicon will break down and becomes conductive, amplifying the carrier to large current flow. This process is known as Geiger discharge. An SPAD operating in Geiger mode can achieve a high gain. The reverse bias voltage creates the high-filed though the junction where the current is generated and flowed out. The series resistor R_Q is act as quenching switch which limits the current drawn by the diode during breakdown. This results in the diode shutdown because the reverse voltage applies on it is below than its breakdown voltage, thus the avalanche process is stopped. The diode then recovered when the bias voltage beyond the breakdown voltage again and be able to detect next photon stream. This cycle of avalanche, quench, and recovery are illustrated in Figure 2.9 (b). As a result, a single SPAD sensor operated in Geiger-mode functions as a photon-triggered switch, in either an 'on' or 'off' state. This results in a binary output. Regardless of the number of photons absorbed within a diode at the same time, it will produce a signal no different to that of a single photon. Proportional information on the magnitude of an instantaneous photon flux is not available [44].

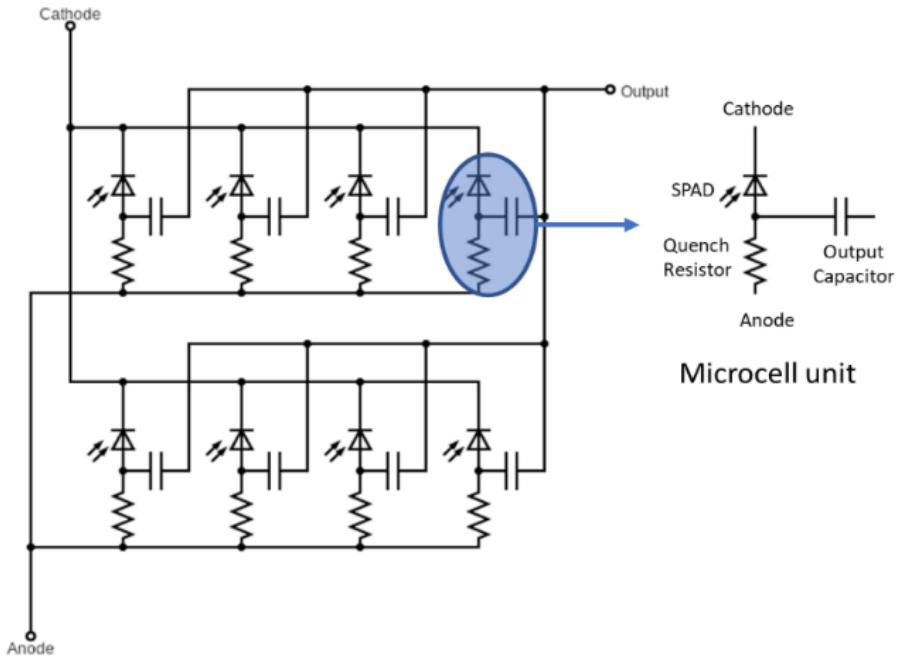

(a)

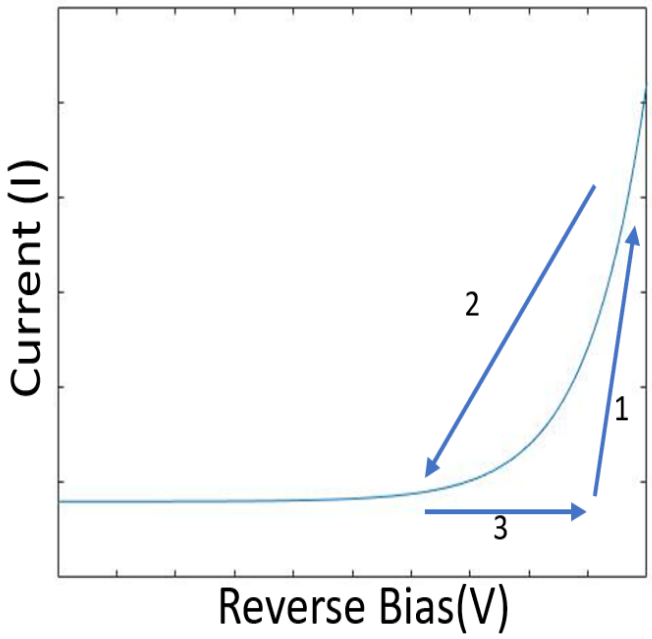

(b)

Figure 2.9 (a) Basic circuit structure of a SiPM receiver and (b) The cycle of Quenching process: 1. Avalanche process: The breakdown reverse bias voltage creates the high-filed to generate the avalanched current. 2. Geiger discharge: The series resistor RQ is act as quenching switch which limits the current drawn by the diode during breakdown. 3. Recovery: The diode then recovered when the bias voltage beyond the breakdown voltage again and be able to detect next photon stream.

2.4 Optical lens

Optical lens is commonly used in OWC systems to focus or disperse light beam propagating in the air. A lens is a pieces of transparent material device with two polished surfaces either both surfaces are curved, or one is curved and one is plane. The types of simple lens can be classed by the curvature of the surface as shown in the figure 2.10.

A Plano-convex lens and a biconvex lens are both types of converging lenses. When parallel rays of light pass through these lenses, they converge to a single point behind the lens. This converging point is known as the focal point, and the distance between the focal point and the lens is called the focal length. The focal length of a spherical lens can be calculated using Eq. 2.19, where the radius of curvature 'R' is another important parameter to describe the curved of the lens' surface, given that the curved surface of the lens is a part of a sphere with radius 'R', as shown in Figure 2.11.

A Plane-concave lens and biconcave lens are called the diverging lens which diverges a collimate light beam emanating from a focal point on the axis in front of the lens.

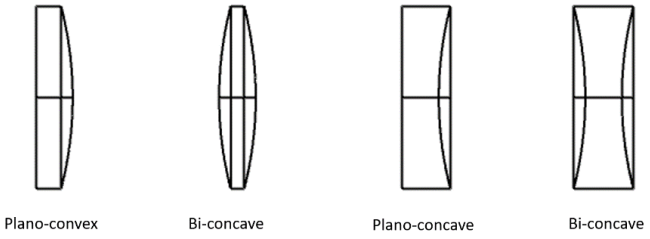

Figure 2.10 The types of different lenses

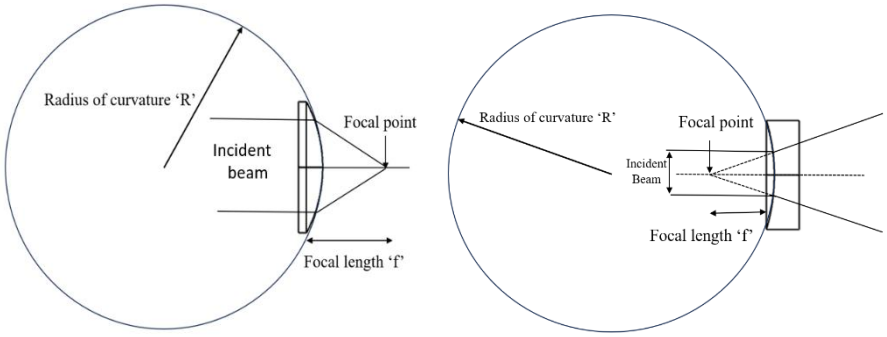

(a) (b)

Figure 2.11 The geometric of lens:(a) Plano-convex lens, (b) Plano-concave lens

The focal length of a lens in air can be expressed as

$$\frac{1}{f} = (n-1)[\frac{1}{R_1} - \frac{1}{R_2} + \frac{(n-1)d}{nR_1R_2}] \quad (2.19)$$

Where: f is the focal length of the lens; n is the refractive index of the lens material; R_1 is the radius of curvature of the lens surface closer to the light source; R_2 is the radius of curvature of the lens surface farther from the light source; d is the thickness of the lens

2.5 Modulation schemes and Equalization techniques

Optical wireless communication systems use various modulation schemes to encode data onto light signals for transmission. These modulation schemes are critical in determining the data rate, spectral efficiency, and overall performance of OWC systems. Multigigabit data rates of laser-based-OWC systems were achieved to improve the capacity of the OWC channel; advanced modulation formats with high spectral efficiency have, therefore, been proposed and implemented to achieve high-speed transmissions. In this section, OWC links employ the most widely used modulation schemes, including On-off-keying and Orthogonal frequency-division multiplexing.

2.5.1 On-Off Keying (OOK)

OOK is the most used modulation scheme for Intensity Modulation/Direct Detection OWC. In OOK modulation, the optical signal is sent by switching a light source on or off. A ‘1’ bit is encoded when the light source is On, and a ‘0’ bit is encoded when the light source is OFF when there is no pulse. The flicker of the light source cannot be sensed by the human eye when the frequency is higher than 60Hz.

There are two types of OOK modulation: return to zero (-RZ) and non-return to zero (-NRZ). In the OOK-NRZ scheme, the pulse duration is equal to the bit duration, while the pulse occupies only the partial duration of the bit in the OOK-RZ scheme. Figure 2.12 (b) shows the signal pulse for the OOK-RZ scheme.

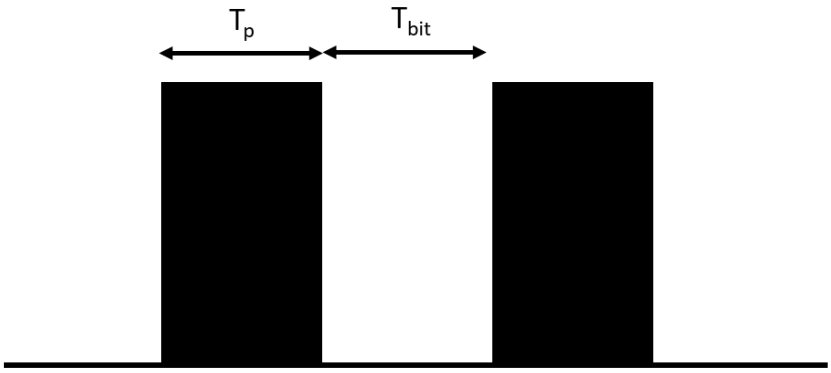

(a)

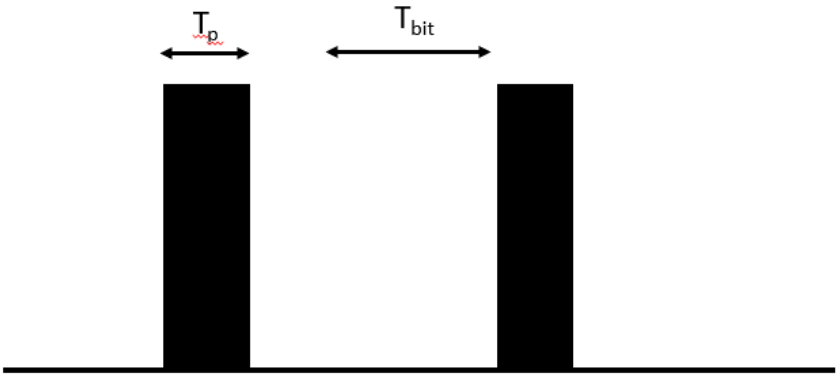

(b)

Figure 2.12 (a)OOK-NRZ and (b)OKK-RZ modulations

The light sources can switch on and off at rates into Gbps using the OOK modulation technique. For example, an aggregate parallel data transmission rate of 1.5 Gbps using OOK modulation for a Complementary Metal-Oxide-Semiconductor (CMOS) controlled GaN-based LED array [45]. OOK modulation in the OWC system is easy to implement, and simple transceiver circuitry is required. However, the effect of inter-symbol Interference is significant at a higher data rate.

2.5.2 Orthogonal frequency-division multiplexing (OFDM)

Orthogonal Frequency Division Multiplexing (OFDM) is a digital modulation technique that has been widely adopted in optical wireless communication systems due to its ability to mitigate the effects of inter-symbol Interference and channel distortion.

OFDM is used to modulate the intensity of the optical carrier signal using a number of subcarriers that are orthogonal to each other. These subcarriers are separated by a fixed frequency spacing, which is typically chosen to be equal to the reciprocal of the symbol duration. The subcarriers are then modulated using different modulation schemes, such as Quadrature Amplitude Modulation (QAM) or Phase Shift Keying (PSK).

In the basic system model for an OFDM-based optical wireless communication system, as shown in Figure 2.13, the crucial components are annotated. The initial data processing involves an M-level QAM constellation mapping and subsequent inputting into serial-to-parallel (S/P) conversion for efficient data representation. The signal undergoes an Inverse Fast Fourier Transform (IFFT) to transition from the frequency domain to the time domain, followed by parallel-to-serial conversion (P/S). A cyclic prefix (CP) is added to mitigate Inter-Symbol Interference (ISI). DC biasing ensures that the OFDM time domain signal remains real and positive.

At the transmitter, Intensity Modulation is applied, and the modulated signal, denoted as y(t), is transmitted through an LED/Laser. A parabolic reflector establishes a line of sight to the receiver, facilitating efficient signal transmission. On the receiver side, direct detection is employed, with a PD converting incoming optical power into the amplitude of an electrical signal.

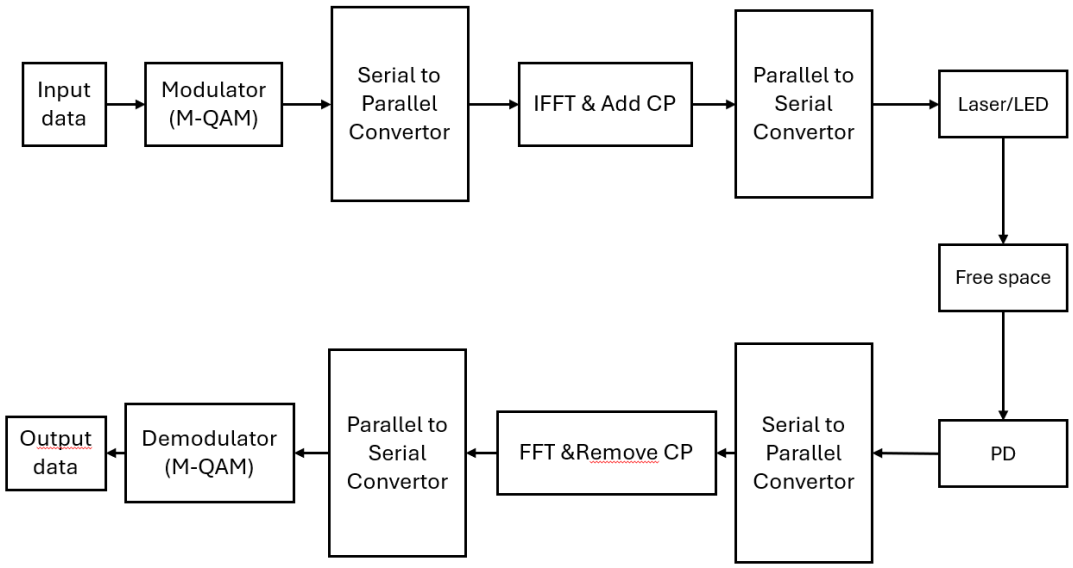

Figure 2.13 The block diagram of OFDM-OWC system

At the receiver, the received signal is first passed through a free space channel, which causes inter-symbol interference and distortion due to the different speeds of the various components of the signal. The received signal is then demodulated using a Fast Fourier Transform (FFT), which separates the subcarriers and allows the receiver to recover the original data.

2.5.3 Equalisation

In OWC links, the optical path arrival to the receiver within a sampling time after the first optical signal received by the PD are the desired signal power. The impulse response of those multipath in each sampling time can be represent as the sum to the pulse, which are also known as Inter-symbol interference.

Equalisation has been widely used in optical communication systems to compensate for Inter-symbol interference and recover the original optical signal [43][44]. The most common equalisation circuit are feed-forward equalisation and decision feedback equalisation, which have already been proven to provide significant performance improvements and extend the transmission capability.

- Feed-forward equalisation (FFE).

A feed-forward equalisation is the simplest type of linear equaliser and significant performance improvements can be achieve using a sequence of feedforward filter (FIR). FIRs get inputs as the sampled received signal with T sampling period, a_{k-n} and each delayed sample is multiplied by its corresponding tap coefficient, c_n, which have been pre-adapted to give the preferable equaliser response. However, the noise from the input signal is amplified during the feedforward equalisation process, resulting noise level enhancement.

$$\mathrm{out(k)} = \sum_{n=0}^{N_{FF}} c_n * a_{k-n} \tag{2.20}$$

- Decision-feedback equalisation（DFE）

A decision-feedback equaliser is a nonlinear equaliser. The previously decided bit values obtained using the decision equipment and multiplies them by the corresponding tap values. The feedback filters are used to get the past decisions of transmitted signal to compensate the noise level and remove the ISI.[43]

$$out(k) = \sum_{i=1}^{N_{FB}} f_i * d_{k-i} \quad (2.21)$$

In this work, the combination of FFE and DFE with Least mean squares (LMS) adaptive algorithm is employed to remove the ISI introduced by the multipath dispersion. The working principle of the adaptive FFE+DFE is shown in figure 2.14. And, its output can be expressed as:

$$d'_k = \sum_{n=0}^{N_{FF}} c_n * a_{k-n} - \sum_{i=1}^{N_{FB}} f_i * d_{k-i} \quad (2.22)$$

Where:

- d' is the decision made by the equalizer.
- c & f represents the weight of FFF and FBF respectively.
- a & d represents the input of FFF and FBF respectively.

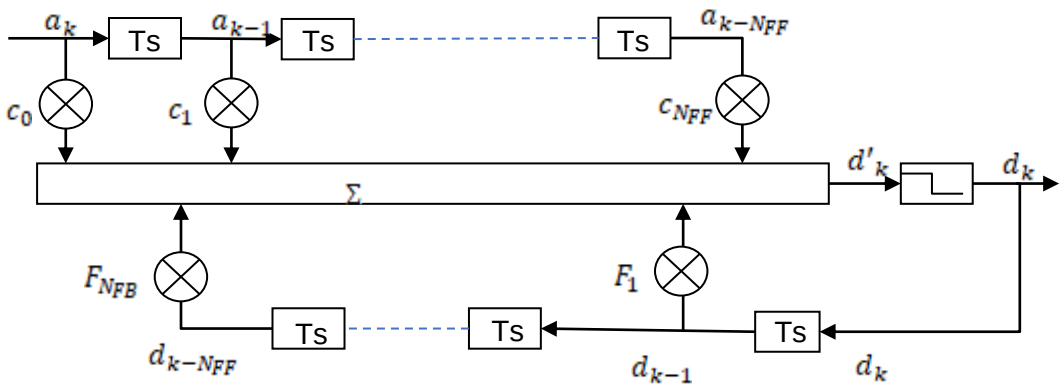

Figure 2.14 Feedforward-Decision feedback equaliser.

- The Least Mean Squares Algorithm

The most used algorithm to adapt the filter coefficients is the Least Mean Squares (LMS) algorithm which is satisfactory in most situations. The LMS algorithm has two parts. In the first part, the output of a transversal filter is computed according to the tap inputs and the error term is generated according to the difference between the filter output and the desired response. In the second part, the adjustment of the tap weights is done according to the error term [46]. The error signal e_k is given by:

$$e_k = d_k - d'_k \quad (2.23)$$

The adjustment process can be expressed as:

$$c'_N(n+1) = c_N(n) + \mu e_k(n) a_N(n) \quad (2.24)$$

$$f'_N(n+1) = f_N(n) + \mu e_k(n) d_N(n) \quad (2.25)$$

To get a satisfactory result from the adaptive equalizers, the equalizers are adapted with a known sequence of symbols, training sequence, which can be pseudorandom sequence. This training period enables the weights to reach a point near to the optimum level, but most of the time it is costly.

2.6 Indoor Optical wireless communication systems

2.6.1 Indoor LED based OWC systems

In optical wireless communication, a modulated electrical signal is applied to a solid-state semiconductor-based source, and the intensity of the source is modulated according to the signal. LED and laser are the two typical optical sources for optical wireless transmitters. In the early stage of the development of indoor OWC technologies, LEDs were widely used as they were cost-efficient and able to provide indoor illumination and data transmission at the same time. Moreover, the wide field of view of LED is another advanced property of LEDs that has low optical intensity in the propagation path. Therefore, an LED transmitter is considered a non-hazardous light source. Up to 4.5 Gb/s data rate, an RGB LED-based WDM system has been demonstrated, which employed RLS-based adaptive equalisation to enhance the channel capacity [47]. Harald Haas et al. demonstrated a 6.36 Gbit/s RGB LED-based WDM MIMO Visible Light Communication System Employing OFDM Modulation within 1.5m free space transmission [48]; they proposed 10 Gb/s visible light communications using WDM RGB LED in 2016. [49] The work wavelengths of LEDs are involved in the visible light spectrum, so an LED-based OWC system is also known as visible light communication. However, the based-OWC system is restricted to achieve higher channel capacity [50][51][52]. One of the main reasons is its relatively lower modulation bandwidth.

2.6.2 Indoor laser based-OWC systems.

Lasers have over GHz modulation bandwidth, which supports laser-based OWC systems to achieve gigabit data transmission. Moreover, the narrow divergence of the laser beam can minimise the multipath dispersion caused by walls and ceiling diffraction in an indoor environment. However, the penalties of using lasers as OWC

transmitters are the risk of high-power levels hazardous to the human body and precise alignment between transmitter and receiver.

Data rate recording for the OWC system using different types of Laser sources is summarised in Figure 2.3. The OWC system using a multichip laser can achieve a higher data rate since multiple light sources are employed. A 20 Gbps data rate OWC link was achieved using RGB Laser; such a system demonstrated a bidirectional signal demodulation VLC system [53]. In [54], a 12 RGB LD-based VLC system was proposed. In the system, each triplet was experimentally demonstrated to achieve an 8.78 Gbps data rate. Therefore, the estimate for the achievable data rate becomes 105.41Gbps.

Recent developments in VCSEL offer a safer wavelength in the infrared spectral range with relatively wide divergence (~20 degrees). VCSEL is considered a more suitable OWC transmitter as the low-cost, well-controlled, circular beam profile and easily 2-dimensional array chip fabricated [55]. VCSELs were investigated for free space interconnect in card-to-card. A 50 Gbps optical interconnect is experimentally demonstrated using 16 carriers-amplitude-phase (16 CAP) symbol modulation and filter-enhanced spatial modulation. In the system, microlens arrays were mounted in front of VCSELs and PD arrays for optical beam collimation and focusing. MEMS mirrors served as the dynamic link selection block for reconfiguration [56]. In [57], A LiFi transmission system with a data rate of 25 Gbps is experimentally demonstrated over a 10 m optical wireless link using a two-stage injection-locked 680 nm VCSEL.

Indoor optical wireless communication OWC systems based on VCSELs have been proposed [58]. Such devices are low-cost, exhibit high power efficiency and relatively large bandwidth (> 5 GHz) and can be readily formed into arrays. As a result, they are ideal sources for low-cost, high-bandwidth NIR indoor wireless optical links. A few such VCSEL-based OWC systems have been presented in the literature [57-62]. For example, an OWC system using a VCSEL array was studied by Sakai et al. in [59]. The system was equipped with a diffuser and a reflective surface to shape the VCSEL array output beams into a pill-box light intensity distribution beam profile. In [60], T. Nakamura et al. studied an OWC system based on a high-power 940 nm VCSEL. Dong et al. proposed a two-user QAM–OFDMA OWC

system using a 940 nm VCSEL array and working over a 2 m distance and demonstrated an aggregate data rate of up to 2.7 Gbps [61]. A 3- 3-meter 850 nm VCSEL OWC system with a 1 GHz modulation bandwidth was proposed by Z. Wei et al. in [62].

2.6.3 The configures of the multibeam OWC transmitter

The VCSEL arrays offer the opportunity to design compact multi-channel optical wireless communication (OWC) links. The transmission through multiple channels increases the aggregated data transmission compared to a single input, single output (SISO) system. Previously, to achieve multibeam system, various OWC systems have been proposed.

- Angle diversity optical transmitter

An angle diversity optical transmitter can realise parallel directional data transmission by activating the lasers that cover only the areas occupied by active users. In imaging diversity transmitters, each laser element/array chip is directed to a particular range of angles, creating a 'cellular' coverage. Independent electrical signals can control different LD elements, which supports MIMO backhaul for high channel capacity achievement. Figure 2.15 (a) shows the multiple narrow-beam laser elements mounted on a semi-sphere access point. Such an OWC system can use space division multiple access (SDMA) to achieve over ten times higher data throughput than a TDMA system using a single laser, which has been studied in [64].

- **Beam steering based OWC transmitter**

Beam steering technology is one of the approaches to achieve a multibeam transmitter, which can orient multiple laser beams propagated into specific areas to enhance user mobility due to location tracking. Different optical beam steering devices have been investigated in OWC, including fibre array, phase array and spatial light modulator (SLM). In [65], O'Brien et al. experimentally demonstrated a 4-meter 25 Gbps bi-directional point-to-multi-point indoor OWC system. A narrow beam was first collimated and orientated in a specific direction—an imaging lens coupling a fibre, which refocused the received beam into the fibre. An IR camera is integrated into the transmitter for precious OWC link alignment. In the system, the position of the receiver is pre-designed. An enhancement of the fibre array system, which

provides over Tbps data rate transmission, was proposed in [66]; Koonen et al. employed a wavelength-controlled two-dimensional IR beam steering OWC system as shown in Figure 2.15 (d). A high port count arrayed waveguide grating router (AWGR) was coupled to a 2D fibre array, and the different beams were orientated in the desired directions using a camera lens. The system achieved 112 Gbps PAM-4 data transmission per beam over a 2.5 m working distance. A total capacity of 8.9 Tbps was projected for this system using an 80-port C-band AWGR. A phase only SLM was used at the access point to route signals from an optical fibre to the users in the downlink with a ± 30° FOV [66]. However, the system has low channel capacity because it can only generate one OW link at the same time. Such systems show great potential but rely on sophisticated and complex optical systems to achieve high capacity and in-room beam steering. In common, the beam steering based OWC systems must incorporate an indoor location system, providing users' location.

- **Advanced optical components for multibeam OWC transmitter**

Advanced optical components are investigated to generate the multibeam OWC transmitter to simplify the configuration of the transmitter. For example, A simple structure of diffusing spots in a line strip multibeam system (LSMS) was simulated and investigated in [67], as shown in Figure 2.15 (b). The transmitter is placed on the floor and emits an optical signal via a diffuse link. A holographic optical diffuser is mounted on the laser source to generate multiple narrow beams illuminating multiple small coverage areas on the ceiling. Although such a system significantly reduced the ISI effect and improved the SNR by 20 dB at the receiver side, the NLOS data transmission links induced the ISI effect, which limits the achievable data rate. The optical diffuser based OWC transmitter has also been developed using a 10 × 10 VCSEL array which is shown in Figure 2.15 (c). [68]. A designed DOE lens interface with the VCSEL array that orientated beams into different directions ensures non-overlapping between the cells. Each VCSEL can illuminate an 88.2 cm ×82.2 cm square area. As a result, the poor uniformity of optical intensity showed in the cell and the system's data transmission capability needs further study.

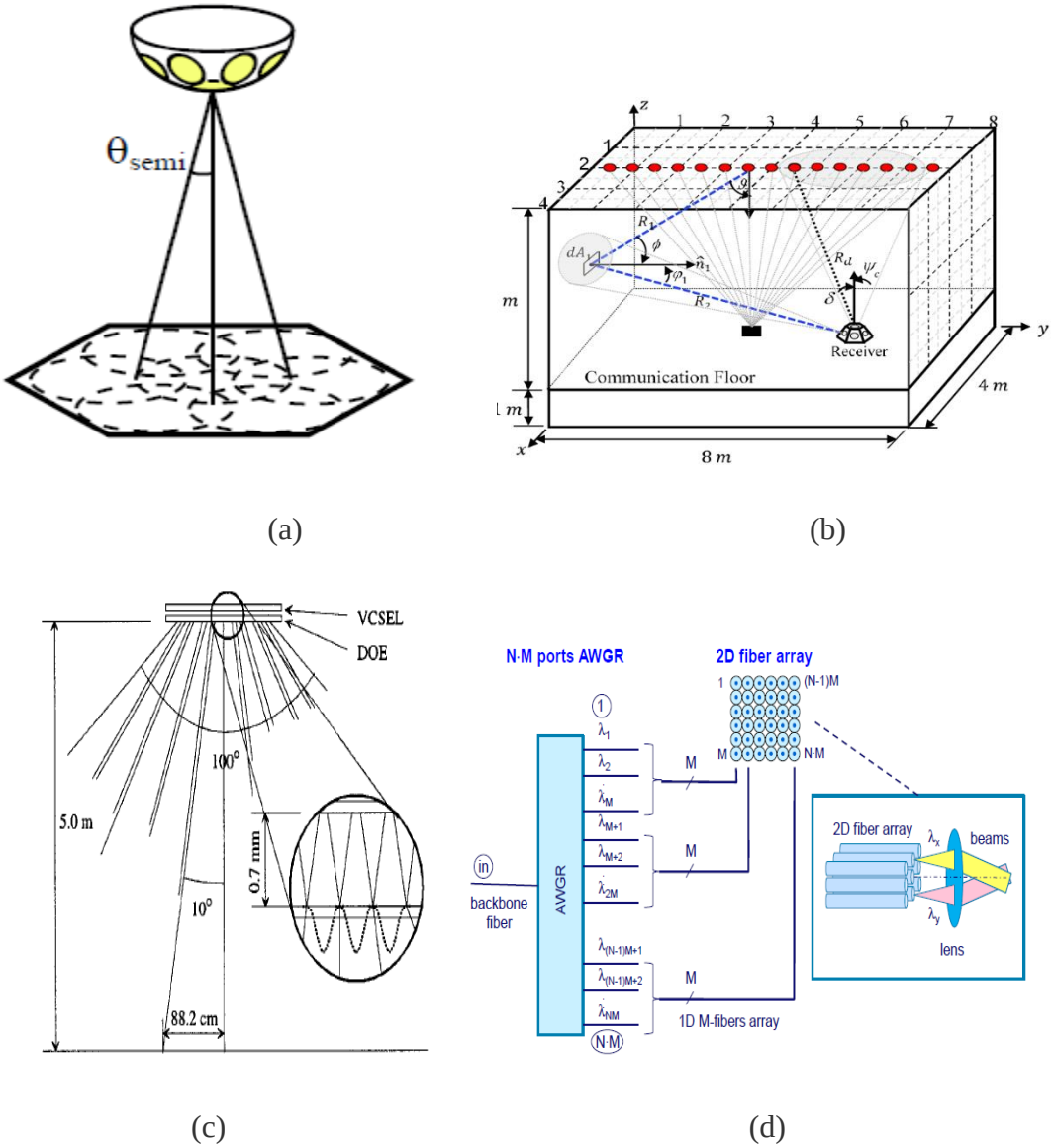

(a) (b)

(c) (d)

Figure 2.15 The configures of the multibeam OWC transmitter (a) the angle diversity transmitter[64], (b) LSMS using holographic optical diffuser[67] (c) diffuser lens[68], and (d) 2D fibre array[66]

2.7 Eye safety consideration

Increasing the output power of the OW transmitter as much as possible could overcome some of the data transmission limitations of OWC systems. A higher emitted optical power could compensate for the power loss in the free space, extending the transmission distance and improving the signal-noise ratio (SNR) due to the higher level of received optical power. However, the optical power is restricted to the risk of optical power level to the human's eye and skin. Eye safety is one of the critical characteristics of indoor OWC applications; the light sources can cause

damage to both the human eye and the skin if their optical irradiance exceeds the specific safety levels [69][70].

In common, the energy power level of optical transmitters does not present a significant risk for the skin, but the human eye is very sensitive to the optical power. Eye can focus light covering the wavelengths around 400–1400 nm onto the retina, and the effects of eye vary under different wavelengths. At the visible light spectral band (550-700 nm), the eye safety regulations are significantly strict as the absorption of the optical energy on the retina is around 90% [69]. Although it is much less strict at longer wavelengths of 1500 nm and above, the cost of optical sources and detectors is relatively costly. The near-infrared (NIR) spectrum is a compromising solution [71][72].

Figure.2.16 illustrates the example results of Maximum permissible exposure (MPE) at different wavelengths of laser under a long exposure duration and the results are presented for four different angular substances. The MPE exponentially raise before 1050 nm and keep constant in the range of 1050 nm to 1150 nm. The MPE remarkable linearly increase when operating wavelength is between 1150 nm to 1200 nm and keep constant after that. Therefore, the MPE is less constrict when large beam diameter is applied or infrared optical source is used.

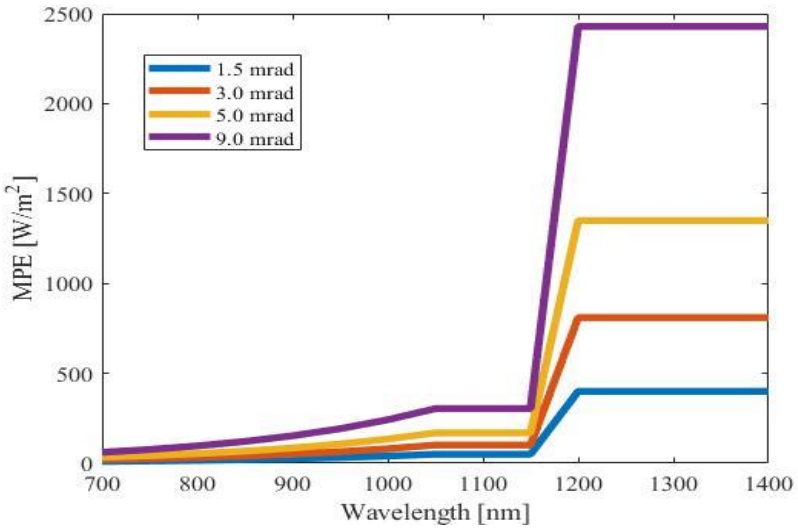

Figure 2.16 The MPE values vs different wavelengths at different beam diameters

LED sources are commonly regarded as eye-safe optical sources because of their wide beam divergence and, therefore, cannot be focused on the retina [72]. On the contrary, the risk of the laser source is unavoidable. There are several standards for the safety of lasers. The International Electrotechnical Commission (IEC 60825-1) determined regulations for laser safety, and its part 12 illustrates the safety of free space optical communication systems [73][74]. The current British standard on laser safety is based on the BS EN 60825-1, which categorises the laser products into 8 classes. Table 2.1 presents the main characteristics and descriptions of the classification system as the classification scheme for lasers indicates the potential risk of adverse health effects, where the higher the class number, the greater the laser radiation hazard posed by the laser. As result, an indoor OWC system, class 1 laser source is required to ensure that human-safety.

Table 2. 1 Laser safety standards [73]

Classification	Description
Class 1	• Safe for direct viewing under normal conditions. • Radiant power is always below or equal to the Maximum Permissible Exposure value. • Output power is considered safe for the eyes.
Class 1C	• Irradiance levels may exceed skin safety limits for intended treatments. • Ocular hazards are prevented during operation.
Class 1M	• Safe for naked eye viewing under normal conditions but can be harmful when viewed using magnifying optical instruments.
Class 2	• Limited to 1 milliwatt output power with a specific wavelength range. • Repeated or deliberate exposure may not be safe.
Class 2M	• Produce large-diameter beams in the wavelength range 400 to 700 nm.
Class 3R	• A maximum output power of 5 mW. • Potentially cause eye injuries but the risk is relatively low for short, unintentional exposure.
Class 3B	• Output power can go up to 500 mW. • Considered hazardous to the eyes, causing potential injury from direct beams and reflections.
Class 4	• Output power is greater than 500 mW with no upper limit. • Capable of causing injuries to the eyes and skin, as well as presenting a fire hazard.

In a recent study about the laser safety for the OWC systems, it defines the eye safe estimation when the optical irradiance lower or equal to the MPE at the most hazardous position (MHP). The study summarised the mathematic formulars to estimate the maximum optical output power for ideal gaussian beam, multimode VCSEL beam and with a simple lens[75]. In[76], the laser based-OWC transmitter with holographic diffuser/Microlens array lens has been studied. These optics increase the size of the apparent source to raise the MPE value, which provides the opportunity for employing higher output power laser increasing the SNR performance. The definition of those laser safety estimation factors is illustrated in below. In laser safety evaluation experiment, a focus stop is placed at the most hazardous position with a 7 mm diameter, which is the same diameter as the cornea.

- Maximum permissible exposure

Maximum permissible exposure (MPE), also known as the admitted exposure limit (AEL), regulars the maximum irradiance level to which the eye or skin can be exposed without consequential injury immediately or a long duration. The MPE is depends on the laser wavelength, the exposure time and the angular subtense of the apparent source. The MPE calculation is summarised in Table 2.2. (The range of wavelength is from 700 to 1400 nm which include most visible light and infrared spectrum)

Table 2. 2 MPE calculation for eye safety power level. [81]

Wavelength[nm]	**700<x<1050**		**1050<x<1150**		**1150<x<1400**	
t_{ex}**[s]**	<10	>10	<10	>10	<10	>10
Point source	$18t_{ex}^{-0.25}C4$	$10C_4C_7$	$90t_{ex}^{-0.25}$		$50C_7$	
Extended source	$18t_{ex}^{-0.25}C4C_6$, if $t_{ex} \leq T_2$		$90t_{ex}^{-0.25}C_6C_7$, if $t_{ex} \leq T_2$			
	$18T_2^{-0.25}C4C_6$, if $t_{ex} > T_2$		$90T_2^{-0.25}C_6C_7$, if $t_{ex} > T_2$			

Where: the factors C_4, C_6, C_7 and T_2 are expressed as:

$$C_4 \begin{cases} 1 & \lambda \leq 700\ nm \\ 10^{0.002(\lambda-700)} & 700\ nm < \lambda < 1050\ nm \\ 5 & 1050\ nm \leq \lambda < 1400\ nm \end{cases}$$

$$C_7 \begin{cases} 1 & \lambda \leq 1150\ nm \\ 10^{0.018(\lambda-1150)} & 1150\ nm < \lambda < 1200\ nm \\ 8 & 1200\ nm \leq \lambda < 1400\ nm \end{cases}$$

$$C_6 \begin{cases} 1 & \alpha \leq \alpha_{min} \\ \dfrac{\alpha}{\alpha_{min}} & \alpha_{min} < \alpha < \alpha_{max} \\ 66.6 & \alpha > \alpha_{max} \end{cases}$$

$$T_2 \begin{cases} 10 & \alpha \leq \alpha_{min} \\ 10 \times 10^{\frac{\alpha-\alpha_{min}}{98.5}} & \alpha_{min} < \alpha < \alpha_{max} \\ 100 & \alpha > \alpha_{max} \end{cases}$$

- Exposure duration

The exposure duration is defined as the time span of laser radiation on the human eye/body. Laser safety standards specify exposure time longer than 10 seconds can be regards as long-term exposure durations.

- Angular substance of the apparent source

The apparent source is the object that forms the smallest retinal image by eye accommodation. The angular substance of the apparent source is the angle subtended by the apparent source as viewed from a point in space as shown in Figure 2.17. It relates to the ability of the eye to focus the laser's power onto a small spot on the retina. The angular substance is calculated as:

$$\alpha = 2\tan^{-1}(\frac{D}{z}) \quad (2.20)$$

Where D_s is the size of light source and z is the distance of the apparent source from the considered position in space.

The size of the angular substance of the apparent source could be separated into point source (smaller than α_{min} = 1.5 mrad) and extended source (greater than 1.5 mrad). The α_{max} is valued as 100 mrad. However, a point source can turn into an extended source by using expander optics.

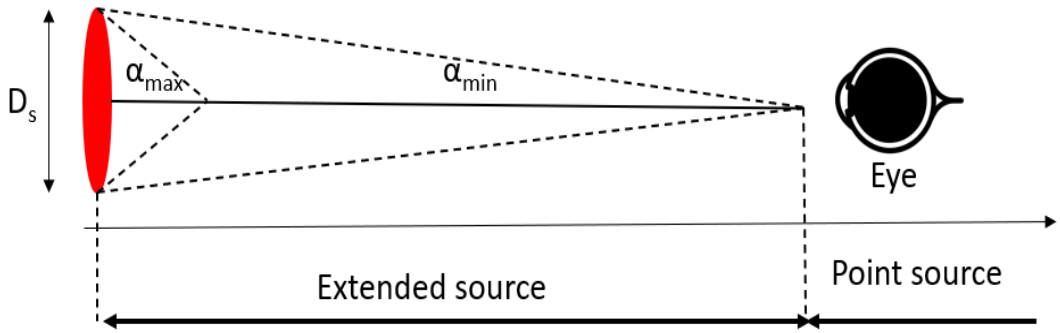

Figure 2.17 Geometric representation of the angular subtense

- Most Hazardous Position

For a given laser beam, the most hazardous position, MHP, denoted by Z_{haz}, is defined as the location at which the ratio of the exposure level to the MPE value is at its maximum.

According to the closest evaluation position which needs to be considered in a retinal hazard MPE analysis is 10 cm from the apparent source. This assumes of a near point of 10 cm, (i.e., 10 cm is the closest position) at which a healthy human eye is able to image the apparent source onto the retina. Closer distances result in higher optical powers entering the eye, but forming blurred, less hazardous images.

2.8 Summary

This chapter illustrates components of an indoor OWC system involving optical sources, receivers, and modulation schemes and summaries of indoor optical wireless communication systems.

Although LEDs (e.g., Micro-LED, PC-LED and OLED) have been studied for OWC systems, a critical limitation of LEDs is their lower modulation bandwidth. In contrast, LDs have significantly higher bandwidth, which can achieve tens of Gbps transmission speed, but penalties by eye safety limit the output power. VCSEL has been proposed as an ideal LD source as it can achieve tens of Gbps transmission speeds while maintaining eye-safety limits (i.e., its operating wavelength in near-infrared).

The PIN detector is formed by a P-N junction with an intrinsic layer at which a single photon absorption generates a carrier. Compared with the PIN structure, the APD detector has an additional multiplication region that generates secondary carriers due to the impact ionization phenomenon. However, SPAD detector is an advanced type of APD which can achieve higher gain because of the Geiger mode. The SiPM (i.e., SPAD array) is used in the OWC network to detect low-power-level optical signals.

IEC 60825-1 standards about laser safety in free space communication are studied for OWC transmitter design. According to the standards, an OWC transmitter can be considered an eye safety when the power intensity at MHP is lower than MPE. In eye safety estimation, the most hazardous point is 10 cm after the transmitter. A 7 mm diameter stop field is set at the MHP to measure the optical intensity of the beam. For different ranges of wavelengths, the limitation of MPE is most serious in the visible light spectrum and rapidly increases in the infrared range.

Chapter 3: Fundamental analysis of indoor VCSEL based-OWC system

To design an efficient indoor optical wireless communication system, it is important to well understand the characteristics of the OW channel. Optical wireless channel is often categorised into two basic schemes: line-of-sight (LOS) and non-line-of-sight (NLOS). LOS links are a direct path between the transmitter and receiver, while NLOS generally relies on the light reflected or diffused by reflecting surfaces such as walls and ceilings. LOS links have the highest power efficiency but can be blocked. The NLOS link, also known as diffusive OWC systems have been developed, which deploy the transmitter on the communication floor or walls, emitting light to the reflective surface and generating multiple diffusive links between the user and the transmitter. The difference typical OWC configurations include point to point, no-directional and diffusive will be discussed in section 3.2.

An amount of work has been published on OWC channel model investigation. In [77], a line strip multibeam system (LSMS) was proposed. The system used a multibeam OWC transmitter to generate multiple atto-cells in the room and significantly reduce the ISI effect. Although NLOS links enable to generate connection even if signal blockage and shadowing, the multipath dispersion causes effects of spread time-delay and ISI that cannot be mitigated, and the poor power efficiency compared to LOS links significantly reduce the signal-noise-ratio. In [78], authors presented a 2 × 2 white LED indoor visible light communication system to analysis the effect of ISI suffered by multipath distortion from the reflection, and they used an adaptive decision feedback equaliser to significantly reduce ISI.

VCSEL is considered a more suitable OWC transmitter as the low-cost, high bandwidth, circular beam profile and easily 2-dimensional array chip fabricated [79]. To design a VCSEL based OWC system which can cover a large indoor environment, the channel model for indoor optical wireless system is simulated using MATLAB. The performance of OWC systems is considered under ambient light noise and

multipath dispersion constraints because background noise and multipath propagation are the major challenges with indoor optical wireless channels and can reduce the received optical power and significantly degrade system performance. The simulation is based on geometrical indoor environment modelling, including multiple reflection orders. An empty 5 m × 5 m × 3 m indoor environment is assumed. To explore a higher SNR performance, the tolerance of transmitter Field-of-View (FOV) has been discussed in late to minimise the multipaths and optical interference. The characteristics of VCSEL is assumed as gaussian beam for concept demonstration.

This chapter discusses the channel characteristics and multipath propagation model in sections 3.2 and 3.3. In section 3.4, VCSEL-based OWC system is simulated to provide an OWC network in an empty 5 m × 5 m × 3 m room. A conclusion about this chapter is presented in section 3.5.

3.2 Channel Characteristics

Indoor optical wireless communication links are most term of intensity modulation and direct detection channel [2]. In an intensity modulation transmission system, the intensity of the light emitting from sources is varied according to some characteristics of the modulating signal. Usually, the amplitude of the modulating signal is taken as the property according to which the instantaneous optical power output is varied.

Direct detection is applicable to all photodetectors in optics, where a proportional current or voltage is produced to the intensity of light that radiates on the active detection area of the photodetector. For general indoor optical wireless applications, a photodetector that employs direct detection is used most frequently.

The drive current of an optical source is directly modulated by the modulation signal $m(t)$, which varies the intensity of the optical source. The optical intensity modulated signal $x(t)$ is propagating in the free space channel until received by the optical receiver, which outputs an electrical current signal y(t) and the level is proportional to the received optical power. Assuming the noise in an Additive White Gaussian Noise (AWGN), the optical wireless channel model can be expressed as follows:

$$Y(t) = \gamma X(t) \otimes h(t) + N(t) \tag{3.1}$$

where $Y(t)$ represents the received signal, γ is the responsivity, $X(t)$ represents the transmitted optical signal, $h(t)$ is the channel impulse response, $N(t)$ represents the AWGN, and the symbol $\otimes$ denotes convolution.

3.3 Propagation model

OWC links may employ various system designs, and it is convenient to classify them according to the link between the transmitter and receiver. These classification schemes are shown in Figure 3.1. In Figure 3.1(a), the point-to-point links employed narrow divergence transmitter and narrow Filed-of-view receiver, which maximises power efficiency as it minimises the multipath dispersion effect and ambient light noise. Nondirected links employ wide angle transmitters which provide large coverage area for remaining mobile terminals connection since they do not require alignment between transmitter and receiver (Figure 3.1(b)). The diffusive links system has been proposed to overcome the shadowing and blockage between the transmitter and detector (Figure 3.1(c)). The robustness and ease of use can be achieved by the non-line-of sight links. The NLOS links rely upon the reflection of light from the ceiling, walls, and diffusely reflecting surfaces.

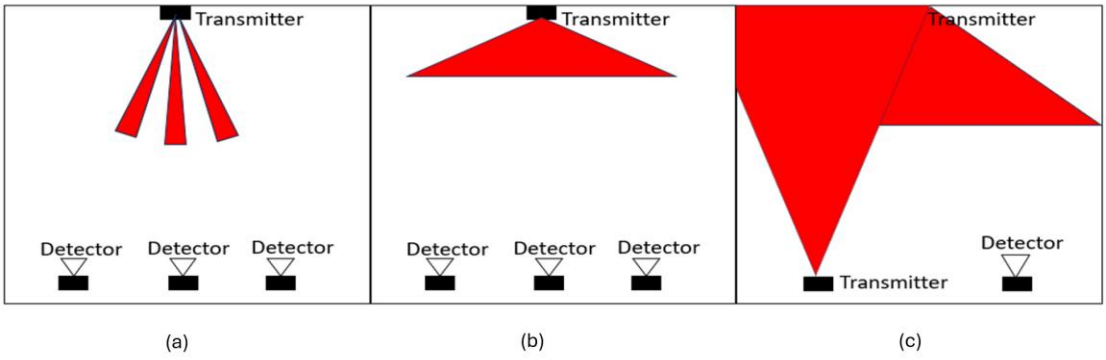

Figure 3. 1 The different OWC systems (a) point-to-point links (b)Nondirectional links (c) diffusive links

The length of propagation path depended on the relative positions of transmitter, reflecting surfaces and receiver. In multipath propagation, the optical signals spread to the receiver at different times can cause inter symbol interference that limits the data rates. Multipath propagation can be characterised by the Channel impulse response. To evaluate the impulse response of indoor optical system, it is characterised as a combination of line of sign propagation model and Non line of sign model, which are discussed in section 3.3.1 and 3.3.2.

In this work, the direct received optical powers and delays for all reflection were sum up to produce the channel impulse response. Theoretically, the received power of an optical signal is significantly dropped after second-order reflection, the direct link and first-order reflections are considered in ray-tracing simulation.

3.3.1 Line of sign (LOS) Propagation Model

In LOS links, the received power is given by:

$$P_r = H_d(0) \cdot P_t \tag{3.2}$$

where: The DC gain $H_d(0)$ is only considering the direct LOS propagation path. P_r is the received power and P_t is the transmitter power.

At the receiver, optical intensity is defined as the received power per active area of PD, which is expressed as:

$$I_s(d, \phi) = P_r / A_{PD}$$

A PDcan be characterised by active area A_{PD}. The radiation incident light in the detector FOV can be received. Thus, the effective active area of the PD is related to the incident angle Ψ, which is given by.

$$A_{eff}(\Psi) = \begin{cases} A_{PD} \cos(\Psi), & 0 < \Psi \leq \pi/2 \\ 0 & , \Psi \geq \pi/2 \end{cases} \tag{3.3}$$

A large active area for the PD can obtain more optical power from the source, however, the junction capacitance is directly proportional to the active area leading receiver bandwidth limits and receiver noise increased. A receiver with an optical band-pass filter of transmission Ts(Ψ), which filter unwanted spectrum light transmit into the receivers. Commonly, the use of the non-imaging concentrator is a cost-effective solution, which focuses multiple optical beams to a small point on the receiver area. The optical gain of an ideal non-imaging concentrator is given by:

$$g(\Psi) = \begin{cases} \frac{n^2}{\sin^2 \Psi_c}, & 0 \leq \Psi \leq \Psi_c \\ 0 & , \Psi \geq \Psi_c \end{cases} \tag{3.4}$$

Where Ψ_c denotes the width of the field of vision at a receiver. n is refractive index of the concentrator.

Therefore, the DC gain for a receiver at a distance between a transmitter and the receiver 'd' and angle ϕ with respect to transmitter can be given by:

$$H_d(0) = \begin{cases} I_s(d,\phi) \cdot A \cdot T_s(\psi) \cdot g(\psi) \cdot \cos(\psi) & 0 \leq \&\Psi \leq \Psi_c \\ 0 & \Psi \geq \Psi_c \end{cases} \quad (3.5)$$

According to Eq 3.3- 3.5, the impulse response can be expressed as:

$$h_{los}(t,d) = \frac{2A_r}{\pi\omega_d^2} exp(-\frac{2r^2}{\omega_d^2}) T_s(\psi) g(\psi) \cos(\psi)\ \delta(t - \frac{d}{c}) \quad (3.6)$$

Where the $\delta(0)$ is the Dirac function and the last term in the expression represent the delay to optical signal propagation. W_d is the beam waist of laser at the distance 'd'. Figure 3.2 shows the LOS OWC link.

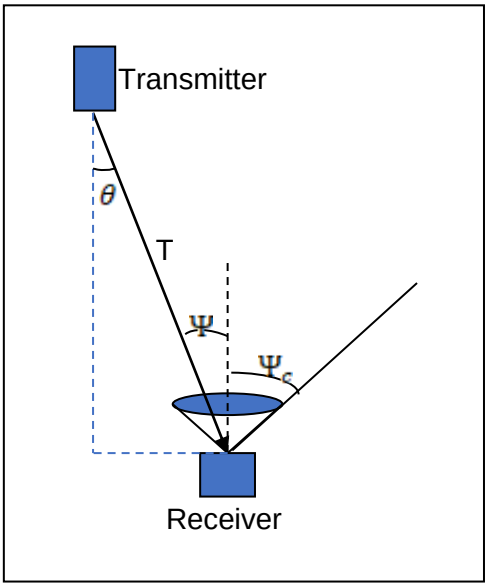

Figure 3. 2 Geometry LOS propagation model

3.3.2 SNR Performance with Inter-symbol Interference

The SNR is one of the critical factors to evaluate the quality of communication, which is defined as the ratio of desired signal power to noise power. In optical wireless communication, the electrical power signal component S is expressed as:

$$S = \gamma^2 p_{rSignal}^2 \quad (3.12)$$

$$p_{rSignal}^2 = \frac{1}{T} \int_{\tau_0}^{\tau_0 + T_{SP}} \sum_{i=1}^{Sources} h_i(t) \otimes X(t)\ dt \quad (3.13)$$

Where the γ represents the responsivity (A/W), $P_{r\ Signal}$ is the received signal power, which is the sum of the powers from each light source. The T_{sp} is the sampling period

which has to greater or equal to two times half symbol time and T is the signal period. T_0 is the time taken when the first signal arrives at the receiver.

OOK modulation scheme is employed as it is the simplest IM/DD modulation. A rectangular pulse shape whose duration equals the bit period. The average transmitted optical power p_t is given by:

$$p_t = \lim_{T\to\infty} \frac{1}{2T} \int_{-T}^{T} X(t)dt \tag{3.14}$$

At the receiver side, the total variance N that is the sum of contributions from shot noise, thermal noise, and inter-symbol interference. In this simulation, the utilize of PIN receiver is considered. The noise expressions are presented as [107]:

$$N = \sigma_{shot}^2 + \sigma_{thermal}^2 + \gamma^2 p_{rISI}^2 \tag{3.15}$$

- Shot Noise

$$\sigma_{shot}^2 = 2q\gamma\left(P_{rSignal} + P_{rISI}\right)B + 2qI_{bg}I_2B \tag{3.16}$$

where q is the electronic charge, B is equivalent noise bandwidth, I_{bg} is background current.

- Thermal Noise

The two terms represent feedback-resistor noise, and FET channel noise, respectively.

$$\sigma_{thermal}^2 = \frac{8\pi T_K}{G}\eta A I_2 B^2 + \frac{16\pi^2 k T_K \Gamma}{g_m}\eta^2 A^2 I_3 B^3 \tag{3.17}$$

where: k: Boltzmann's constant, T_K: Absolute temperature, G: The open-loop voltage gain, η: The fixed capacitance of photo detector per unit area, Γ: The FET channel noise factor and gm: The FET transconductance.

- Inter-symbol Interference

It is defined that the optical path arrival to the receiver within a sampling time after the first optical signal received by the PD are the desired signal power. The impulse response of those multipath in each sampling time can be represent as the sum to the pulse. Therefore, the received power by inter-symbol interference P_{rISI} are expressed respectively as:

$$p_{rISI}^2 = \frac{1}{T}\int_{T_{SP}}^{\infty} \sum_{i=1}^{Sources} h_i(t) \otimes X(t)\ dt \quad (3.18)$$

3.4 Simulation of a fundamental indoor OWC link

3.4.1. System modelling

VCSEL based-OWC system examples considered in this chapter. An indoor open space as shown in Figure 3.3. The room size is 5 m × 5 m × 3 m. The deployment of transmitters is displaced on the celling with the same distance. The purpose of transmitters deployment is designed to provide maximum optical coverage (i.e., the floor) and minimise the overlap area between cells to achieve the high SINR.

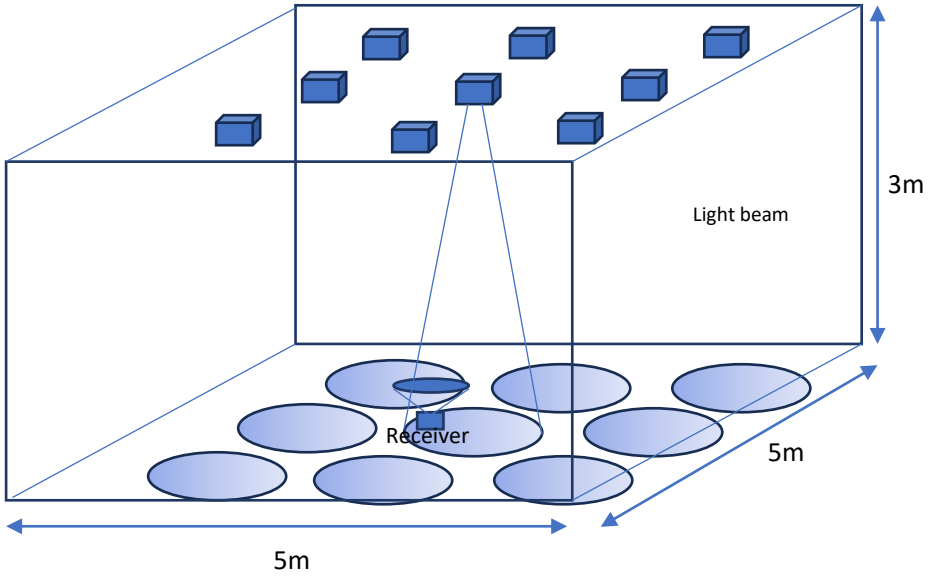

Figure 3.3 The concept of the indoor VCSEL based-OWC system

In multipath mode, the first order reflections were considered, noting that reflections higher than first order have little influence on the received optical power. The walls and receiver surface were divided into small areas to simplify the computation. Therefore, each surface inside the room was divided into small equal areas, dA, with a reflection coefficient of ρ. It is shown in [21] that plaster walls and walls with similar surface roughness reflect light rays close to a Lambertian pattern. Thus, each element in walls inside the room is modelled with a reflection coefficient equal to 0.8 for ceiling and walls. Therefore, elements in each surface were considered as small emitters that reflect the received signal in the shape of a Lambertian pattern with emission order equals to 1. The element's area has an inverse relationship with the temporal resolution of the impulse response results. However, to

simplify the computation process, the area of the element for the first-order reflection was chosen to be 10 cm × 10 cm, and the receiver's area was selected to be 1 cm × 1 cm.

3.4.2 Simulation of VCSEL based-OWC links.

In this numerical examples, the following parameter values is chosen[20]: $T = 295\,K$, $\gamma = 0.54\,A/W$, $G = 10$, $gm = 30\,mS$, $\Gamma = 1.5$ and $\eta = 112\,pF/cm2$ (Table 3.1). And we assume the background current from direct sum light [42].

Table 3. 1 Parameters of the PIN receiver

Parameter	
Output optical power [mW]	20
Open-loop voltage gain	10
Fixed capacitance[pf/cm2]	112
Fet channel noise factor	1.5
Fet transconductance [ms]	30
Absolute temperature [K]	298
Background light current [μA]	5100
Field of view at a receiver [deg.]	60
Detector physical area of a pd $[cm^2]$	1.0
Gain of an optical filter	1.0
Refractive index of a lens at a pd	1.5
O/E conversion efficiency [A/W]	0.53

To simulation SNR performance of OWC system using VCSEL source, Gaussian beam is assumed to present the beam spot of VCSEL and the parameters of VCSEL is referred on a realistic VCSEL source (ULM850-10-TN-N0104U). Each VCSEL is assumed to emit optical signal directly into free space without any camera lens employed. The parameters of VCSEL source are shown in Table 3.2.

Table 3. 2 The parameters of VCSEL (ULM850-10-TN-N0104U)

Parameter	
Output power of each VCSEL [mW]	6
Beam divergence [deg.]	20
Emission wavelength [nm]	850

- **Eye safety estimation**

According to Equations 2.4 - 2.6, the maximum output optical power of each transmitter is to be expressed as:

$$p_{t\,max} = \frac{1}{(1-\exp\,(\frac{-2r^2}{W(Z_{MPH})}))}\pi r^2 MPE \tag{3-27}$$

Where: r is the radius of stop filed = 3.5 mm, and Z_{MPH} = 10 cm.

Assuming the beam directly emits into free space, the maximum permissible exposure can be determined as 19.95 W m^{-2}. Therefore, we can find out that the maximum output power of each VCSEL transmitter is determined as 13.84 mW. The minimum received beam intensity is assumed as 65% of the output beam is assumed in this work.

The distribution of the received power in the room are evaluated based on Equations 3.2 - 3.6 and the results are shown in Figure 3.4. Each VCSEL array chip illuminated a circular atto-cell covering 0.79 m^2 in a 1 m × 1 m area and the cells interface at tangent of circulars. In each cell area, the maximum received power is -26.54 dBm at which the receiver directly under the VCSELs and the minimum received power is -31.05 dBm. The optical power distribution inside the signal coverage area is seen as approximately Gaussian. Therefore, the optical intensity reaches its peak at the beam centre, and its gradually decreasing as moves away from the central point. To ensure robust high-speed wireless connectivity in the entire coverage area of the beam, the power at the edge of the beam must exceed the receiver's sensitivity threshold. In this case, the optical power around the beam centre is much higher than the required power level, in other words, the optical power at the receiver side is not efficiently utilized. Otherwise, the smaller cell coverage is shown since the optical power at the beam's edge smaller than the receiver sensitivity.

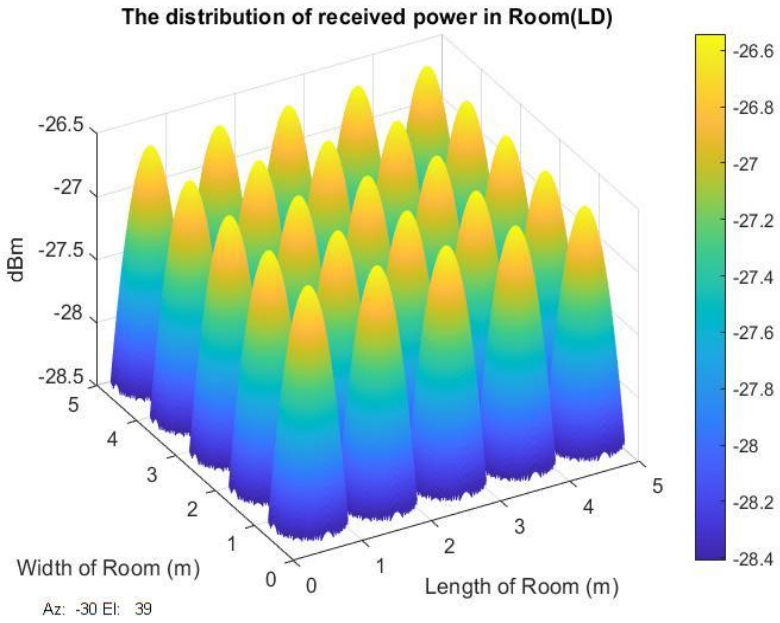

(a)

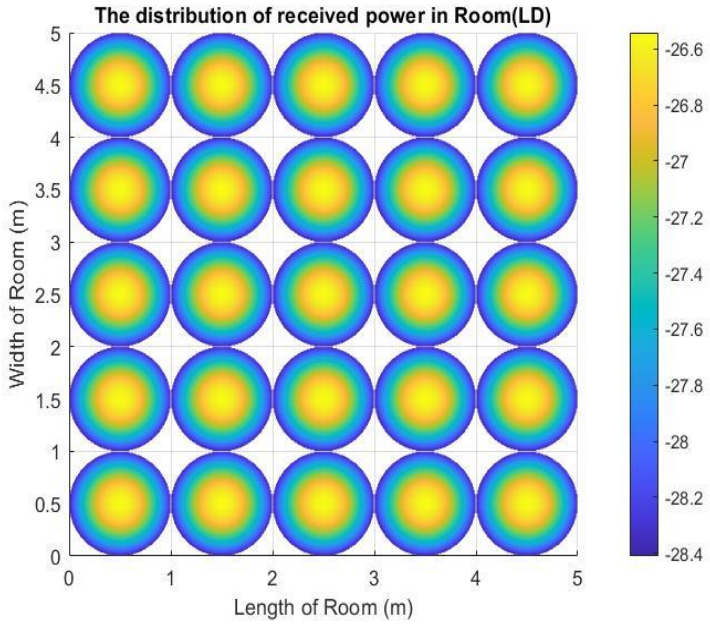

(b)

Figure 3.4 The optical power distrubution of VCSEL based-OWC system:(a)3D map (b) 2D map

Figure 3.5 shows the SNR intensity distribution map of the VCSEL based-OWC system when the 1Gbps data rate of the OOK modulation scheme was employed. The SNR performance was significantly improved since the effect of multiple dispersion was mitigated due to narrow divergence. At the receiver (0.5 m, 0.5 m, 0 m), where is the centre of a VCSEL beam, the highest data rate can be

achieved for each VCSEL is 9 Gbps (i.e. SNR > 13.6 dB) as shown in Figure 3.6. Therefore, the theoretical aggerated capacity of 5 × 5 VCSEL array OWC system is 225Gbps.

Although this VCSEL array based-OWC system has low interference between adjacent cells and a low multipath dispersion effect, the no signal area (i.e., the white area shown in Figure 3.4(b) between the cells causes unstable user connectivity. Beam steering technologies are one of the promising solutions to overcome this issue. They can shift the direction in which light is emitted to increase signal coverage and can be used to provide user mobility [103][104].

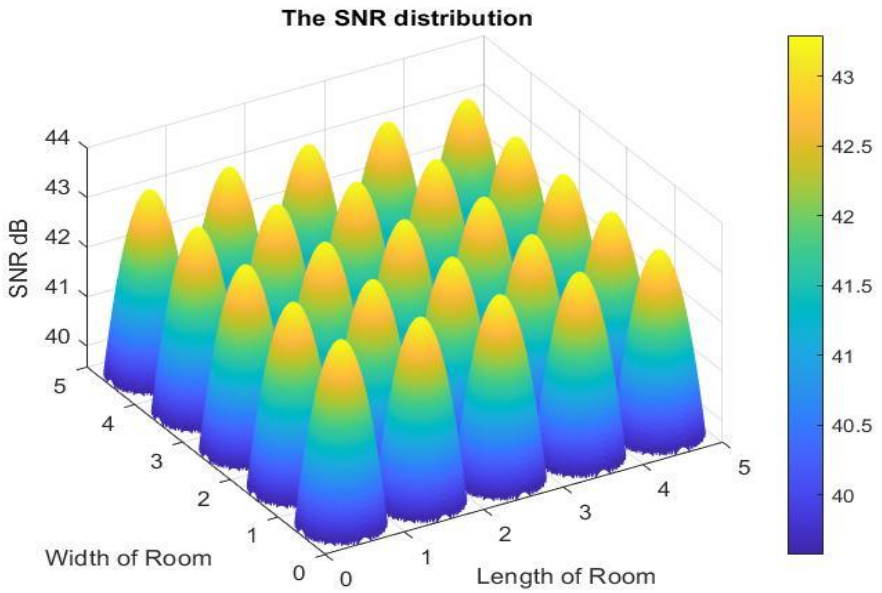

Figure 3.5 The SNR distribution of the VCSEL based-OWC system.

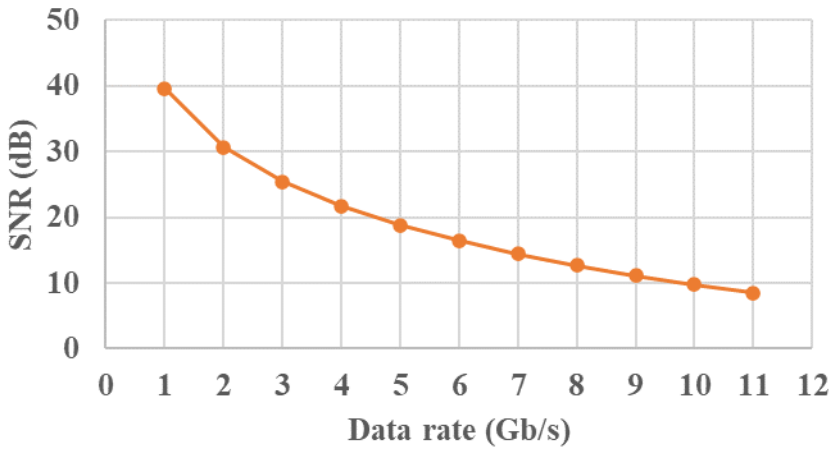

Figure 3.6 The SNR value of each cell with varies data rate.

Figure 3.7 shows the optical irradiance map of a realistic VCSEL array source; the ‘doughnut-shape’ beam profile indicates a no signal area at the centre of each VCSEL beam, causing less optical signal coverage area. While a precision alignment between transmitter and receiver is required. Beam shaping techniques are for more efficient signal distributions in indoor OWC systems [94]. More evenly distributed inside the signal beam coverage area.

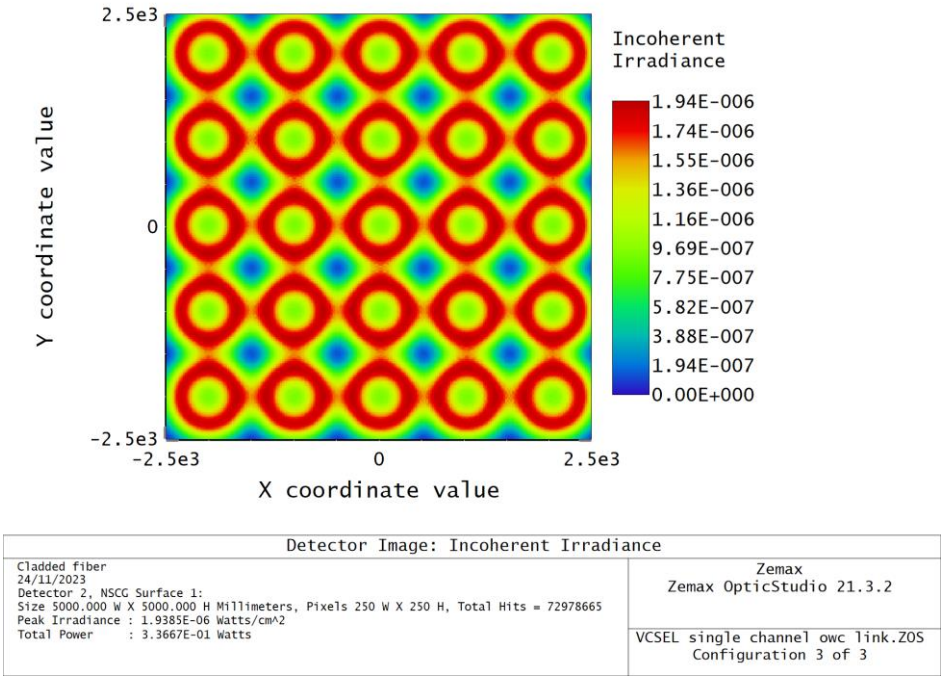

Figure 3.7 The optical irradiance map of the 5×5 realistic VCSEL array based-OWC system.

3.5 Summary

This chapter uses an indoor 5×5 VCSEL based-OWC system to cover a 5 m × 5 m indoor room with minimum optical interference between the atto-cells. To present this concept, the simple OOK modulation scheme was employed to evaluate data transmission.

At transmitter side, the narrow beam divergence VCSELs were employed, and the average emit power of each VCSEL is 1.73 mW. According to laser safety regulations, the maximum output power of a transmitter is valued at 13.84 mW to meet the MPE (19.95 W m^{-2}) at MHP. Each VCSEL transmitter illuminated a circular atto-cell covering 0.79 m^{-2} area in a 1 m × 1 m space, in which the maximum received power is -26.54 dBm and the minimum received power is -31.05 dBm. The Gaussian distribution of the output power beam induced the low optical power area in the

coverage area. Therefore, the next chapter considers beam-shaping techniques for more efficient signal distributions in indoor OWC systems. More uniform power irradiance is distributed inside the signal beam coverage area, and smaller transmission power and robust high-speed OWC links between transmitter and mobile receivers can be used.

The SNR was significantly improved as the no multiple dispersion links affected the receivers. Each VCSEL can achieve 9 Gbps data rate using OOK modulation. However, to meet the high-capacity OWC system with wide coverage and relatively low optical interference, a VCSEL array based-OWC transmitter is designed and presented in the next chapter.

Chapter 4: A novel multiuser VCSEL array based optical wireless transmitter with wide uniform converge

4.1. Introduction

Optical wireless communications (OWC) are a promising solution to this problem as it can provide high-speed data access into the hundreds of Gb/s and can support communication for multiple users. The available spectrum of OWC, which includes the visible (380 - 750 nm) and infrared (IR) spectrum (750 nm-1 mm), offers more than 20,000 times the bandwidth capacity of the RF spectrum, and is license-free. The main two categories of OWC that are currently considered for use include visible light communications (VLC) and IR-based systems[80]. The use of LED-based VLC systems in indoor environments has obvious advantages, as such systems can simultaneously provide illumination and data transmission. Thanks to the development of Class I safety laser source, a lot of laser-based VLC system has been demonstrated However, the achievable data rates are limited by the relatively low bandwidth of LEDs (up to a few hundred MHz for small LED pixels [81]), while VLC systems can suffer from light dimming, glaring issues and connectivity availability when no illumination is required in the room. As a result, laser sources emitting near-infrared (NIR) wavelengths are considered for use in indoor environments as they can overcome these issues.

In this chapter, a multiuser VCSEL array based OWC system is proposed, comprising multiple VCSEL array transmitters that directs beams in specific directions covering a 1 m^2 area, each of which is equipped with a 5 × 5 square VCSEL array. To solves the issue of signal power variation at the moving receiver end in atto-cellular area, microlens arrays (MLA) are employed to obtain square shape beam profile of atto-cells with uniform optical intensity, which guarantees stable communication link. The VCSEL array based-OWC multibeam transmitter using

MLA is designed and verified using ZEMAX software. The realistic multimode VCSEL source based on the ULM850-10-TN-N0104U product is simulated. Meanwhile, the maximum emitted optical power satisfies the Maximum Permissible Exposure (MPE) at the most hazardous position which ensures the transmitter meeting class-1 eye safety standards is estimated.

The remainder of the chapter is organised as follows. Section 4.2 illustrates the aim of the VCSEL array OWC transmitter, and Section 4.3 describes the schematic of the transmit optical system and working principle of the microlens array-based homogeniser. Section 4.3 provides the ray tracing model of VCSEL array based-OWC transmitter by ZEMAX software, and Section 4.4 provides the conclusions.

4.2 The VCSEL array-based OWC transmitter design

An access point using an array of VCSEL array to provide wide coverage and aggregated data rate of Tbps has been proposed, as illustrated in Figure 4.1(a) [83]. The system relies on the use of multiple transmitters, each one oriented in a different direction to cover the entire space. Each transmitter includes a square 5 × 5 VCSEL array to cover a 1 m × 1 m area, with each VCSEL illuminating a 20 cm × 20 cm area, as shown in Figure 4.1(b). Assuming no multiplexing techniques are employed, each VCSEL in the array can serve one user within its illumination area. As a result, the proposed VCSEL-based transmitter can serve 25 users in a 1 m × 1 m area.

A square microlens array (MLA) pair, working as a homogeniser, is employed to reshape the narrow divergence doughnut–shaped VCSEL beam profile into a flat-top square spot, illuminating a uniform signal-noise-ratio (SNR) distribution area in the cellular. The homogeniser is one of the beam-shaping technologies used to modify the incident light beam into a nearly uniform optical intensity beam [84]. The shape of the output beam depends on the shape of the microlens. Therefore, different microlens arrays, such as square, cylindrical, or hexagonal, can be used to generate different shapes of cellular area. However, the VCSEL array transmitter generates a grid cellular network in this work. Thus, the square shape is relatively simple to compose the cellular network without overlap among adjacent cells. Meanwhile, The MLA expands the beam width and transforms the VCSEL source from a point source into an extended source, resulting in a significant relaxation of the MPE level. [85]

All in all, this transmitter has advantages of (i) each VCSEL generates a uniform power intensity atto-cellular and therefore can offer reliable high data rate communication to the user(s) present in this particular illumination, (ii) interference between atto-cells is kept as low as possible to increase the achievable signal to noise and (iii) individual beams practically do not overlap in space relaxing the eye-safe concerns related to the use of VCSEL arrays, if MLA homogeniser employing.

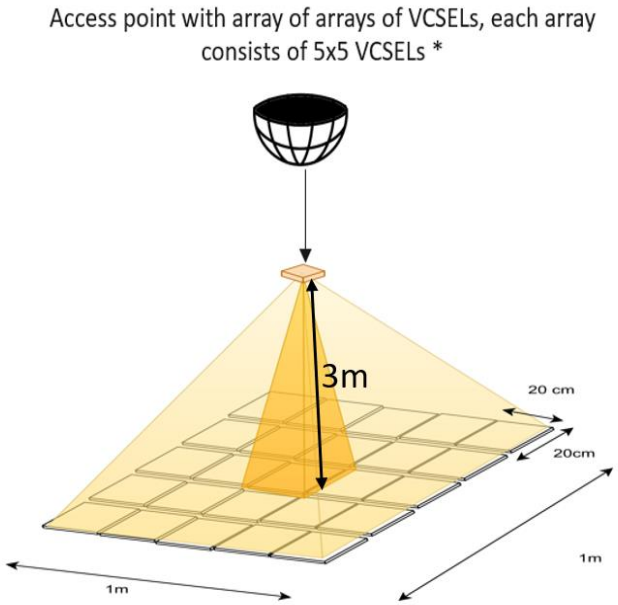

(a)

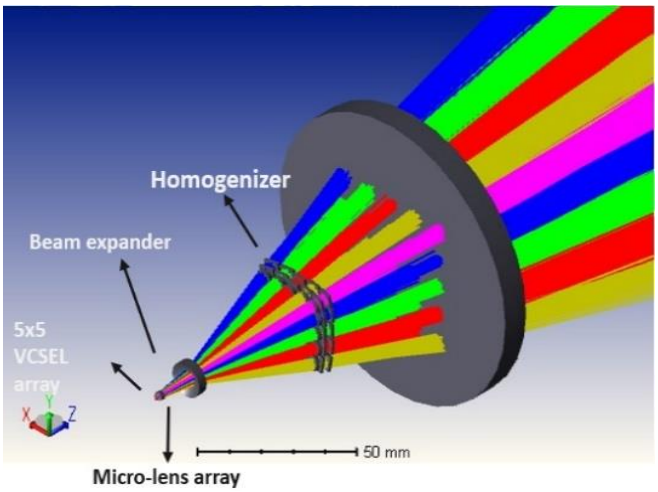

(b)

Figure 4. 1(a) The concept of Arrays of Arrays of VCSELs system, (b) the schematics of each VCSEL array transmitter

The main components of the OWC transmitter annotated are shown in Figure 4.2.(a) and the parameters of lenses area summarised in Table 4.1. The total length of the designed transmitter optical system is 11 cm. The structure of the transmit optical system is composed by four parts: a) Collimation lens array (MLA1), b) beams splitter (PCV1 & PCV2), c) homogeniser system (PCX1, MLA2 and MLA3) and d) large scale plano-convex lens (PCX2). Each part is described as follow:

a) The beam emitted from each VCSEL on the VCSEL array is first collimated using a microlens array (MLA1) with the same pitch as the VCSEL array.
b) A pair of Plano-concave lenses (PCV1 & PCV2) is placed 1 mm behind the MLA1. They are used to generate the required separation between the output beams and allow the insertion of a beam homogeniser system (i.e., PCX1, MLA2 and MLA3) on each beam path. The angle of beam in space is illustrated in Figure 4.3 which shows the angle of respective homogeniser need to tilt. The centre of PCV1 and PCV2 is along with the Z-axis, and the space between them is 14 mm.
c) Each VCSEL beam is recollimated by a plano-convex lens (PCX1) at 24 mm behind PCV2; the parallel incident beam through the MLA pair (i.e., MLA2 & MLA3) ensures the highest efficiency of beam intensity uniformity and is shaped into a flat-top profile by the respective beam homogeniser. According to the angle of beam in space as shown in Figure 4.3, the homogenisers at the second layer are tilted ± 6^{o} based on its local X/Y axis and the outside layers homogenisers are tilted ± 12^{o} based on its local X/Y axis. The specific tilt angle of each homogeniser is shown in Figure 4.4. The space between the homogeniser is 1 mm.

   The size of the uniform beam on image plane is dependent on microlens' pitch, its focal length, and working distance. The working principle of MLA homogeniser is explained in next section.

d) The last plano-convex lens (PCX2) converges to form the desired seamless 25 squares illuminating on the image plane.

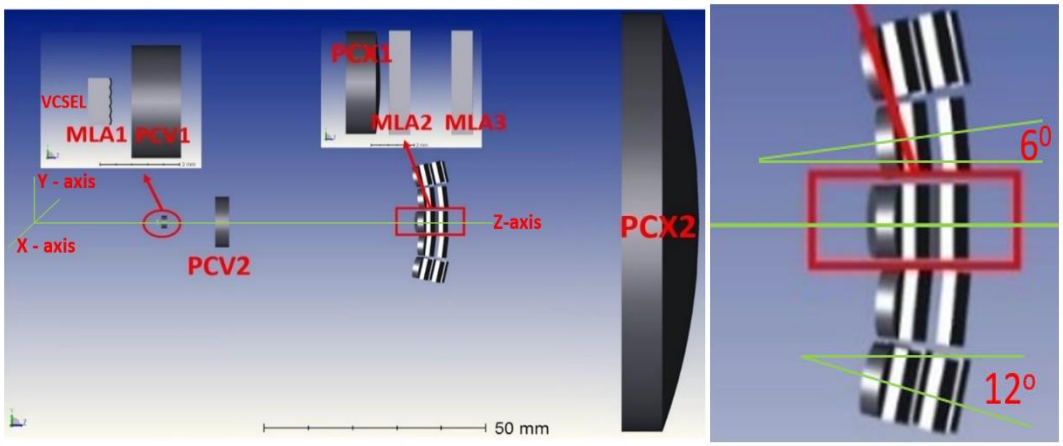

(a) (b)

Figure 4.2 (a) The downlink transmitter optical system design and (b) Detail of homogeniser part

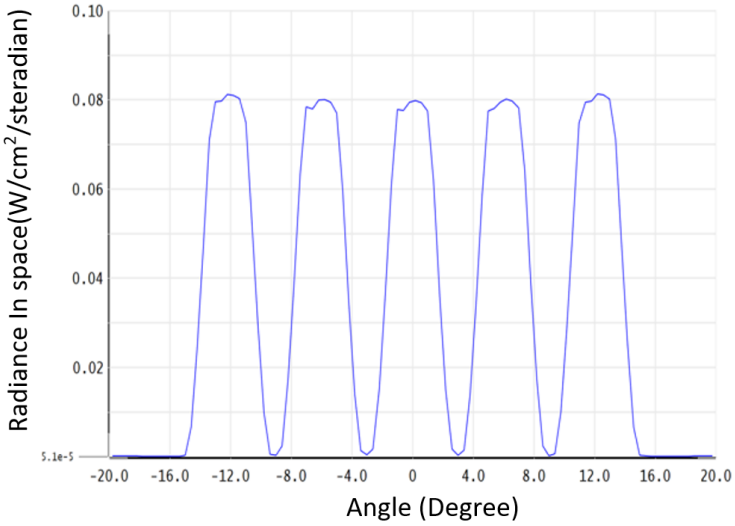

Figure 4.3 The radian in angle space cross-section map

X =12⁰ Y =-12⁰	X = 12⁰ Y = -6⁰	X = 12⁰ Y = 0⁰	X=12⁰ Y=6⁰	X=12⁰ Y=12⁰
X = 6⁰ Y = -12⁰	X = 6⁰ Y = -6⁰	X = 6⁰ Y = 0⁰	X=6⁰ Y=6⁰	X=6⁰ Y=12⁰
X = 0⁰ Y = -12⁰	X = 0⁰ Y = -6⁰	X = 0⁰ Y = 0⁰	X=0⁰ Y=6⁰	X=0⁰ Y=12⁰
X = -6⁰ Y = -12⁰	X = -6⁰ Y = -6⁰	X = -6⁰ Y = 0⁰	X=-6⁰ Y=6⁰	X=-6⁰ Y=12⁰
X = -12⁰ Y = -12⁰	X = -12⁰ Y = -6⁰	X = -12⁰ Y = 0⁰	X=-12⁰ Y=6⁰	X=-12⁰ Y=12⁰

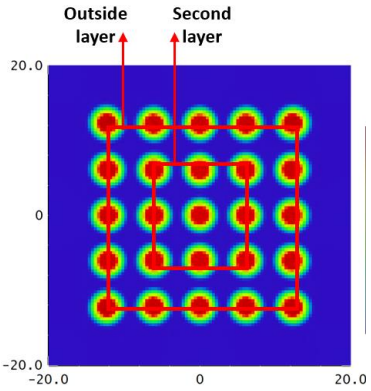

(a) (b)

Figure 4.4 (a) The angle of tilt about each homogeniser and (b)the 2D map of the beams in angle (Unit: Degree)

4.2.1 MLA homogenisation technologies for OWC transmitter

Mircolens array (MLA) using for homogenisation of the laser beam is a considerably simple solution. The working principle of the homogeniser is that microlens array divides an incident beam into multiple beamlets and recombine them in the far field generating a near uniform beam. Microlens array-based homogeniser is used for applied in high-precision laser cutting and uniform light illumination. In this work, the MLA homogeniser is investigated in optical wireless communication application.

Diffractive Optical Elements (DOE) and fly-eye type MLA are the two different structures of advanced optical MLA. The DOE optics consists of a number of irregulars microlens units, and its lens structure is shown in Figure 4.5 (a). The DOE transfers the incident light into a controllable divergence and near uniform beam. In work [87], a large DOE lens has been proposed to build up a multibeam VCSEL array based-OWC transmitter. A DOE lens that directly interfaces with the VCSEL array orientated each VCSEL output beam in a different direction. However, the undesired ‘doughnut-shape’ beam profile was shown in atto-cells in resulting a discrete optical power distribution. The fabrication of DOE lens is complexity and expensive that is another limitation for applying DOE lens in multibeam OWC transmitter.

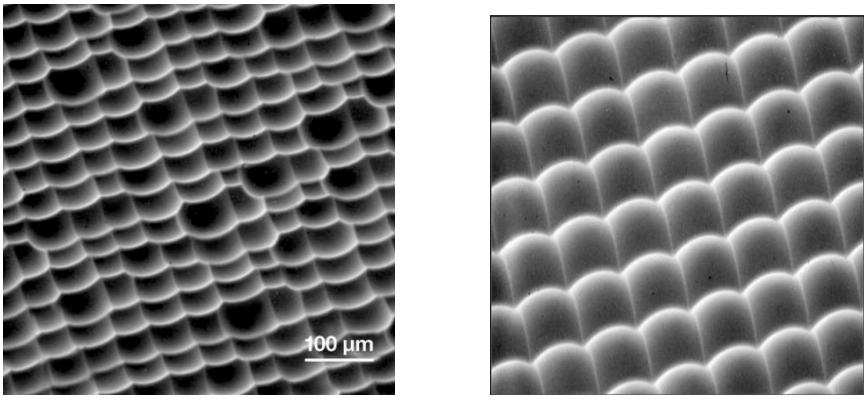

Figure 4.5 SEM Picture of (a) Engineered Diffuser and (b) MLA[86]

Compared with the DOE, fly-eye type MLA is composed of regular mircolens units (Figure 4.5 b) which has relatively low-cost and easy fabrication. The structure of the fly-eye MLA homogeniser is shown in Figure 4.6. It consists of a pair of

microlens arrays (MLA2 & MLA3) and a Fourier lens (FL). The incident beam is divided into multiple beamlets by MLA2, while MLA3 acts as an objective lens array, superimposing the image of each sub-beamlet in the MLA2 [88]. These two MLAs have the same size, material, and radius of curvature for lens alignment convenience. The diameter of the flat-top beam profile generated by the optical system can be expressed by:

$$D_{FT} = P_{LA}\frac{f_{FL}\cdot(f_{LA2}+f_{LA3}-a_{23})}{f_{LA2}\cdot f_{LA3}} \tag{4.1}$$

Where: P_{LA} is the pitch of the MLA2 and MLA3, f_{LA2} and f_{LA3} are the focal lengths of the MLA2 and MLA3 respectively, a_{23} is the spacing between the MLA2 and MLA3. F_{FL} is the focal length of the Fourier lens. The separation between two microlens arrays is chosen to equal the focal length of MLA2 in order to fulfil the imaging conditions [89]. As a result, Eq. (4.1) can be simplified as:

$$D_{FT} = P_{LA}\frac{f_{FL}}{f_{LA}} \tag{4.2}$$

Eq. (4.2) indicates that the homogenised beam profile's diameter depends on the microlens array's pitch and the microlens array's focal length. We assume that the working distance has been determined by the geometry of our OWC system (i.e., The distance of the last plano-convex lens to the imaging plane). [90]

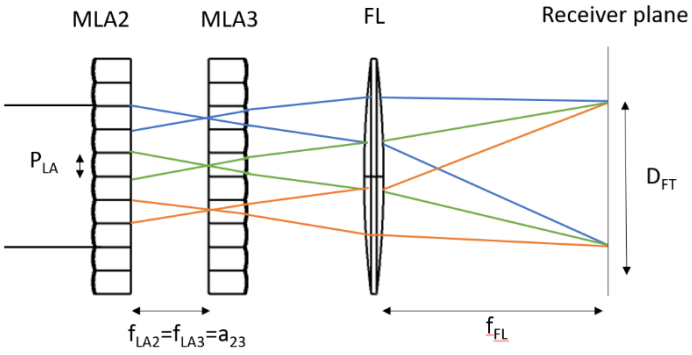

Figure 4.6 Structure of the beam homogeniser using a pair of microlens arrays.

In practice, the second microlens array cannot ideally deploy at the focus point of the first microlens array due to manufacturing error causing an image project at the plane of the second microlens array. To avoid the loss of light and overfilling of the

lens aperture, the diameter of each beamlet at the second microlens array must be smaller than the lens pitch P_{LA} [88].

Although high resolution pixel number of a microlens array can achieve higher uniformity of the output beam, the number of pixels is limited by the manufacturing technologies. A demonstration of the beam uniformity after the homogenizer versus a different number of lenses microlens arrays is shown in Figure 4.7. In simulation, a simple MLA homogeniser based on the structure has been established in ZEMAX. A single multi-mode 850nm VCSEL is set as light source, and the size of MLA keeps as a 5 mm × 5 mm square. The focal length of MLA remains constant as 4.8 mm. The uniformity is defined as the ratio of the lowest to the largest intensity across the flat-top area of the illumination spot. It can be expressed as:

$$\eta_1 = \left(\frac{P_{Min}}{P_{Max}}\right) \times 100\% \tag{4.3}$$

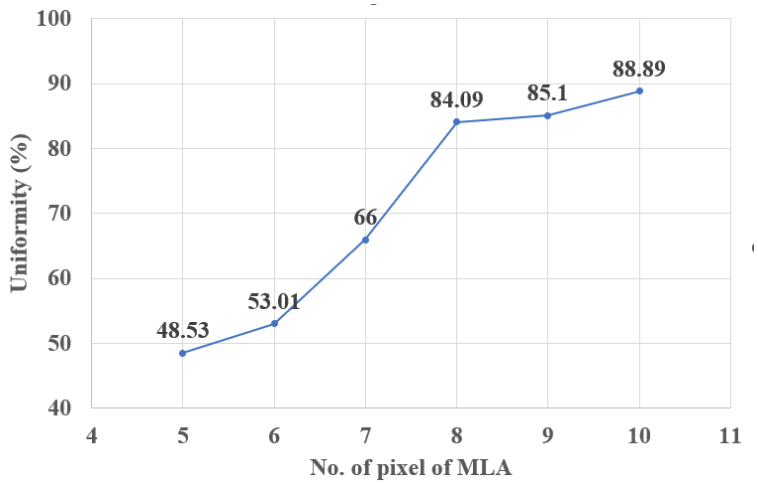

Figure 4.7 The optical irradiance distribution verse different number of pixels in an MLA

The uniformity of the beam is linearly increased with the number of pixels until a sufficient uniformity (>80%) is achieved when the number of lenses increases to 8 × 8. The larger numbers of lenses can slightly improve the uniformity and size of beam spots. Therefore, the minimum resolution of MLA to achieve a high uniformity is valued as 8 × 8 when the size and focal length of MLA is determined. Figure 4.8 shows the optical irradiance map of different number of lenses microlens arrays.

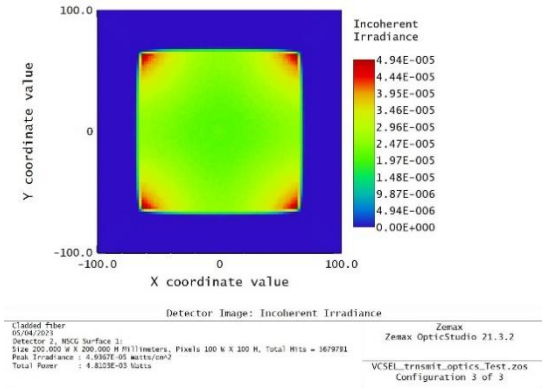

(a)5×5 pixels MLA, Uniformity 48.53%

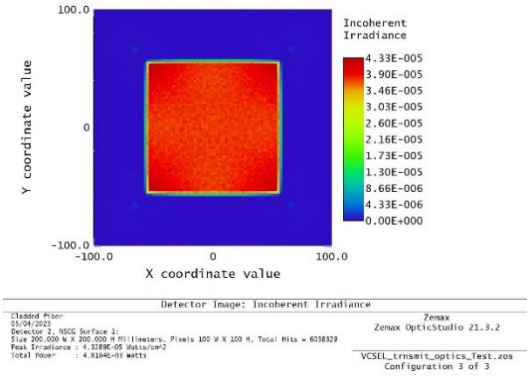

(b)6×6 pixels MLA, Uniformity 50.00%

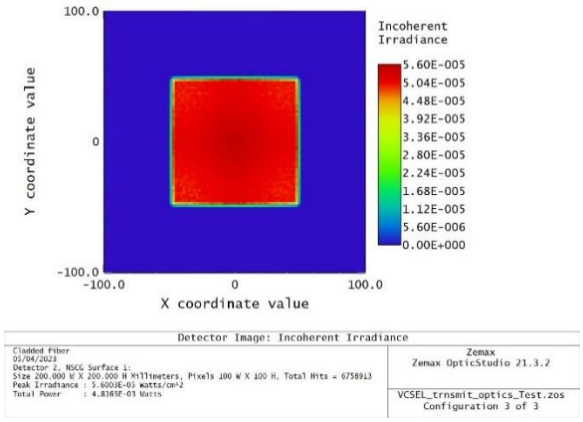

(c)7×7 pixels MLA, Uniformity 66.00%

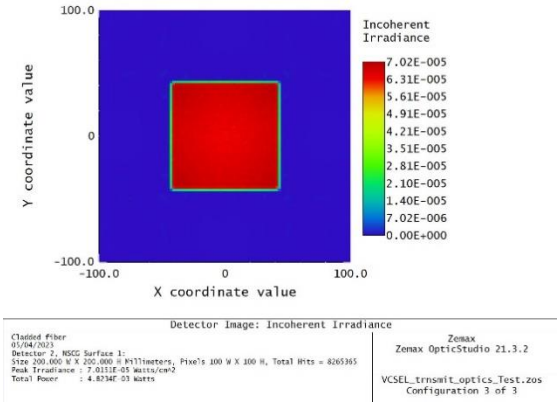

(d)8×8 pixels MLA, Uniformity 84.09%

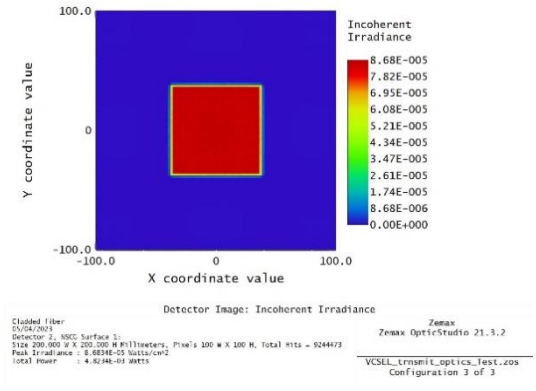

(e)9×9 pixels MLA, Uniformity 85.10%

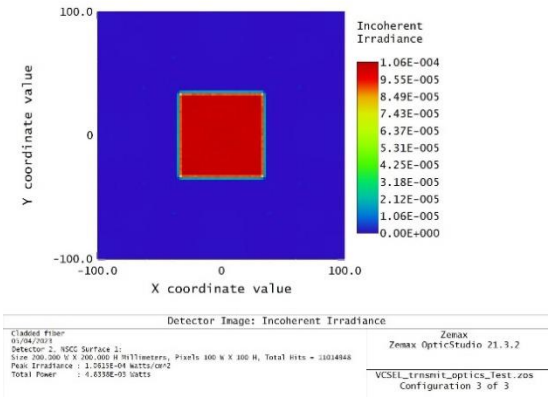

(f)10×10 pixels MLA, Uniformity 88.89%

Figure 4. 8 The optical irradiance distribution verse different number of lenses MLA

4.3. Ray tracing simulations

4.3.1 Simulation of VCSEL array OWC transmitter

The design of the optical transmitter system was verified with the ZEMAX ray tracing software. In the ZEMAX, a 1 m × 1 m rectangle detector surface is set at 3 m

with a 500 × 500 pixels receiver unit and the ray number of each VCSEL is set as 5E06. Increasing the number of rays can enhance the image's detail, but it takes plenty of time to progress the simulation.

A 5 × 5 VCSEL array is simulated using the realistic parameters of the ULM 850nm VCSEL product, such as VCSEL element pitch, beam wavelength and beam profile. A doughnut-shaped output beam profile was assumed for each VCSEL, while the VCSEL pitch of VCSEL was set to 250 μm to match the standard pitch of conventional VCSEL arrays. The output power of each VCSEL is 6 mW, which is the maximum output power of the VCSEL (ULM850-10-TN-N0104U) product.

In the simulation, the beam spot shape transformation at each stage of the transmitter is illustrated in Figure 4.9. In the figures, the red area indicates high intensity, and the green area indicates low intensity. The VCSEL laser provides a doughnut-shaped beam profile (Figure 4.9a). However, a nearly Gaussian beam profile is generated after the beam expander because it is set at the focal point of the microlens array (Figure 4.9b). The beam spot is transformed into square beams with uniform power intensity after the homogeniser (Figure 4.9c). Finally, a 1 m × 1 m square coverage area is shown at the receiver plane at 3 m consisting of 25 square beams. The measurement position of which stages is indicated in Figure 4.9.

Table 4. 1 the parameters of lens components (ROC: radius of curvature).

Components	ROC (mm)	Diameter (mm)
1. Microlens array 1	0.22	0.25
2. Plano-Concave lens 1	5	3
3. Plano-Concave lens 2	10	9
4. Plano-Convex lens 1	15.5	4.9
5. Microlens arrays 2&3	3.5	0.50
6. Plano-Convex lens 1	75	150

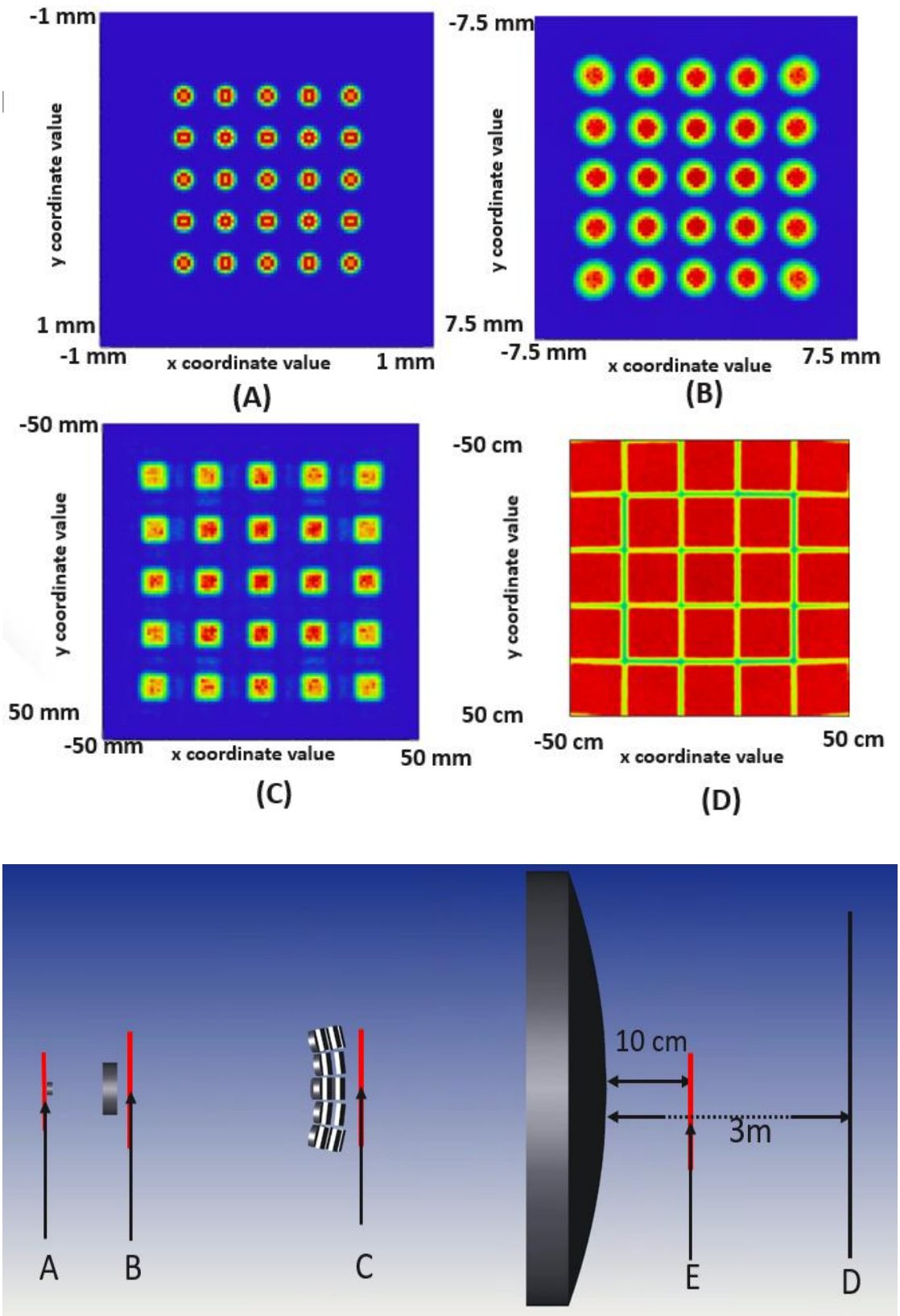

Figure 4.9 The 25 VCSEL beam spots after each stage of the transmitter (*A*) microlens array (*B*) beam expander (*C*) homogeniser (*D*) receiver plane.

The power intensity distribution of the proposed OWC transmitter is simulated, and it can be clearly seen that the output of each row (or column) of the 5×5 VCSEL array is transformed into five well-separated flat-top illumination spots on the image plane for the optics systems. The width of each spot is around 20 cm. In this work, the working distance of the transmitter (i.e., 3 meters) is much longer than the facial length of the Fourier lens. As a result, the lens slightly refocuses at the far field, showing a nearly square wave of the flat-top beam profile at the received plane. The heatmap of the full 2D illumination area at the image plane is shown in Figure. 4.10 (a), and the cross-section of the column is shown in Figure 4.10 (b). It can be noticed that sufficient uniformity is achieved with the value of 88.89%. The power intensity coverage for the system in the 1 m^2 is ~97%, which indicates that the proposed system design significantly reduces the probability of getting no signal while ensuring a uniform signal across the floor. The gap between the cell is around 1 cm from the full width at half maximum (FWHM) to the adjacent beam's FWHM to provide near-ubiquitous coverage with minimal interference. The average irradiance of each cell raised to 82 mW m^{-2}.

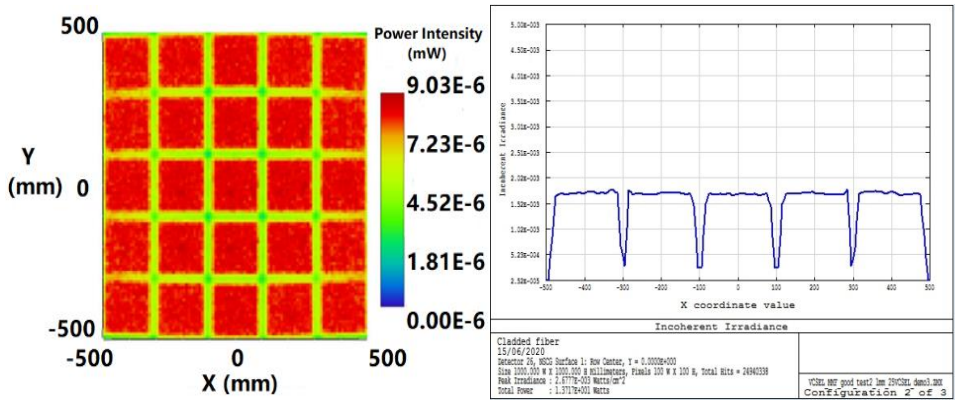

(a) (b)

Figure 4.10 The power intensity distribution of the OWC transmitter (a) full map (b) cross-section of column

4.3.2 Eye-safe estimation for the VCSEL array based OWC transmitter

In laser safety estimation, a 7 mm diameter stop field sets at MHP to represent the eye corn and measure the optical power of the laser beam passing through the hole [84]. An eye safety OWC transmitter can be determined when the optical intensity at the MHP is lower than MPE. The long-term exposure durations (t_{ex} > 10s) and 850 nm

VCSEL's working wavelength with 6 mW output power are assumed in this work. To specific value of the MPE, the angle substance needs to be determined.

In Zemax, the stop field was set at the 10 cm after the last optical lens as shown in the Figure 4.11 where is the MHP in resulting the angular substance of the each VCSEL beam is regarded as a point source and the MPE of the transmitter is calculated to be 19.95W m^{-2}. The beam spot detected at the MPH position is shown in Figure 4.12. As results, the received optical irradiance at the MHP is 12.57 W m^{-2} which is significantly lower than the MPE. Consequently, the VCSEAL array transmitter meets to the eye-safe requirement.

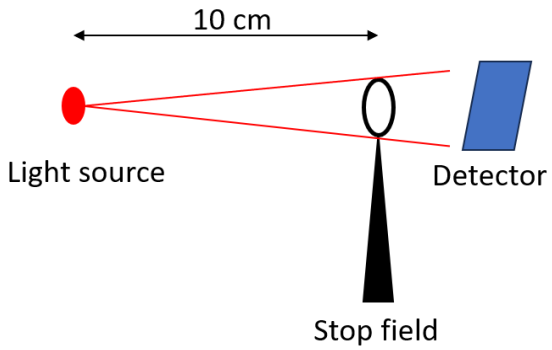

Figure 4.11 The structure of eye safety evaluation set up

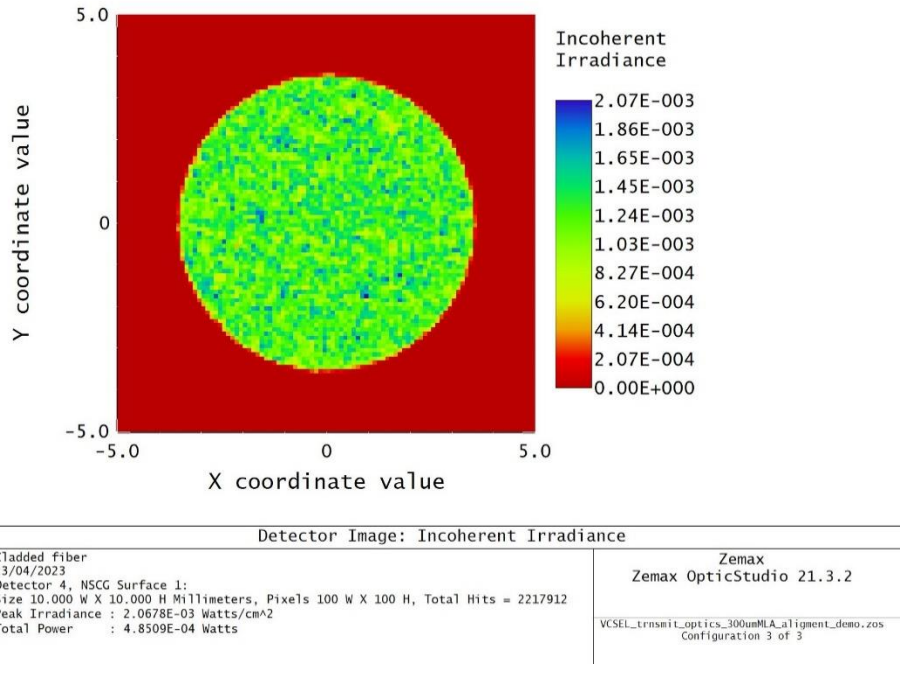

Figure 4.12 The optical power distribution of the VCSEL array OWC transmitter at MHP

4.4. Summary

In this chapter, an array of VCSEL array transmitter is proposed to provide wide uniform coverage from one access point. Each VCSEL array transmitter orients into a specific direction to cover a 1 m × 1 m area, while each individual VCSEL illuminating a 20 cm × 20 cm area.

A OWC transmitter employing microlens homogeniser has been presented to achieve the proposed OWC transmitter, which provides a 1 m^2 area coverage by 25 individual atto-cells. Each cell can service for a user terminal assuming no multiple division technology employed. The gap between the adjacent cell is kept as low as possible to improve the SINR performance. The transmit optics is consisted of collimation microlens array, beam expander, homogeniser, and Fourier lens.

Microlens array homogeniser is first time employed in indoor laser based-OWC transmitter to provide uniform SNR distribution in the illumination area. In this work, the "doughnut-shape" Multimode VCSEL beams was transferred into squares. In the homogeniser system, the beam size of the beam at the receiver surface is dependent on the lens pitch, working distance and lens's focal length. The uniformity relies on the number of pixels in the microlens array. In practice, 8 layers usually can provide a satisfied uniformity (>80%), and the high resolution microlens array slightly enhance the quality of the image.

A simulation of the lens products system is verified in ZEMAX. In this simulation, the result is shown that each VCSEL generates >80% beam uniformity across a square atto-cell of 20 cm × 20 cm with low interference to adjacent cells. The gap between the adjacent cells is 3 cm at FWHM, however it can be eliminated when optimised lens products employs. Meanwhile, the simulation result proof that the proposed OWC transmitter meet the eye-safety requirement.

Chapter 5: Demonstration of VCSEL array based-OWC system using commercial components

5.1 Introduction

A VCSEL array-based transmitter in an optical wireless communication system can provide multi-channel wider coverage as explained in Chapter 4. In addition to wider coverage, high speed data transmission capability of VCSELs can help to achieve Tb s^{-1} aggregated data rates using such transmitters. Previously, a theoretical Tb s^{-1} multiuser VCSEL-based-OWC system has already been described in [91]. The system used nine 5 × 5 VCSEL array chips and each chip orients into specific direction to cover a 5 m × 5 m area. However, the performance of the OWC transmitter using simple lens mounts on the VCSEL array results in uneven optical power distribution on the receiver surface with no signal areas in each atto-cell. For instance, Figure 5.1 shows the beam of a 5 × 5 multi-mode VCSEL array transmitter interfacing with a 3 mm diameter plano-convex lens. The discrete illumination of these 25 ‘doughnut-shape’ VCSEL spots causes the null coverage area between the atto-cell, while the small atto-cell size requires high precision alignment between the optical transmitter and an optical receiver. To provide stable user’s connectivity and to minimize the interference between atto-cells, the proposed VCSEL array based-OWC transmitter provides uniform beam. Each atto-cell of 5 x 5 VCSEL array provides 20 cm x 20 cm coverage with a total covered area of 1 m^2.

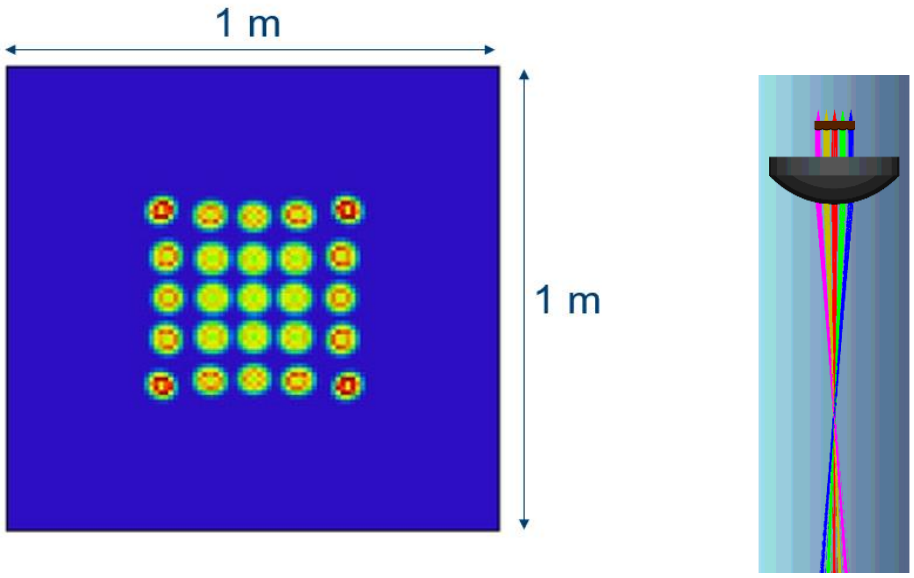

Figure 5. 1 (a)The spots of a 5 × 5 VCSEL array with simple lens and (b) its simulation model

At the receiver side, the P-i-N (PIN) receiver and avalanche photodiode (APD) receiver are the most common optical receivers in OWC. Unfortunately, PIN receivers have no internal gain layer, and APD receivers generate excess shot noise, which limits their SNR performance. In the VCSEL-based-OWC system, the lower output power level of the laser source ensures eye safety; moreover, path loss in free space propagation at the usual working distance of ~3 m results in very low received power levels. As mentioned in Chapter 2, SiPM is an array of SPADs with high sensitivity and no excess shot noise. Therefore, SiPM receiver has been considered as a suitable optical receiver to achieve high-speed OWC system when received optical power is very low. For example, a 3.45 Gbps data rate VLC link is achieved using a SiPM receiver and simple OOK modulation scheme [92].

Although the SiPM has high sensitivity, its potential to achieve high-speed data transmission is limited by saturation and inter-symbol interference (ISI) caused by finite output pulse width. The SPAD unit experiences a quenching process when absorbing photons, while it blinds to new incident photons until saturation. This short period of recovery time, 'dead time', can cause nonlinear effects, which are limitations of maximum power detection due to the saturation and low modulation bandwidth due to inter-symbol interference induced.

Equalisation techniques are a promising solution to improve the data rate. The decision feedback equaliser is one of the most common equalisation technologies, which will be described in Section 5.3.

In this chapter, a single channel of the proposed transmitter is demonstrated using commercial off-the-shelf optical components. Although ideal components with the parameters used in the simulations are not available, off-the-shelf components are selected with similar lens parameters to provide 79.43% uniformity at the receiver plane.

Due to the transmitter system's centre axis being symmetrical, only the centre channel is experimentally demonstrated initially, showing the proof of concept. The central channel provides a 21 cm × 21 cm uniform IR image at the receiver plane. The eye safety of the transmitter is verified as the measured irradiance value at MHP (i.e., 10 cm behind the transmitter) is less than the maximum permissible exposure (MPE) class 1 eye-safe limit of 19.95 W m^{-2} at 850 nm. To demonstrate the data transmission, a single VCSEL OW link using the commercial SiPM receiver has been established. An 8 Gbps data transmission OW link over 3 meters is achieved by employing an OOK modulation scheme and decision feedback equaliser (DFE) at the receiver side. The VCSEL array based OWC transmitter can achieve a total data capacity of 200 Gbps.

The remainder of the chapter is organised as follows. Section 5.2 describes the simulation of the transmitter employing off-the-shelf lens production and presents the obtained results. Section 5.3 provides the link implementation and the experimental results for the 8 Gbps OW transmission, and the conclusion is presented in Section 5.4

5.2 Ray tracing of simulation

5.2.1 The “off-the-shelf” transit optics

Although the ideal optical components shown in Chapter 4 could be custom-made, the available off-the-shelf components which closely match with the designed transmitter optics are selected for ensuring low-cost system design. The parameters of commercial lens components and the ideal optical components are summarised in Table 5.1. Most off-the-shelf lenses (i.e., MLA, PCV1, PCV2, PCX1 and PCX2) properties closely match to the ideal system. However, the homogenizer components i.e. MLA2 and MLA 3 deviates from the original design with different ROC and diameter. Therefore, homogenizer is redesigned using Zemax with ROC and diameter of 2.2 mm and 0.3 mm respectively. The space between the MLA2 and MLA3 is

adjusted to 4.4 mm based on Eq. 4.1 to achieve the 20 cm × 20 cm IR image at receiver plane.

The system using off-the-shelf optical lens products is simulated in ZEMAX and compared to the results based on the ideal lens components. The output power of VCSEL is set as 6 mW which is the maximum optical output power of the VCSEL (ULM850-10-TN-N0104U).

Table 5. 1 the parameters of the custom components and the off the shelf components (Unit: mm)

Components	Custom components		Off the shelf components		
	ROC	Diameter	ROC	Diameter	Product
MLA1	0.22	0.25	0.25	0.25	SUSS 18-00696
PCV1	5	3	4.71	3	Edmund #67-979
PCV2	10	9	9.42	9	Edmund #67-988
PCX1	15.5	4.9	15.5	5	Edmund #87-920
MLA2&3	3.5	0.50	2.2	0.3	SUSS 18-00157
PCX2	75	100	73.2	100	Edmund #27-502

It can be seen that the output of the VCSEL beams is transformed into well-separated flat-top illumination spots on the image plane for both optics systems, as shown in Figure 5.2. The width of each spot is around 20 cm. However, the 300 μm pitch MLA homogeniser was applied in the "off-the-shelf" lens case, which caused the smaller coverage area of each VCSEL beam. As a result, the unwanted non-signal area between adjacent cellular happens. The average irradiance of each cell was raised to 110 mW m^{-2} in an off-the-shelf case.

The shape of the full 2D illumination area at the image plane is shown in Figure. 5.3a & Figure. 5.3b for both systems. Nevertheless, satisfied uniformity is achieved in both cases, with values of 88.89% and 79.43% recorded for the system with ideal and off-the-shelf components, respectively. The power intensity coverage in the 1 m^2 area for both cases is ~97%, which indicates that the proposed system design significantly reduces the probability of getting no signal while ensuring a uniform optical power across the floor. In the off-the-shelf scenario, the gap between the beams is 3 cm from the full width at half maximum (FWHM) to the adjacent

beam's FWHM to provide near-ubiquitous coverage with minimal interference. The gap between the cells (highlighted as blue in Figure 5.3 b) is regarded as no-signal areas due to the optical signal power being lower than the half maximum. However, the gap between the cells can be minimised when the 500 µm pitch MLAs employed.

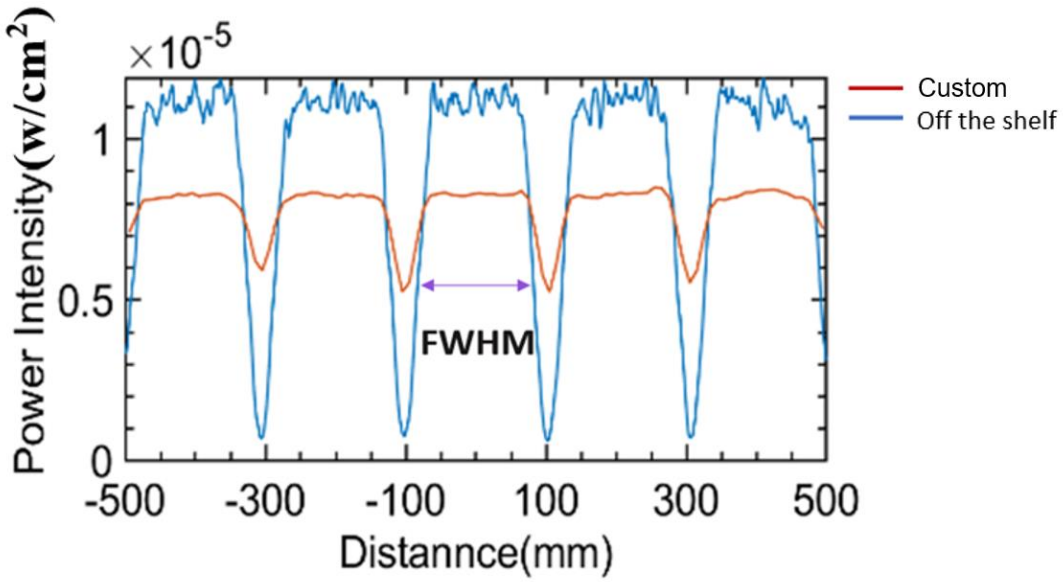

Figure 5.2 The cross-section intensity distribution of both systems

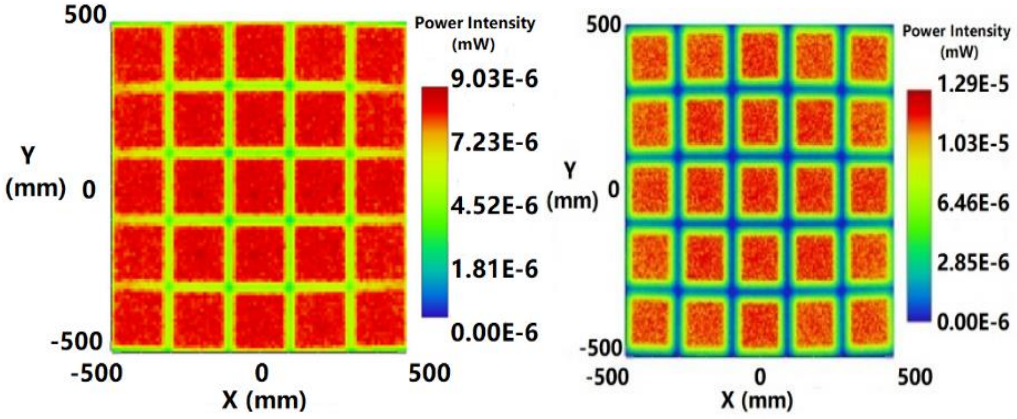

(a) (b)

Figure 5.3 The power intensity distribution full map of (a) the optimised, (b) the off-the-shelf components

5.3 Experimental demonstration

5.3.1 Setup of the VCSEL based-OWC transmitter.

At the transmitter side, a 1×4 linear VCSEL array (ULM850-10-TN-N0104U) with 250 µm pitch is integrated into a custom designed PCB to generate an optical intensity signal. The average output power of each individual VCSEL is 1.7 mW. Figure 5.4 illustrates the transmit optics employed for the demonstration. To experimentally test the transmitter designed in Zemax, 3D holders are designed for mounting optics. For MLA1, a metallic holder is designed as it requires very high precision and needs to be positioned just 0.16 mm away from the VCSEL active area. 3D holders for the beam expander and homogenizer are formed by SLA printing with a precision of 0.1 mm (3Dprintuk company). The holders' design for the beam expander and homogenizer are shown in Figure 5.4. The holders set at three different 3 axis stages for lens alignment. To provide proof of concept and avoid the complexity, the VCSEL transmitter is designed for three channels, out of which initially single channels' coverage is verified. The demonstration of three-channels multibeam transmitter is presented in Chapter six.

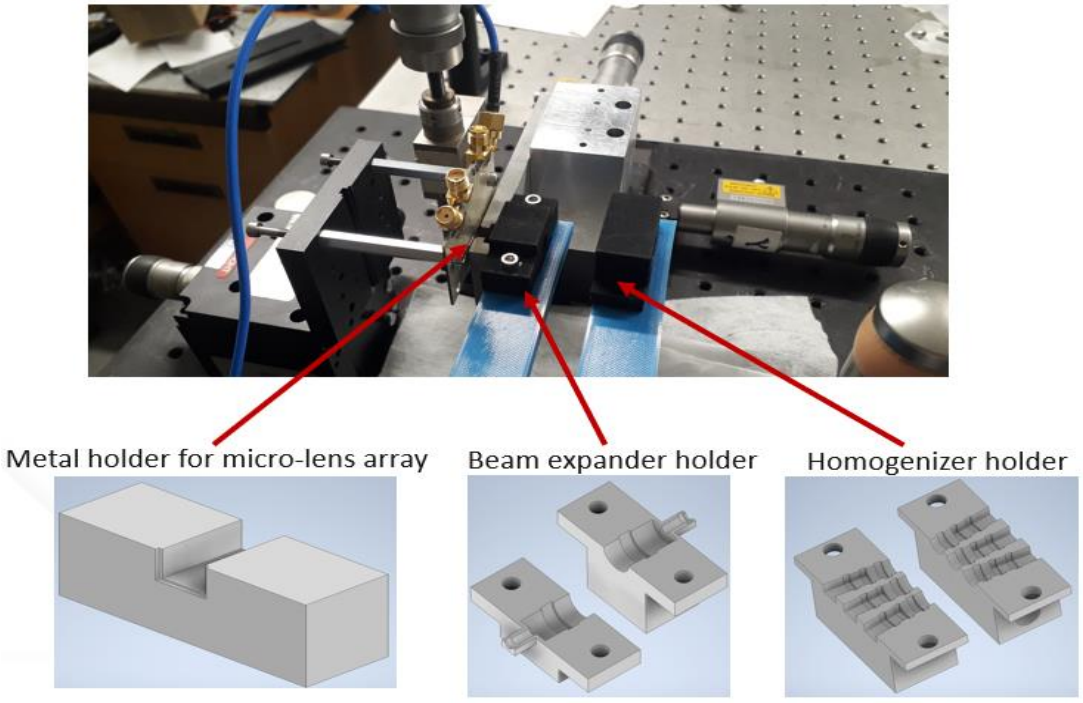

Figure 5. 4 3D housing lens holders for microlens array, beam expander and homogenizer

5.3.2 Optical irradiance measurements

A 5 mm diameter of the power meter (HP 81520A Silicon Optical head) is used to evaluate the eye safety of the transmitter by measuring the optical irradiance at the 10 cm distance in front of the transmitter. The uniformity of the VCSEL beam at the receiver plane is investigated by measuring the power level crossing the image area with 1 cm displacement.

An IR camera Raspberry Pi captures the beam profile projected onto a white screen at the 3m distance, the profile of a single beam is shown in Figure 5.5 demonstrating 21 cm x 21cm cells, where the receiver power in the square area is 21.87 mW m^{-2}. The converging lens (PCX2) unemployed in the system causing the spot is slightly larger than the desired size.

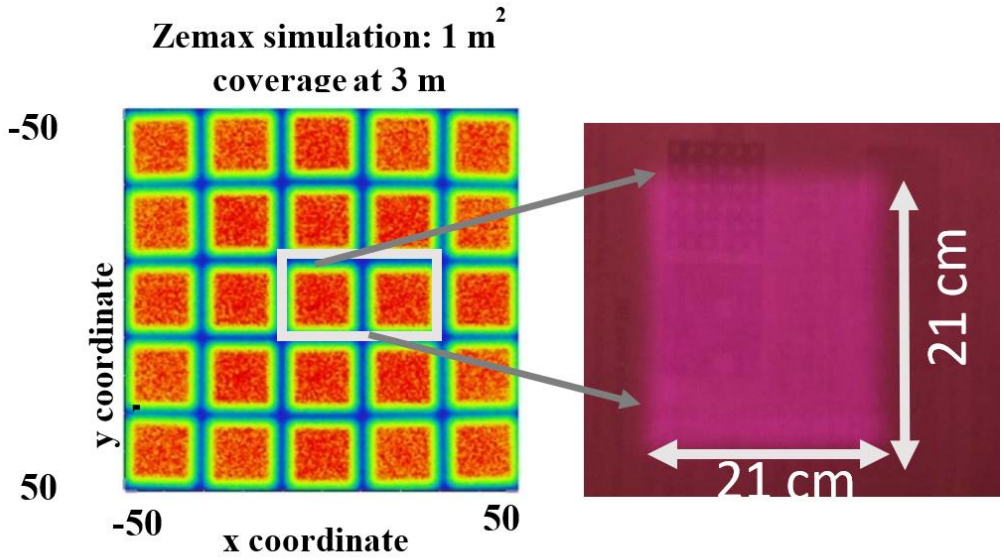

Figure 5. 5 Two channels coverage at 3 m without FL lens (Image obtained using an IR Camera)

Figure 5.6 shows the column cross-section of the optical power in the cell and the displacement is set as 1 cm. A flat-top beam profile showed in the figure proofing a satisfied uniformity in the square cell, where the average received power is -33.67 dBm which is 1 dB lower than the simulation result where the VCSEL output power is 1.7 mW. The lower optical power distribution in the cell happened because of the light coverage area expanded.

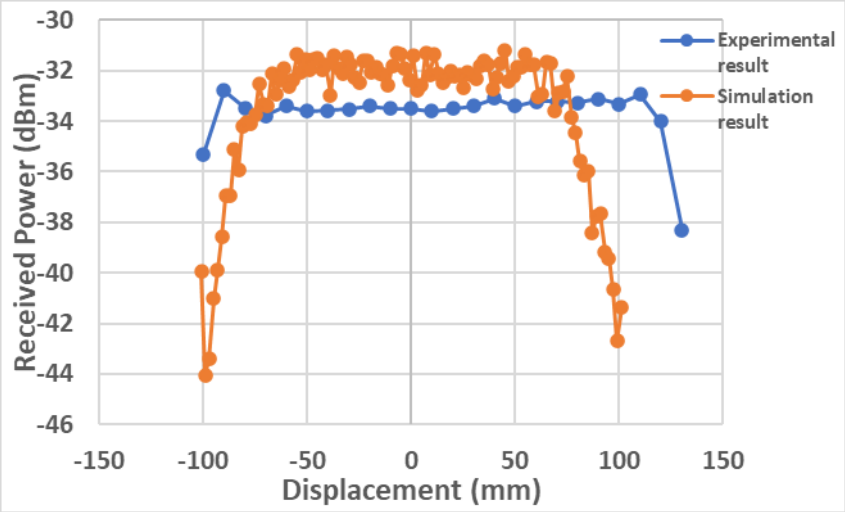

Figure 5. 6 The cross-section of the beam profile

- Eye safety evaluation

As mentioned in Chapter two, the eye safety of the transmitter is evaluated by measuring the irradiance from the transmitter at 10 cm distance. In this work, the same 5 mm diameter of the power meter (HP 81520A Silicon Optical head) placed at the Most hazardous point (i.e., 10 cm after the PXC2 lens) and the measured irradiance value is 8.5 W m^{-2} which is less than the maximum permissible exposure (MPE) class 1 eye-safe limit of 19.95 W m^{-2} at 850 nm.

5.3.3 Data transmission

The designed transmitter is then employed to perform data transmission using the experimental setup shown in Figure 5.7 and Figure 5.8. The receiver consisting of a 1 mm^2 SiPM is placed at a 3 m distance. SiPM is selected due to its better sensitivity compared to APDs and PIN photodiodes. The SiPM has a full-width and half maximum pulse width (FWHM) of 0.6ns and 3dB bandwidth of 310MHz but higher data rates can be obtained thanks to its slow frequency roll off as shown in Figure 5.9. The SiPM is enclosed in a box while a colour glass filter RG-780 nm with 97.00 % spectral transmittance is placed in front of it to block any ambient light as shown in Figure 5.7(b). Figure 5.10 shows the spectrum with the long pass filter (RG-780) response of the OWC link under 500 lux of ambient light generated using Philips 18 W warm white LEDs. A 5 cm plano-convex lens is placed in front of the SiPM receiver to focus light on its active area.

On-Off-Keying (OOK) modulation data with 8b10b coding is generated using Arbitrary Waveform Generator (AWG). An amplifier is used after AWG to provide peak-to-peak voltage of 600mV because AWG peak-to-peak voltage is limited to 500mV. A VCSEL in the 1 x 4 array VCSEL chip is biased at 4 mA and directly modulated using signal from the AWG. The signal from the SiPM is then amplified and recorded in the real time oscilloscope. Finally, the signal from oscilloscope is post-processed offline. It was low pass filtered to minimize noise and for reducing the Inter-symbol interference (ISI), Decision Feedback Equalization (DFE) is applied and operated in MATLAB programme.

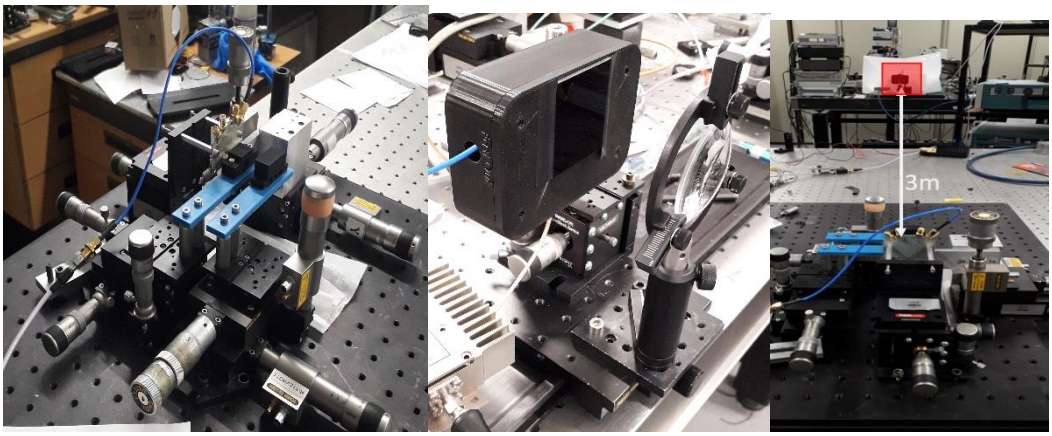

(a) (b) (c)

Figure 5. 7 The experimental set up for OWC link (a) Transmitter (b) SiPM receiver block (c) the whole system

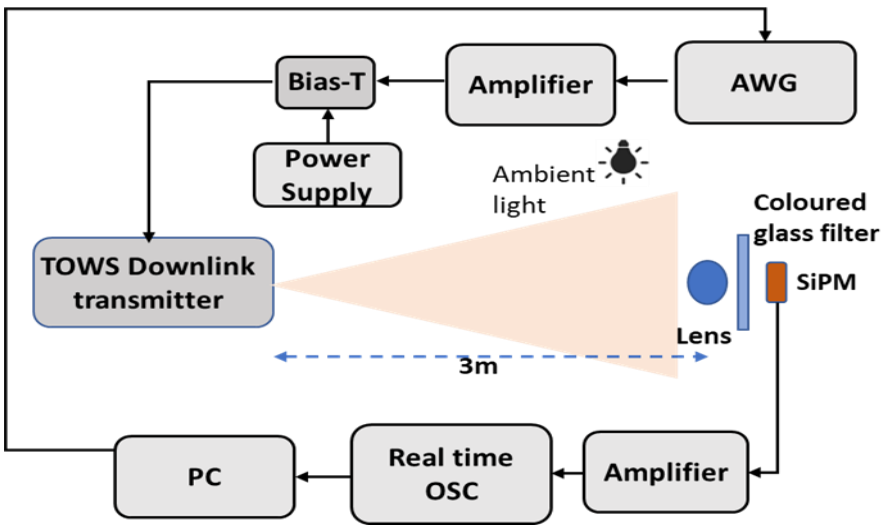

Figure 5. 8 The VCSEL array based optical wireless communication link.

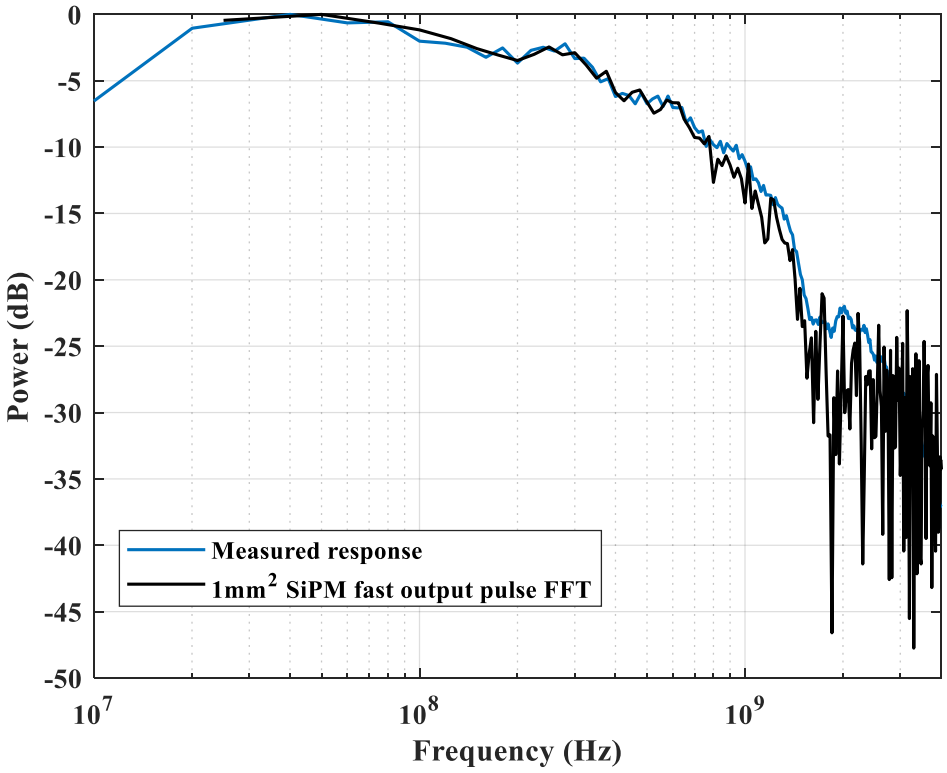

Figure 5. 9 Measured and estimated frequency response from fast pulse

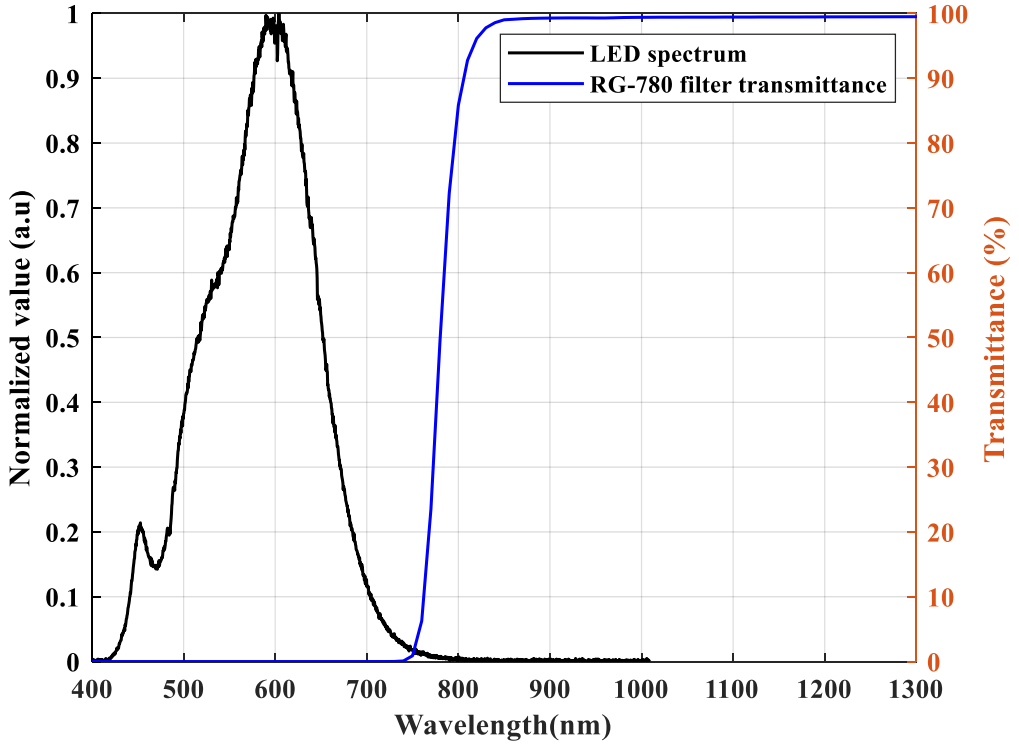

Figure 5. 10 Philips WLED normalized spectrum and RG-780 colour glass filter transmittance.

The experimental setup provided data transmission of 8 Gbps at BER of < $3.8x10^{-3}$. An eye diagram for 8 Gbps is shown in Figure 5.11. The value 3.8 x 10^{-3} (or 0.0038) is commonly used as a threshold for Bit Error Rate (BER) in communication systems. A BER of 3.8 x 10^{-3} signifies a bit error rate of approximately 0.38%, which translates to a data transmission accuracy of over 99.62%. As we assume that each VCSEL performs at its maximum data rate (8 Gbps), the transmitter can achieve an aggerated capacity of at least 200 Gbps.

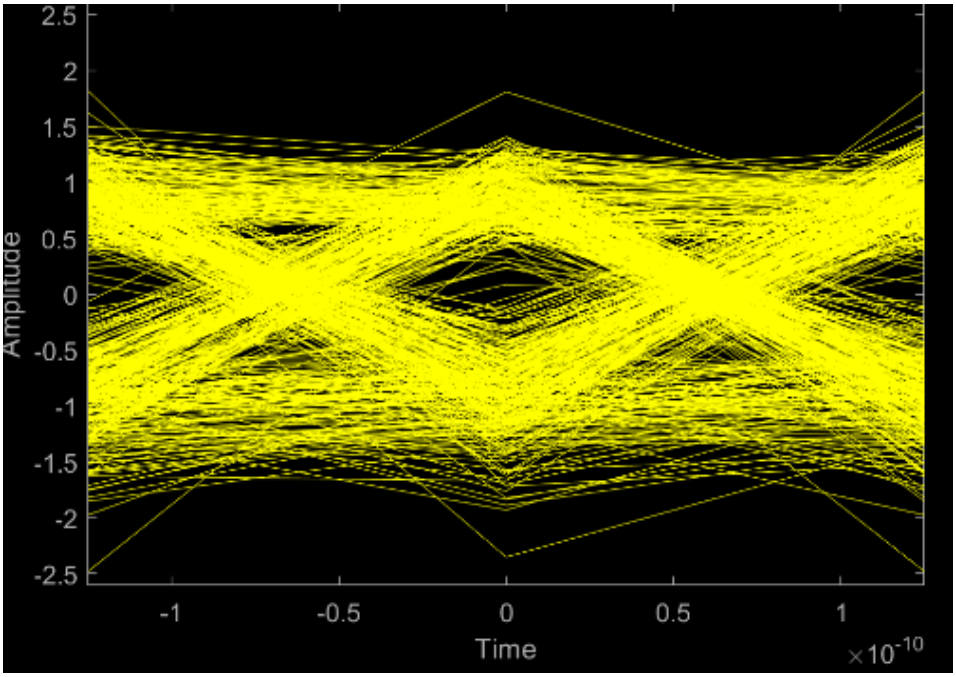

Figure 5. 11 The Eye diagram of transmitter at 8 Gbps

5.4 Summary

This chapter first time demonstrates the high-capacity VCSEL array-based OWC transmitter with uniform coverage using off-the-shelf lens component products. 25 square atto-cell was achieved in the image plane with a 20 cm ×20 cm area. The uniformity is achieved in both cases, with values of 88.89% and 79.43% recorded for the system with ideal and off-the-shelf components, respectively. The power intensity coverage for both cases is approximately 97%.

To experimentally test the transmitter designed in Zemax, 3D holders are designed for mounting optics. Both the simulation and experimental studies have presented that the designed transmitter can provide a uniform power intensity atto-cell

and, therefore, can offer high data rate communication to the user(s) present in this illumination.

A single VCSEL experimentally achieves 8 Gb/s data transmission using OOK modulation and DFE over a 3 m link using a Silicon Photomultiplier (SiPM) receiver. The capture IR image shows a 21 × 21 cm^2 cell where the receiver power in the square area is 21.87 mW m^{-2}. The class 1 eye-safe transmitter is demonstrated as the measurement of optical power at the MPH is less than the MPE limitation. An aggregate capacity of up to 200 Gb/s over a one m^2 area can be achieved, meeting future wireless demands.

Chapter 6: Demonstration of a high capacity multibeam VCSEL array OWC system with wide coverage

6.1. Introduction

In this chapter, the proposed low-cost, compact and high-capacity VCSEL array based-OWC transmitter has been further investigated for multichannel data transmission. To verify proof-of-concept principle, three channels are experimentally demonstrated and characterized. It is shown that all three channels provide near uniform coverage of 20cm x 20cm with negligible optical interference amongst them. A ~10 Gbps maximum data transmission is demonstrated with all three channels at 3 m transmission distance with a BER of $< 2x10^{-3}$ by employing an APD based receiver. All channels achieved 9.8-10 Gbps for approximately 7 cm coverage, thanks to wider transmitter coverage and better FOV of the receiver.

The remainder of the chapter is organised as follows. In section 6.2, the challenge of the lens alignment has been discussed and the result of the optical power distribution is presented in section 6.4. To achieve targeted 10 Gb/s data transmission of each channel, a higher modulation bandwidth APD receiver is employed with OFDM modulation, and the results is shown in section 6.4.

6.2 Experimental investigation of multibeam VCSEL optical power distribution

6.2.1 Setup of the multibeam VCSEL array transmitter

The transmitter designed using ZEMAX is verified experimentally by initially designing precise 3D holders for mounting optics. A 1×4 linear VCSEL array with a pitch of 250 µm is integrated to a designed PCB to generate optical intensity signal. The average output power of each individual VCSEL is 1.7. Figure 6.1 and Figure 6.2

shows the transmit optics employed for the demonstration. VCSEL and lens holders are precisely positioned according to ZEMAX simulation values using three-axis stages. To provide proof of concept and avoid complexity, three channels are demonstrated. Therefore, homogeniser of the transmitter is optimally designed for three central channels. An IR camera Raspberry Pi is used for beam alignment and obtaining the IR image at a 3m distance.

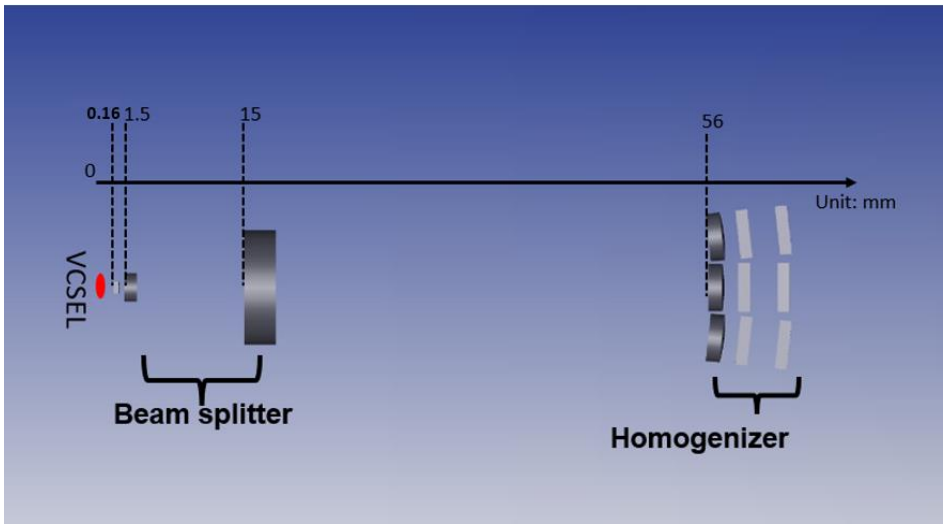

Figure 6. 1 The structure of 1 × 3 VCSEL array OWC transmit optics.

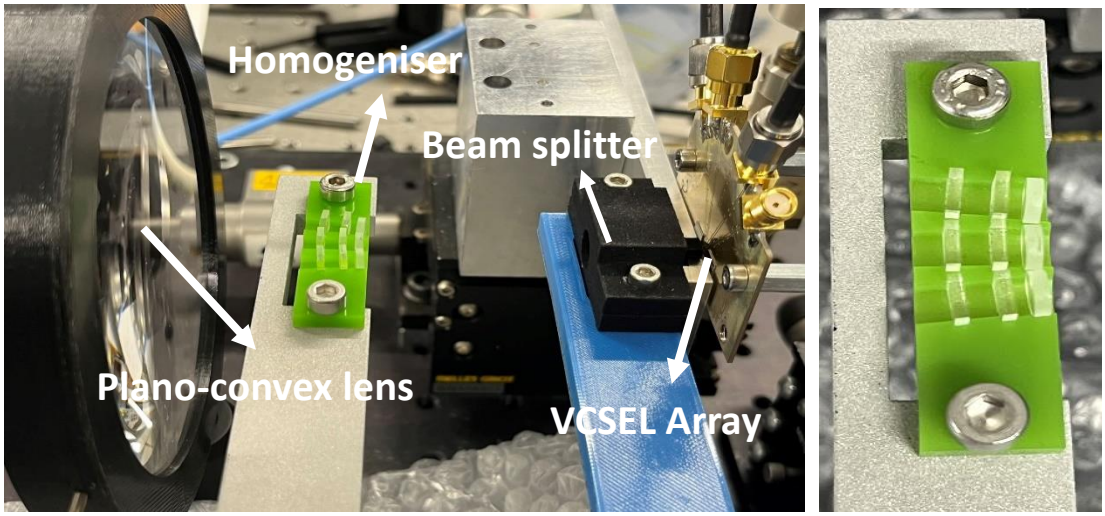

Figure 6.2 VCSEL array full transmit optics and new 3D printing holder

- **Lens alignment**

A 1×3 multibeam VCSEL array OWC transmitter is developed based on the commercial off-the-shelf components mentioned in the Chapter 5. The demonstration of multi-channel transmitter is more challenging because high precision is required to position the homogeniser lenses. Any lateral or angular tilts of the lenses results in

nonaligned beam spots at the receiver plane. Therefore, it is paramount to keep the lenses aligned with high precision.

The misaligned channels coverage is obtained when 3D printed holder using SLA printing technology with 0.1 mm tolerance is employed for placing homogeniser lenses. The SLA printing technology can provide good resolution however, the precision is still not good enough to position homogeniser lenses with negligible misalignment. The resolution of 0.1 mm results in wider or smaller width for lens spaces which results lens angular and lateral misalignments.

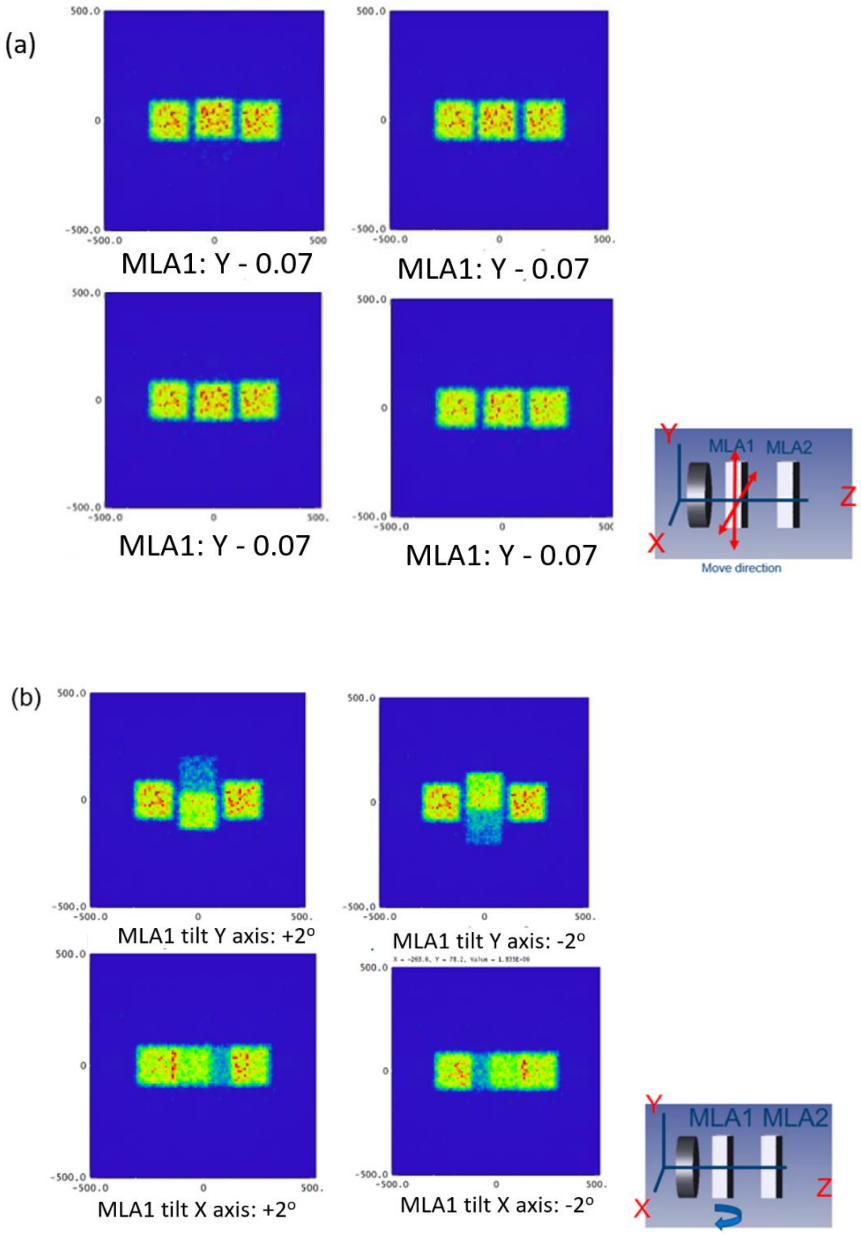

Figure 6.3 The IR image caused by homogeniser misalignment (a) lens angularity (b) lens shift.

The minimum tolerance to the lens holder is verified in Zemax as well. Figure 6.3 shows the IR image of the central channel under the maximum tilt angle and maximum lens shift of MLA1, respectively. In Figure 6.3(a), the lens shift of MLA 1 slightly change the IR image, and it did not induce interference to adjacent cells. Although the MLA1 tiles along the X/Y axis caused the incident beam to split into dense and weak, the dense part also did not overlap with the adjacent cells, as shown in Figure 6.3 (b).

6.2.2 Experimental results of optical power measurement

An IR camera capture the beam profile projected onto a white screen at the 3 m distance. The spot of the three adjacent beams is shown in Figure 6.4, 20 x 20 cm^2 cells, where the average optical irradiance in each square area is 21.81 mW m^{-2}, 23.05 mW m^{-2} and 23.28 mW m^{-2} (from left to right). The dotted array in the cells is due to the coherent light interacting with a periodic structure of the microlens arrays. Although the IR image shows the unwanted grating inference effect, the illumination area is still can be regards as a uniform SNR distribution. a microlens array is a periodic structure with pitch PLA, which can cause effects like grating inference and talbot self-imaging on the image. When a periodic structure interacts with light, the resulting propagation will always exhibit traces of the original periodicity. This periodicity often leads to undesired modulation in the homogenization plane. The homogenization process splits the incident beam into multiple beamlets to regenerate and overlap in the imaging plane.

The power meter (HP 81520A Silicon Optical head) is placed at 3 m distance and sampled the optical power with 1 cm displacement crossing the cells. The power levels of each channel are measured using an optical power meter (with a 5 mm diameter active area) at 3 m distance. Figure 6.5 presents the results showing that each channel can provide -32 dBm of power at 3 m distance. The results in Figure 6.6 are obtained when all the three channels are ON. The periodic pattern of the received signal resulted in around 2 dB power fluctuation in received signal, which can be mitigated by placing lens in front of the receiver. The gaps between adjacent channels are also visible in Figure 6.4, ensuring negligible optical interference among adjacent channels. The interference is further evaluated by turning on one channel at a time. The results in Figure 6.5 show that each channel only covers ~20 cm^2 area and do not cause any optical interference to adjacent channels. The simulation results are also

plotted in Figure 6.5 which matches well with the measurement results. Moreover, the optical irradiance at the MHP has been valued as 8.5 W m^{-2} which meets the class 1 laser safety requirements (< MPE: 19.95W m^{-2})

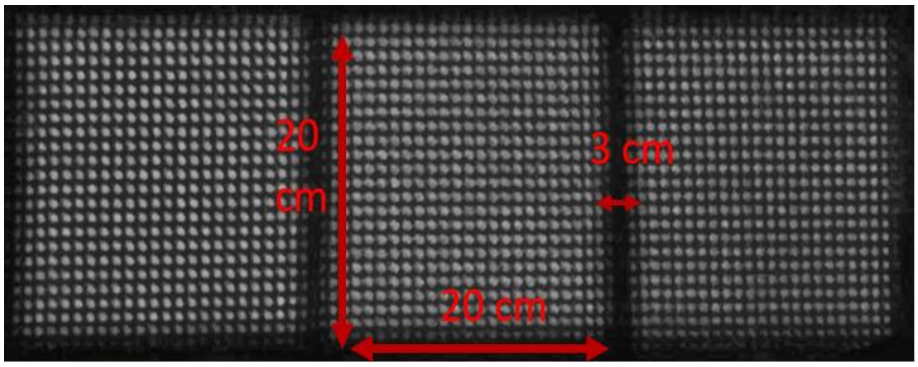

Figure 6.4 Three channels coverage at 3 m with Fourier lens

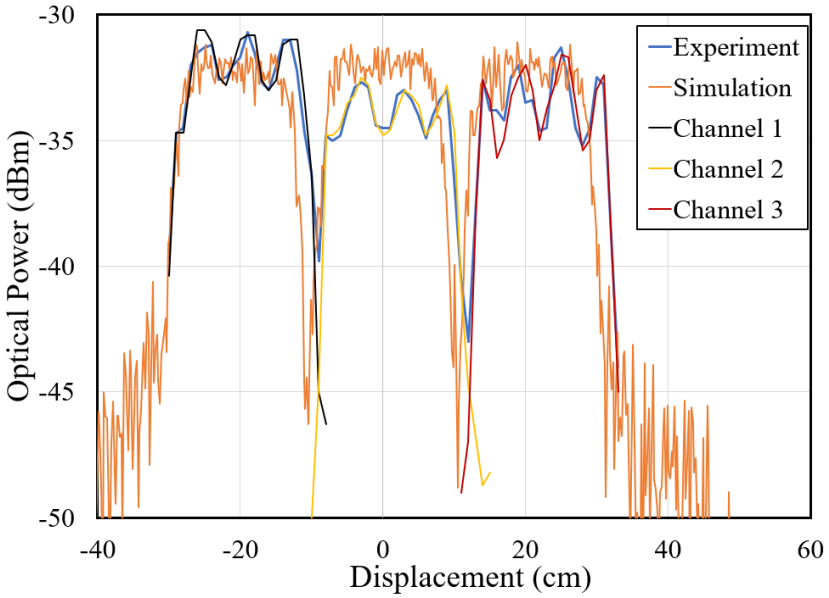

Figure 6.5 The comparison of the power distribution in simulation and experimental measurement

6.3 Experimental investigation of multibeam VCSEL array-APD data transmission

6.3.1 Setup of the multibeam VCSEL array - APD OWC links

The experimental setup of OWC link based on the designed three channel transmitter and a custom-designed receiver is shown in Figure 6.6. A APD optical receiver chip coupling with a large convex lens is set at receiver part. The receiver area of APD is 3 mm^2. In order to establish the OW channels at side, the APD receiver is perpendicular to the incident beam in the cells, which is tiled ± 6 degrees. In this work, higher-order OFDM modulation is considered to achieve high data rate.

Each OFDM frame consists of 1024 carriers and a cyclic prefix (CP) of 3 to minimize effects of Inter-Symbol-Interference (ISI). To maximize the data transmission rate, A bit power loading algorithm [106] is implemented.

At the transmitter side, the signal waveform is fed into an Arbitrary waveform generator (AWG) (50 GS/s, 15 GHz Tektronix A7000). The output from AWG is amplified to obtain an optimum peak-to-peak voltage of 850 mV which is then used to directly modulate the VCSEL transmitter. Due to lab setup limitations, each channel is tested individually. A VCSEL bias current of 5 mA is set for each channel to obtain a high SNR while producing an optical output within the maximum permitted exposure limits for eye-safe operation. The optical receiver is placed at a transmission distance of 3 m.

The receiver consists of a 1.3 GHz APD, amplified by an integrated trans-impedance amplifier (TIA), packaged in a transistor-outline-Can which ensure highly reliable package with a very low thermal resistance. A custom PCB board is designed carefully for the APD. The PCB board is enclosed in a custom designed metal cage to avoid external interference. An aspherical condenser lens (Thorlabs-16mm focal length) is used in front of the APD for focusing received signal at its active area.

The received signal is detected by the receiver, captured by an oscilloscope and then further post processed offline to demodulate the signal and estimate Bit Error ratio (BER). A target BER of $2x10^{-3}$ is considered such that error free transmission could be achieved by employing FEC.

The designed transmitter channels transmit each channel beam at various angles to obtain a coverage of 1 m^2. Particularly, channel 1 and 3 as demonstrated in section 6.2 transmit signal at + 6 degree and -6 degree respectively. Without using any optics in front of the receiver, the received power varies with cosine law however, FOV of the receiver reduces significantly if optics is used [93]. High speed angle diversity receivers could be designed for such OWC links [94]. In addition, recently demonstrated steerable receiver [95] can also be employed for achieving high speed data transmission and coverage with designed transmitters.

To verify performance of three channel OWC link, data transmission for channel 1 and 3 is performed by tilting the receiver by -6 degree and +6 degree

respectively. The receiver is mounted on an optical rail for evaluating all three channels' data transmission and coverage performance.

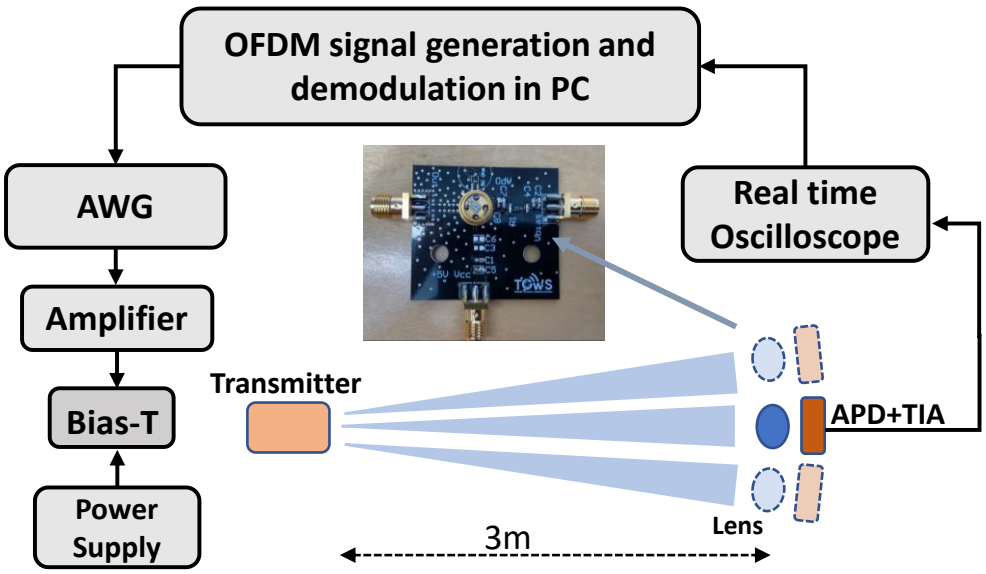

Figure 6.6 Experimental setup of OWC link

The OFDM system utilizes bit and power loading algorithm which needs prior knowledge of each sub-carrier. Therefore, the SNR is evaluated by transmitting an OFDM pilot frame that consists of random binary phase shift keying (BPSK) symbols. SNR values are obtained through Error Vector Magnitude (EVM) estimation on each subcarrier. The pilot symbols are also used to estimate channel response, which help to correct magnitude and phase of received data symbols.

6.3.2 Experiment results of data transmission

With a MATLAB program generating the OFDM signal offline, the OWC link achieves a maximum data rate of 10 Gbps for all three channels at BER of $\leq 2 \times 10^{-3}$. The BER as a function of data rate plot is shown in Figure 6.7. There is small variation of SNR among all the three channels which also leads to slight change in the BER results of Figure 6.8. Each channel has its own Bias-T and RF cables which may resulted in some small SNR variation. The coverage of all the three channels of the OWC link is evaluated by positioning the receiver at the required coverage area and then performing radial displacement. The data transmission results as a function of radial coverage are presented in Figure. 6.9 which shows that all channels achieved 9.8-10 Gbps for approximately 7 cm coverage. A satisfied 12 cm diameter coverage can be achieved for all channel when the target data rate is over 4 Gb/s. The detail of

coverage about each channel has been summarised in Table 6.1. The maximum OFDM signal bandwidth of 1.81 GHz is used, limited due to the APD bandwidth. At misaligned positions, the reduction in received power lowers the subcarriers SNR, majorly impacting the higher frequency subcarriers. Therefore, bandwidth of OFDM signal is adjusted accordingly when receiver is misaligned to obtain maximum possible data transmission within target BER. Outside the reported coverage values, the SNR is not sufficient to perform data transmission within the target BER.

These results are a significant step to develop Tbps OWC link for indoor environments. An aggregated capacity of 250 Gbps can be obtained with 5 × 5 VCSEL array transmitter having each channel achieving 10 Gbps transmission. Four such transmitters within a room or office scenario will result in total capacity of Tbps. The receiver design also shows that low cost off-the-shelf APDs and optics can be used to achieve high speed data rates and wider coverage. In future, FOV of receivers will be improved along with designing angle diversity receivers.

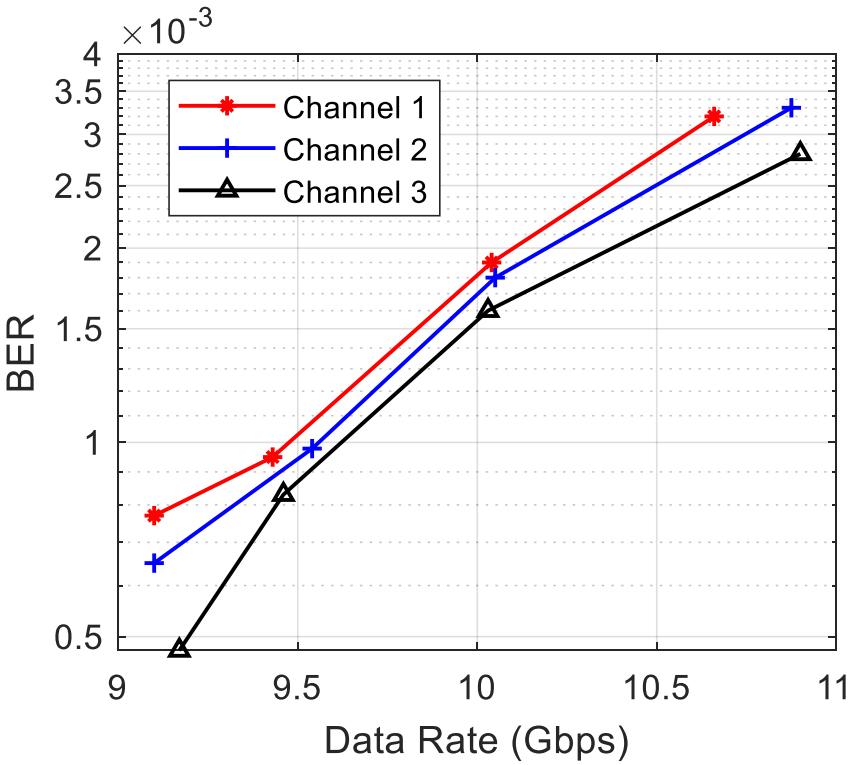

Figure 6.7 BER as a function of data rate.

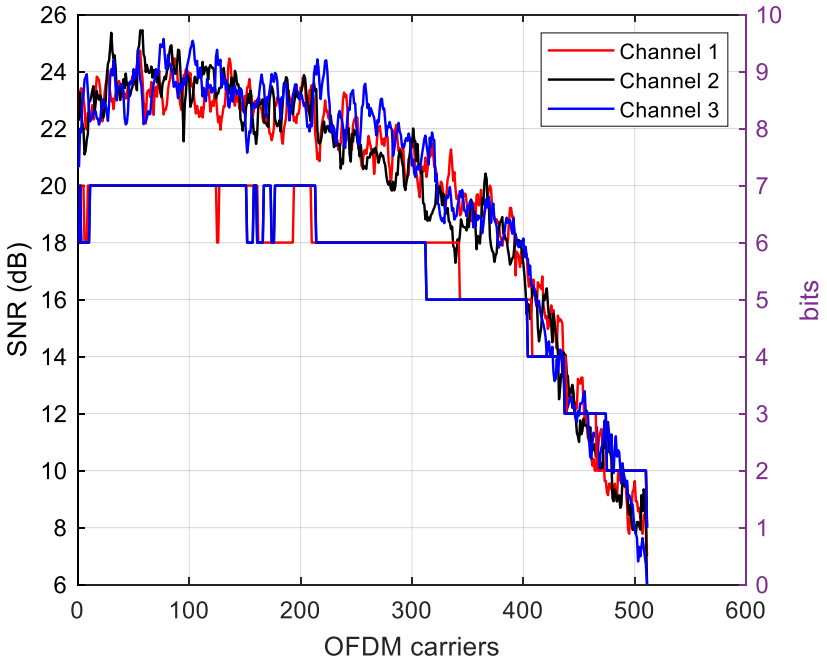

Figure 6.8 Bits allocation and SNR of OWC link for all three channels resulting in 10 Gbps.

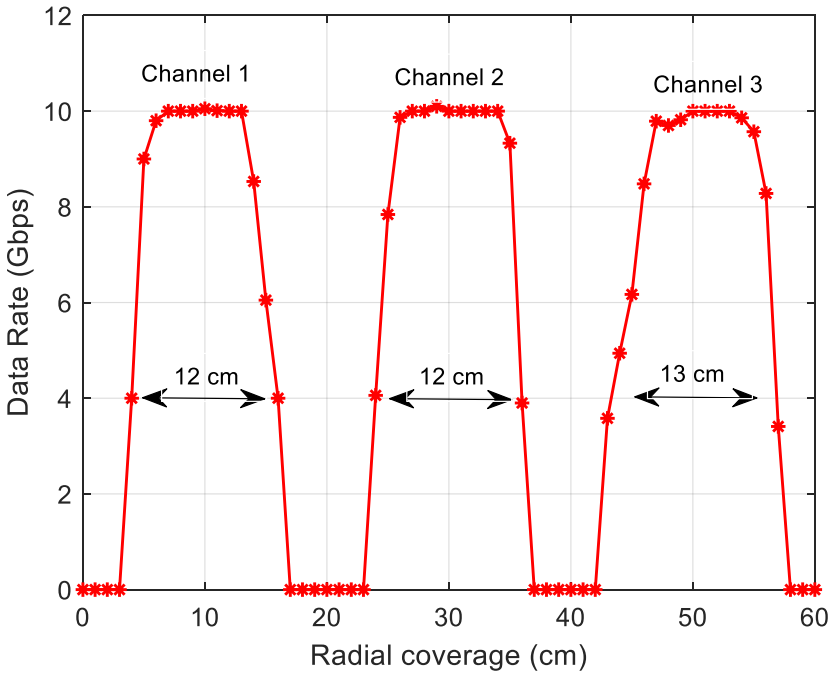

Figure 6.9 OFDM data rate obtained at various lateral position for all three channels with APD based receiver.

Table 6.1 Data transmission coverage summary for all the three channels

Channel	R_{max} and bandwidth	Coverage
1	10.01 Gbps at 1.81 GHz	>=9 Gbps within 8 cm > =4 Gbps within 12 cm
2	10 Gbps at 1.81 GHz	>9 Gb/s within 9 cm >=4Gbps within 12 cm
3	10 Gbps at 1.81 GHz	>9 Gbps within 8 cm > 4 Gbps within 13 cm

6.4 Summary

The experimental investigation presented in this chapter focuses on a low-cost, high-capacity VCSEL array-based optical wireless communication (OWC) transmitter designed for multichannel data transmission. The primary objective is to enhance parallel optical wireless (OW) transmission channels, thereby improving the overall data rate through the simultaneous transmission of multiple data streams.

A three channel VCSE VCSEL array based- OWC transmitter is demonstrated experimental using a 1 × 4 850nm VCSEL array, 3 groups of microlens array homogeniser products and a APD receivers. The 20 cm × 20 cm coverage area for all channels are shown into 3 m distance, where the average optical irradiance in each square area is 21.81 mW m^{-2}, 23.05 mW m^{-2} and 23.28 mW m^{-2}. The 1D power distribution measurement shows the minimum gap between beams is achieved as the value 3 cm proof the do not cause any optical interference to adjacent channels.

The experimental setup involves a 1x4 linear VCSEL array integrated into a designed PCB for optical intensity signal generation. The study investigates the challenges of lens alignment, optical power distribution, and data transmission performance.

Further, the experimental investigation of multibeam VCSEL array-APD data transmission includes the setup of the OWC link and the performance evaluation of three channels. The use of higher-order OFDM modulation and a bit power loading algorithm contributes to achieving a maximum data rate of 10 Gbps for all three

channels, with a bit error ratio (BER) below $2x10^{-3}$. The study also explores the coverage and radial displacement, indicating the feasibility of achieving high data rates for indoor environments.

Chapter 7: Demonstration of a low-cost high-capacity OW fronthaul using VCSEL based-free space optics

7.1 Introduction:

With recent advances in radio access networks (RAN), the last few metres of fronthaul will become a bottleneck for cost-effective ultra-dense network deployment as a huge number of optical fibre links are required to be installed to support high-capacity and multiband remote units. Optical fronthaul is required due to the large bandwidth demand led by the fronthaul protocols such as common public radio interface (CPRI), or low-split evolved CPRI (eCPRI). Both protocols are crucial for 4G and 5G networks, enabling seamless coordination between controllers and radio equipment for efficient data transfer and management. The CPRI protocol defines the interface between Radio Equipment Control (REC) and Radio Equipment (RE) in base stations, specifying key criteria for transport interfacing, as shown in Figure 7.1. The current solution to relieve the high bandwidth requirement is to use upper split options defined in eCPRI. However, this solution will inevitably increase the complexity and power consumption of the distributed remote units (RU). CPRI-based fronthaul links are still more commonly deployed for the final drop of RAN.

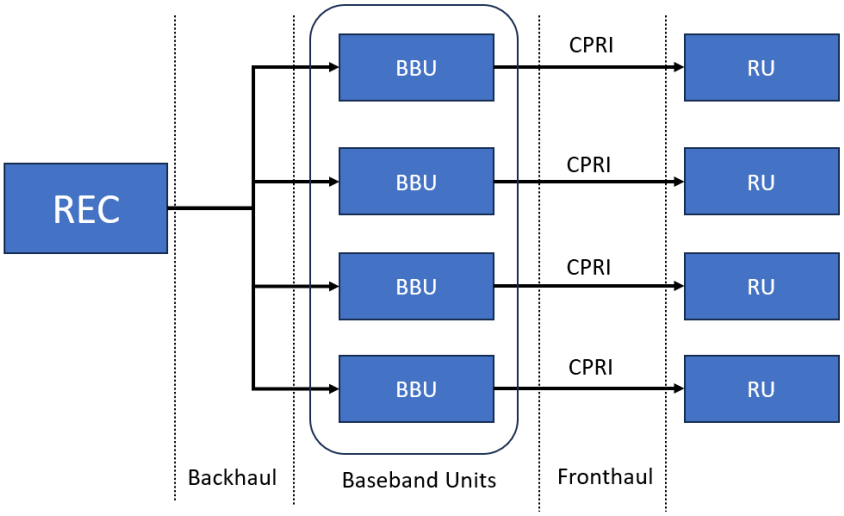

Figure 7. 1 The block diagram of radio access networks (RAN)

Cell-Free MIMO, leveraging massive MIMO processing and distributed antenna systems, has gained traction in Beyond 5G and 6G scenarios [96]. This technology excels in extending coverage and boosting capacity by employing a multitude of antennas to serve all user terminals, eliminating conventional cell boundaries. The benefits include enhanced spectral efficiency, increased capacity, and improved mobility. However, a substantial challenge emerges due to the extensive interconnections required between Baseband Units (BBUs) or Central Processing Units (CPUs) and distributed antennas, with the fronthaul being a critical bottleneck for cost-effective network deployment in practical applications. In this case, new solutions that ease fibre installation will become more attractive, especially for complex cable deployment (densely populated areas, inter-building, disastrous zones, rivers, etc.). A solution is to carry fronthaul traffic over either microwave or free-space optics (FSO) links.

Wireless fronthaul bridging using millimetre wave (mmW) and terahertz carriers (THz) previously demonstrated in [97][98]. In the work, they demonstrated a low-cost indoor wireless network using digital radio over fibre (DRoF). So that, the multiple compressed digitised RF services can be transport both using optical fibre and wireless mmW links. However, the mmW/THz techniques face the challenge of the spectrum becoming increasingly congested, resulting in spectrum regulation and costly licensing. In recent research, free-space optics (FSO) have been proposed as they can provide bandwidth similar to optical fibre and are license-free. Conventional

FSO links create a point-to-point (PtP) narrow beam for line-of-sight (LoS) communications, requiring careful or active alignment.

7.1.1 VCSEL-based FSO fronthaul link

VCSELs have been considered a cost-effective laser source for FSO links as their high bandwidth, invisible working wavelength and energy efficiency. However, they have the drawback of low output power which however may be compensated by high gain optics although that requires careful alignment. In the future fronthaul, a large number of remote antennas are densely distributed at fixed locations or in some cases mounted over unmanned aerial vehicles for capacity enhancement. These scenarios require more relaxed alignment and inherently eye-safe operation. In this work, a VCSEL array with lens system is proposed to diverge the beam so that large and uniform coverage is created, and non-expert alignment is possible. Figure. 7.2 shows the concept of the proposed system. Using multiple VCSEL arrays to create extended cells capable of spatial multiplexing, a huge amount of optical fibre links is saved together with easy optical alignment in indoor distributed and cell-free massive MIMO scenarios.

In this chapter, a VCSEL array-based FSO link for fronthaul transportation is demonstrated. This offers a promising solution for replacing fibre connections with optical wireless links utilizing VCSEL arrays, eliminating the need for cable infrastructure in the final link. Additionally, a microlens array homogeniser system provides wide uniform optical beams at the receiver, significantly improving link alignment area. A data compression technique is implemented to enhance the spectral efficiency of the fronthaul link, achieving successful 1 Gbps data transmission with SiPM receiver while carrying two 20 MHz-bandwidth RF signals over the FSO link.

Simultaneously, a VCSEL-APD based FSO fronthaul has been extend explored and a significant milestone - a 4 Gbps fronthaul transmission supporting an aggregated RF bandwidth of 160 MHz has been achieved. RF Dynamic range and Error Vector Magnitude (EVM) performance are measured to underscore the feasibility of real-world deployment. Importantly, this new setup is designed to seamlessly integrate with commercial-off-the-shelf (COTS) components, enabling direct interfacing with any commercial fronthaul system that features small form factor pluggable (SFP), SFP+, or Quad SFP transceiver modules. Therefore, this

demonstration represents a pivotal leap forward toward the commercial deployment of future FSO-based Fronthaul solutions.

The rest section presented as: Section 7.2 presented the optics design and eye-safety evaluation. In section 7.3, an experimental demonstration of the VCSEL - SiPM FSO fronthaul is presented at first time. A VCSEL – APD FSO fronthaul is demonstrated to achieve high data transmission and relatively wide converge in section 7.4. Section 7.5 gives conclusion of this chapter.

Figure 7. 2 VCSEL-array based FSO Fronthaul for Indoor Scenario

7.2 Transmitter Design and eye-safety evaluation

In chapter 6, a multibeam VCSEL-based transmitter was previously demonstrated to obtain a uniform coverage area at a 3 m distance. To further explore applications of the transmitter, it is demonstrated using a short-range FSO fronthaul links. Figure 7.3 (a) shows the transmit optics structure for a single VCSEL OW link and a 20 cm x 20 cm uniform beam profile as shown in Figure 7.3 (b).

The average output power of the VCSEL is 1.7 mW, resulting in a uniform irradiance of 26.32 mW m^{-2} in the coverage area at the 3 m receiver plane. The eye-safe estimation is evaluated as 8.5 W m^{-2}, which is smaller than the MPE 19.98W m^{-2} requirement meeting class 1. Utilising the benefits of 1D/2D VCSEL arrays, optics will be designed for each channel, providing coverage for massive MIMO RUs deployed for indoor scenario.

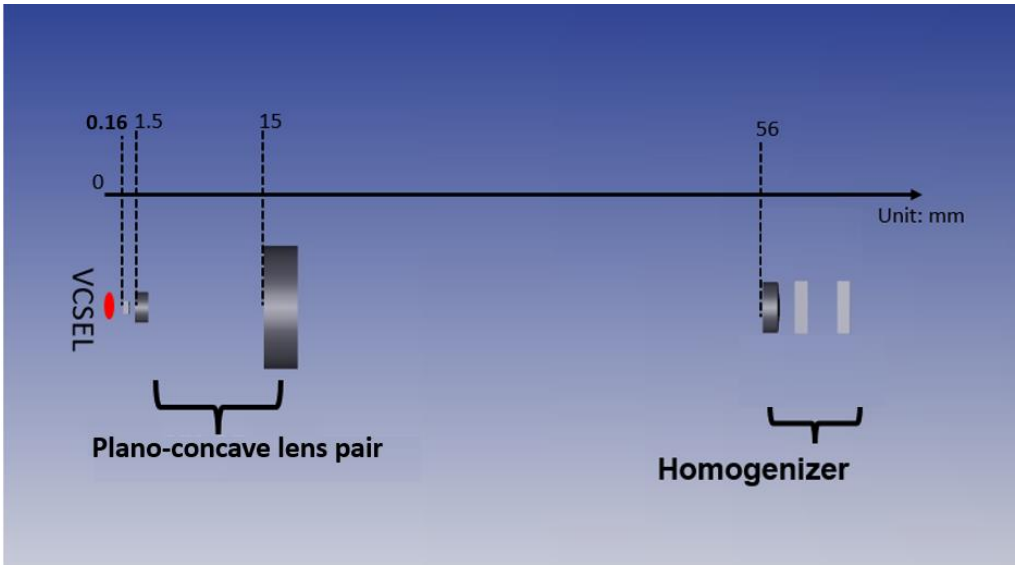

(a)

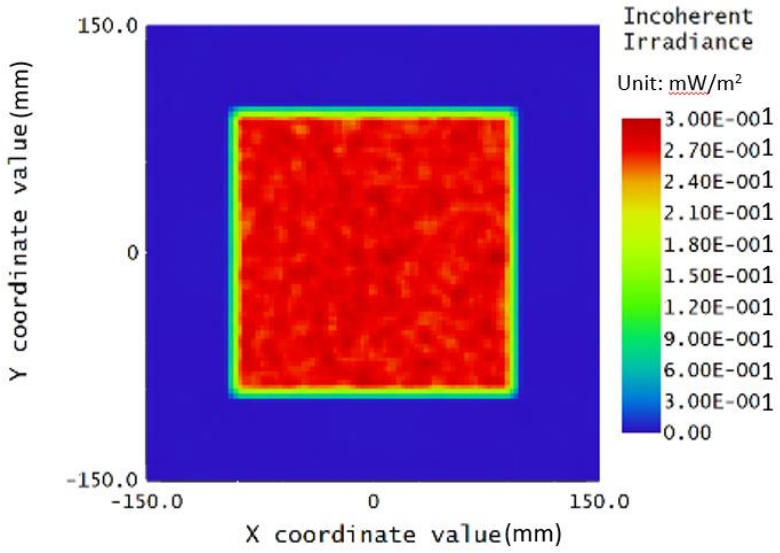

(b)

Figure 7. 3 (a) single channel VCSEL Transmitter Design and (b) Zemax Simulation Result

7.3 Experimental demonstration of the VCSEL - SiPM FSO System

7.3.1 FPGA based Digital Signal Processing

A Field-Programmable Gate Array (FPGA) is an integrated circuit that can be programmed or reprogrammed after manufacturing. It consists of an array of

configurable logic blocks (CLBs) connected via interconnects, allowing users to define the functionality of the device based on their specific requirements.

The FPGA processing chain in this experiment has illustrated in Figure 7.4, it begins with the RF input being down-converted to an intermediate frequency (IF) before undergoing digitization via an analog-to-digital converter (ADC). Subsequently, it passes through the digital downconverter (DDC) and compression module. The resulting data is then replicated into 8 streams, each containing identical information, simulating a multi-band scenario. These streams are subject to 8B/10B encoding and synchronization coding. 8B/10B encoding is a line code that maps 8-bit data words to 10-bit symbols to achieve DC balance and bounded disparity in telecommunications. This encoding ensures a minimum number of transitions and provides error detection capabilities. Next, the FPGA transceiver module performs parallel-to-serial (P/S) conversion and clock synchronization. The high-speed serial data is then transformed into optical information via the SFP module. Upon reception, the signal from the SFP module undergoes a reverse process to recover its original format before being routed to the digital-to-analog converter (DAC) and the Analog Front End (AFE) for RF transmission.

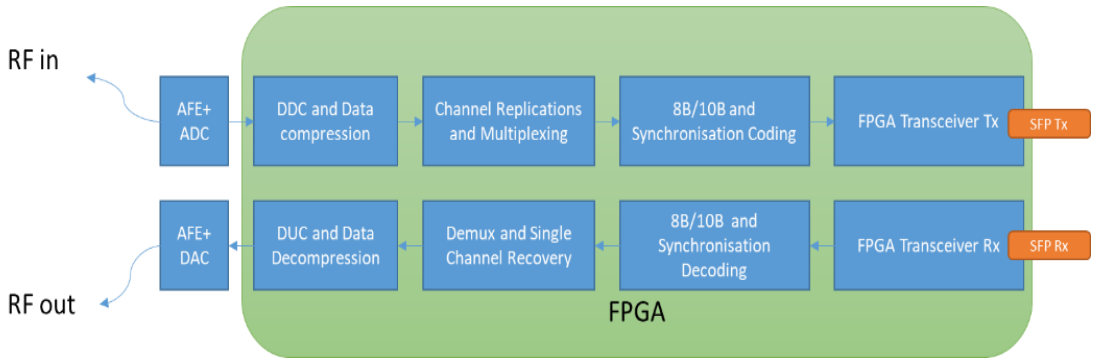

Figure 7. 4 The FPGA Processing Chain

7.3.2 Experiment set up

The experimental setup for the FSO link is shown in Figure 7.5. As an initial proof of concept, one element of a 1 x 4 850 nm wavelength VCSEL array (ULM850-10-TN-N0104U) is used. Each VCSEL has a 3-dB bandwidth of 7 GHz.

To verify the transmitter design of section 7.2, the output beam of a single VCSEL passes through the lens system with custom 3D-printed holders for collimation and homogenization so that at the receiver side, a 20 cm x 20 cm coverage

area is created at a 3 m distance. The eye safety of the transmitter is verified by measuring the irradiance at 10 cm distance from the homogenizer part of the transmitter. The measured irradiance is 8.5 W m^{-2} which is less than the maximum permissible exposure (MPE) class 1 eye-safe limit of 19.95 W m^{-2} at 850nm. The signal is detected by a 1 mm^2 silicon photomultiplier (SiPM) after passing through a 5 cm diameter optical lens.

The SiPM has a 3dB bandwidth of 310MHz, but its slow roll-off frequency response can allow it to achieve over 1Gbps operation. A colour glass filter (Schott RG 780) is used in front of the SiPM to block ambient light.

An LTE-compatible RF input signal is generated with 64QAM modulation format using a Rhode and Schwarz SMW200A vector signal generator (VSA). This signal has a 20MHz bandwidth and a carrier frequency of 2GHz. At the fronthaul central unit (CU), the AFE performs down-conversion, shifting it to 37.5MHz, which aligns with the centre frequency of the first Nyquist zone of the following 14-bit and 150Msamples/s ADC. The resulting 2.1Gbps digital signal then undergoes further down-conversion to the baseband and compression on the FPGA. Ideally a 20MHz clock rate is used to sample the filtered signal. This experiment re-samples the signal at 25MHz to avoid clock jittering caused by fractional down sampling. Thus, the data rate after compression is 400Mbps (8×25×2 Mbps) for the 8-bit IQ data. The data is subsequently duplicated to create an 800 Mbps stream carrying two 20 MHz-bandwidth RF signals. This reduced bit-rate data is replicated into eight identical streams and then organized through time-division multiplexing (TDM), preparing it for subsequent 8B/10B channel coding. To accommodate the 8-channel data, the FPGA transceiver is configured to operate at 1 Gbps.

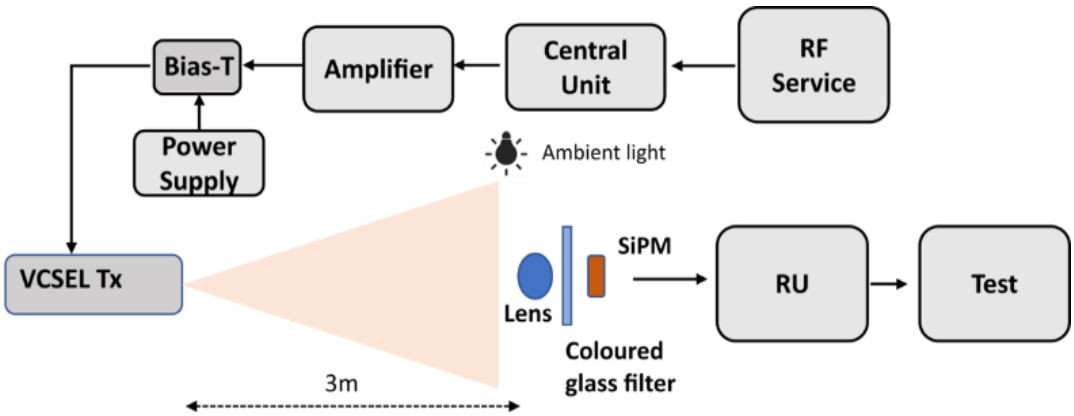

(a)

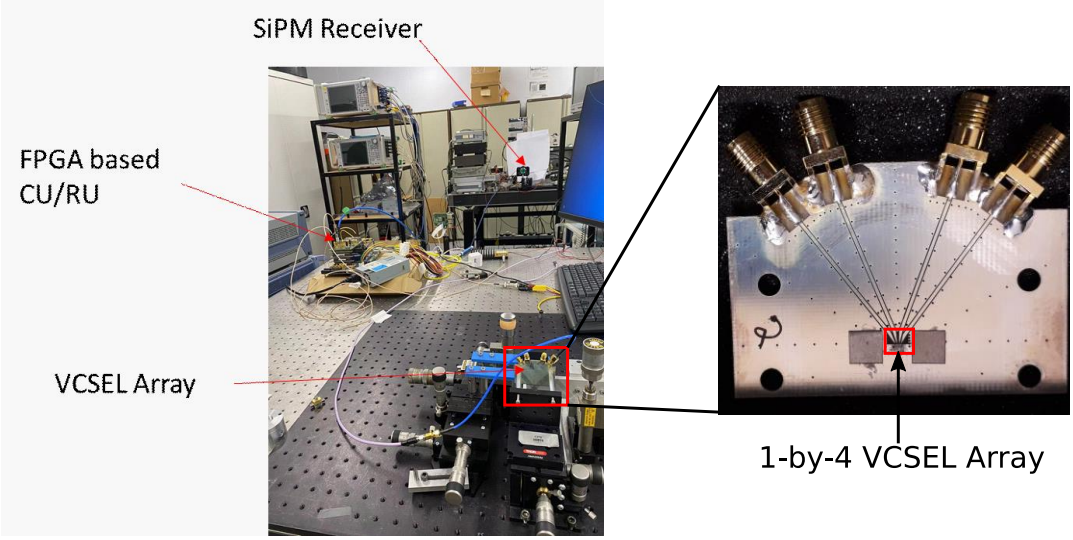

(b)

Figure 7. 5 Experimental Setup (a) Block Diagram (b) Lab Setup and 1-by-4 VCSEL Array

7.3.3 Experiment results

To test the dynamic performance of the system, error vector magnitude (EVM) is measured at different RF input power and received optical power. The received optical power is varied by placing Neutral Density (ND) filters in front of the receiver and optical power values are measured by replacing the receiver with a power meter. As shown in Figure 7.6 (a), the lowest EVM achieved is 1.1% at an RF input power of -10dBm. The RF dynamic range is over 45dB for <8% EVM for 64QAM inputs. In terms of the optical dynamic range, a 6 dB budget is presented, which indicates that a doubling of transmission distance is possible. The current transmission distance is limited by the size of the lab and the devices available. A 1 Gb/s real-time OWC data transmission is demonstrated.

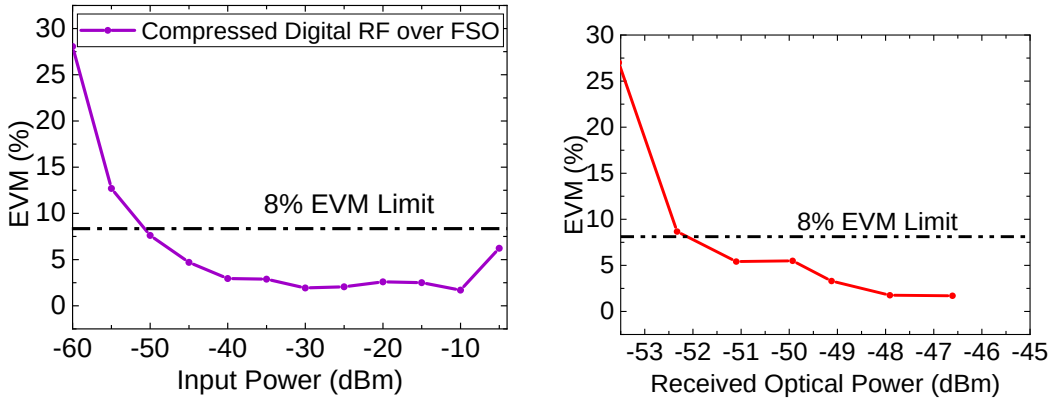

(a) (b)

Figure 7. 6 Experimental Results (a) EVM vrs RF Input Power (b) EVM vrs Received Optical Power.

7.4 Experimental demonstration of the VCSEL - APD FSO System

7.4 1. Experimental Setup of the system

To further demonstrate higher speed real-time OWC links, a VCSEL – APD based OWC link is established as shown in Figure 7.7(a). The receiver consists of an APD (First Sensor AD230-8-2G, 0. 23mm diameter) with a built-in transimpedance amplifier (TIA) and a single focusing lens, as shown in Figure 7.7(b). An -3dB bandwidth of 1.25 GHz and -10 dB bandwidth of 1.8 GHz are measured, as shown in Figure 7.7(c). To improve the received power and provide a wide field of view (FOV), an aspheric condenser (AC) lens with a 25.4 mm diameter and 16 mm focal length is placed in front of the receiver, while a metallic shielding box (i.e., RF cage) is manufactured and grounded to minimize the interference from external RF signals. In the experiment setup show in Figure 7.8 and Figure 7.9.

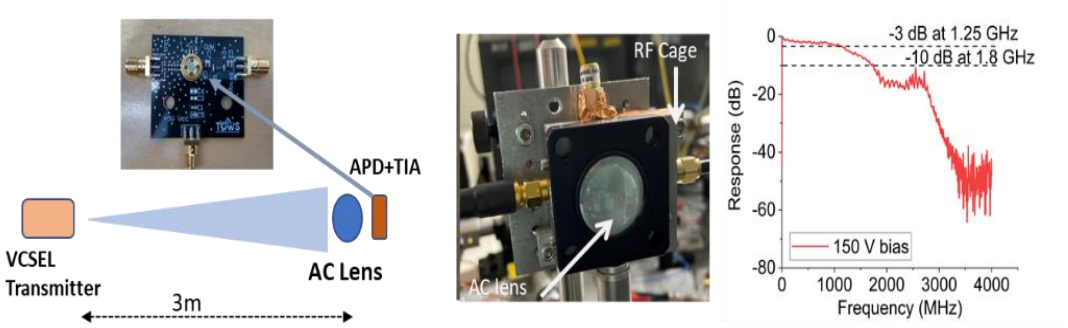

(a) (b) (c)

Figure 7. 7 (a) FSO System block diagram utilizing VCSEL transmitter [2] and (b) Aspheric condenser (AC) lens and APD receiver in RF cage aligned with AC lens (c) receiver bandwidth

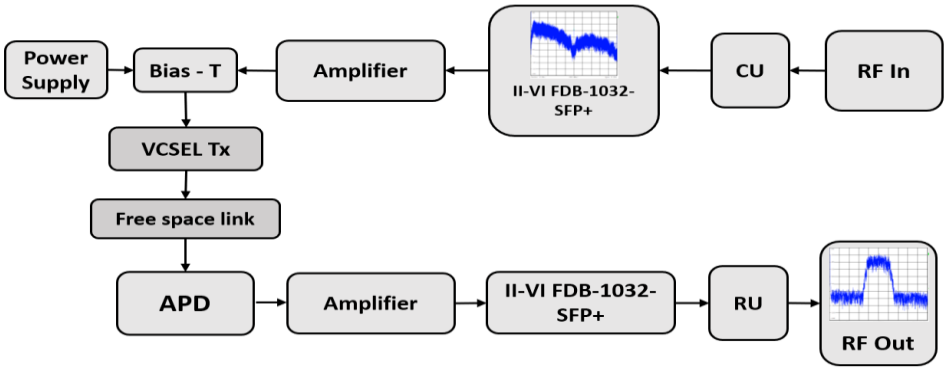

Figure 7. 8 The block diagram of experimental Setup

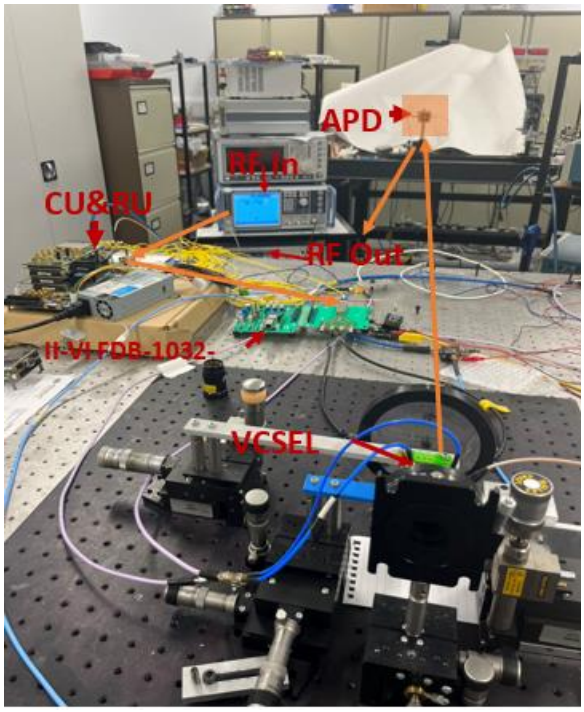

Figure 7. 9 The experimental Setup

In the FSO system, the II-VI FDB-1032-SFP+ Evaluation Board is used, serving as an optical-electrical-optical interface between COTS SFP, SFP+, or QSFP modules and the FSO platform, enabling seamless integration and data transfer with any standard fronthaul interfaces with various wavelengths and unknown optical mode pattern. The signal output from the evaluation board is fed into an amplifier to achieve a peak-to-peak voltage of 700 mV, which is then used to directly modulate a VCSEL biased at a current of 5 mA. The VCSEL bias current is carefully selected such that the minimum possible EVM is obtained while the optical output power does not exceed the maximum permitted exposure (MPE) limits for eye-safe operation. The transmitter and receiver are separated by 3m. The measured received power at the receiver positioned at 3 m is -32 dBm. Subsequently, the II-VI FDB-1032-SFP+ evaluation board receives the signal from the APD based receiver. At the fronthaul remote unit (RU), the signal is restored to its original RF state for testing and analysis as described in the previous section.

7.4.2 Experiment results

Figure. 7.10 (a) illustrates the impressive RF dynamic range, showcasing minimum achieved EVM below 1.5% alongside a wide RF dynamic range exceeding 40 dB for EVM <8% as specified by 3GPP. Comparing this performance with the 1Gbps link rate, we observe no RF degradation. In addition, an optical dynamic range is obtained by varying received power using Neutral Density (ND) filters in front of the receiver presented in Figure 7.10 (b). The power levels are measured using power meter. The minimum EVM of 1.24 % is obtained at -32 dBm receiver power. A power budget of ~7 dB is observed which can be used to extend the transmission distance. We further stress-tested the FSO link by replacing it with a bit error rate tester (BERT) to explore its limits. Figure 7.10 (c) demonstrates that the system can transport 3.072 Gbps CPRI-equivalent data with error-free transmission ($<1x10^{-12}$). In parallel, we evaluated the alignment active area, as detailed in Figure 7.10 (d). The system showcased a 4 cm diameter steady signal receiving area at the receiver end, offering flexibility and non-expert alignment capabilities.

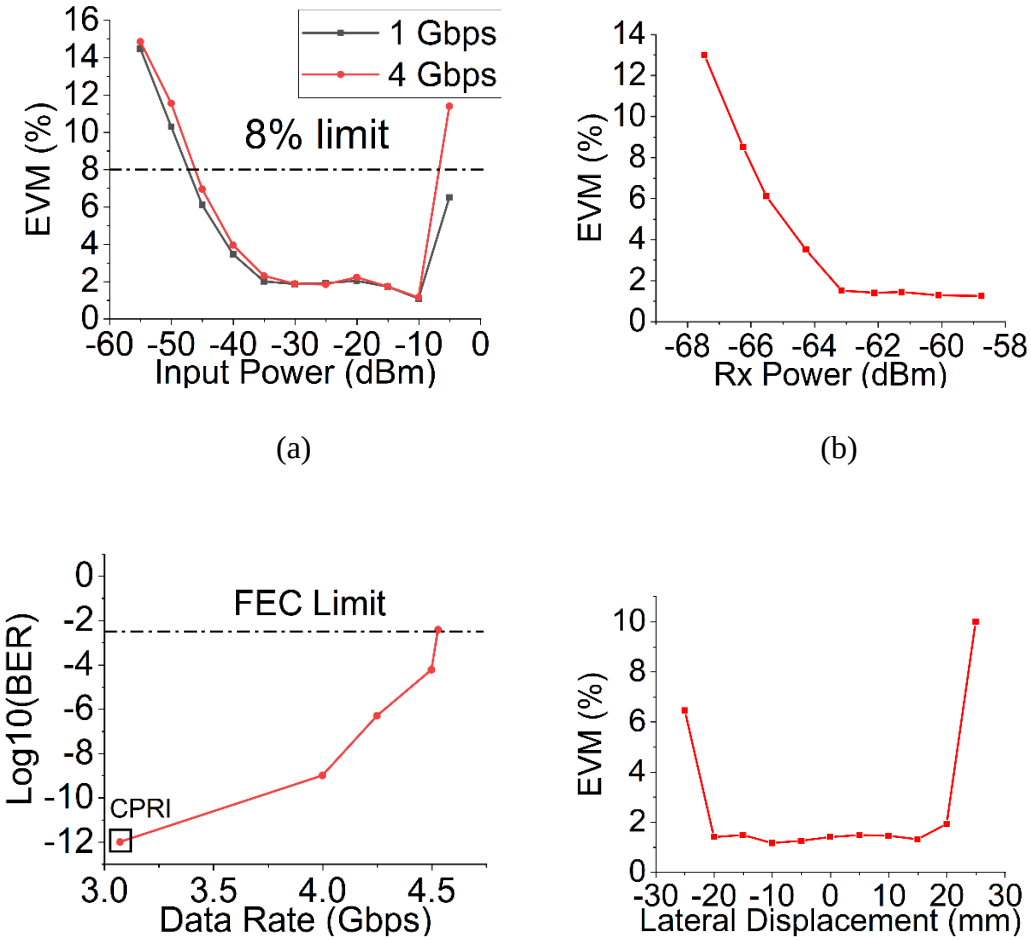

Figure 7. 10 Experimental Results (a) EVM vrs RF Input Power (b) EVM vrs Received Optical Power (c) BERT results: BER vrs data rate (d) EVM as a function of receiver's lateral displacement.

7. 5 Summary

In this chapter, A VCSEL-array-based FSO fronthaul link with easy alignment for next-generation RAN is demonstrated. With a lens system, a 20cm x 20 cm area coverage is created at a 3m distance. In the experiment, two 20MHz-bandwidth 64QAM RF services are successfully transported over the 3-m VCSEL-SiPM based FSO link, showing the lowest EVM of 1.1% and 45dB RF dynamic range.

Moreover, a real-time implementation of FSO-based fronthaul transmission, achieving a remarkable data rate of 4Gbps without any digital post processing. With comprehensive measurements of both RF and digital performance, we confirm the system's feasibility for fronthaul transmission. While the lab limited FSO distance

reaches 3 meters, it's worth noting that the VCSEL output could be increased by 3.6 dB while remaining eye safe, therefore the transmission distance can be expected to be extended longer than 3 m.

Furthermore, the system exhibits non-expert alignment, featuring a ±2cm alignment area. This advancement is poised to significantly reduce infrastructure costs for future Cell-Free MIMO deployments.

Chapter 8: Conclusions and Future work

8.1 Conclusions

Optical wireless communication (OWC) has been a considerable solution for short-range communication within indoor environments. In contrast to conventional RF wireless technologies such as 5G, Wi-Fi, and mm-Wave, OWC leverages the advantages of the light spectrum, offering a large unlimited bandwidth. To address the anticipated surge in network traffic demand, research efforts have focused on enhancing the capacity of cost-effective visible light communication (VLC) to accommodate bandwidth-intensive services.

This work proposes the concept of a high-capacity optical wireless system using VCSEL array arrays, offering multi-user connectivity within a designated area. A VCSEL array transmitter optics has been designed to achieve relatively wide coverage and ensure uniform signal-to-noise ratio (SNR) distribution for each atto-cellular unit. The regular deployment of atto-cellular ensures the non-optical irradiance overlapping. Furthermore, adherence to the standard laser safety regulations for free-space optical transmission transmitters has been meticulously examined and deliberated upon to ensure the design's compliance with eye safety standards. This thesis focuses on VCSEL array transmitter designs, presenting transmitter optics to provide multi-user communications at high data rates (10 Gbps) with no optical interference between adjacent cellular. The microlens array homogeniser is involved in the optical system to generate a uniform optical irradiance that sustains the link connectivity. However, the challenge about lens alignment inquires high resolution 3D printing housing holder to build the designed transmitter optics.

The experimental set-up was established on the off-the-shelf component to demonstrate the concept of the system.A SiPM receiver and an APD receiver have been employed as optical receivers for the designed VCSEL transmitter. The SiPM received allows for smaller optical irradiance. However, the bandwidth of the SiPM is

limited, and only a 1Gbps data rate is recorded due to the PDF effect. However, DFE can reduce the PDF effect and raise the data rate performance to 8 Gbps. Additionally, the smaller active area of SiPM (1 mm^2) limited the receiver FOV inquiring about high precious optical path alignment. To improve the possibility of user mobility, the APD receiver has been employed, and it has a wide FOV. The 10 Gbps data rate of the APD-based OWC links with the OFDM modulation scheme has been recorded, and the steady high data rate links can be ensured in a 12 cm diameter area. The designed VCSEL array transmitter has been proven to work with wide convergence without the active alignment mechanic.

Subsequently, a VCSEL-array-based FSO fronthaul link with the designed transmitter optics for next-generation radio access network (RAN) is demonstrated. With the designed lens system, a 20 cm x 20 cm area coverage is created at a 3m distance. In the experiment, a real-time implementation of VCSEL- APD FSO-based Fronthaul transmission has been presented to achieve a data rate of 4 Gb/s. Furthermore, the system exhibits non-expert alignment, featuring a ±2cm alignment area. This advancement is poised to significantly reduce infrastructure costs for future Cell-Free MIMO deployments.

In summary, we believe that a high capacity VCSEL array based OWC transmitter is developed, which offering multiuser connectivity, low-complex link alignment between the transmitter and receiver and low interference among adjacent atto-cellular. An aggregated capacity of 250 Gbps can be obtained with 5 × 5 VCSEL array transmitter having each channel achieving 10 Gbps transmission. Four such transmitters within a room or office scenario will result in total capacity of Tbps.

However, the designed transmitter has several limitations. Firstly, the size of the atto-cell is proportional to the transmission distance, which means the VCSEL beam will be overlapped when the transmit distance is greater than 3 m, where the optical interference happened. Therefore, the designed transmitter is more suitable for indoor office or house environments where the work distance is around 3 meters. In additional, smaller lenses must be employed to build the designed transmitter optics when a large-scale VCSEL array is applied. Still, the lens alignment could be a challenge and require a higher resolution 3D printer to print the lens holder.

8.2 Future works

8.2.1 Mitigate Nonlinearity of SiPM

Chapter five has demonstrated an 8.2 Gb/s data transmission OW channel over 3 meters using a SiPM and OOK modulation and DEF equaliser. The main challenge of using SiPM to build the high-speed receiver is the mitigation of distortion caused by the nonlinearity within SiPM. Addressing this challenge could involve the application of machine learning techniques, and neural networks to learn the mapping between the SiPM's distorted output and the actual input light intensity. Neural networks can model complex nonlinear relationships[x].

8.2.2 Enhancing Receiver's Field of view.

In chapter six, the multibeam transmission of the proposed OWC system has been demonstrated using a 1 × 3 VCSEL array and an APD receiver, which achieved a maximum 8.8 Gb/s data rate for each channel. The performance of data transmission is limited by the narrow field (FOV) of view of the receiver. To achieve better communication performance, the advanced receiver has been studied.

Angle diversity receiver relies on multiple optical receivers oriented in different directions, offering a promising solution for signal enhancement. The incorporation of a compound parabolic concentrator (CPC) as an optical concentrator for photodetectors (PD) provides efficient signal collection. A broad FOV is achievable despite the narrow FOV of individual receivers. Imaging diversity receivers is another approach to improve data transmission. The imaging lens focuses the signal light onto the PD array. Key advantages include the potential for compact, cost-effective receivers and the realization of system-level integration. Integration of an optical concentrator for all detector elements introduces increased compactness.

The fly-eye lens system is tolerant to fluctuations in beam shape, beam size, number of beams, beam incident position, and beam incident direction. It was widely studied in the optical wireless power transfer system. In [99], the result shows the proposed lens system significantly improves the allowable incident angle. Therefore, it is interesting to investigate an OWC system using this novel fly-eye lens system.

8.2.4 Extending to Long-Range High-Speed Free-Space Optical Communication

The scope of this work could be broadened to encompass applications in long-range free-space optical (FSO) communication. Chapter Seven delves into investigating significantly high maximum permissible exposure (MPE) levels for the VCSEL-based OWC transmitter using beam homogenizer technology. This suggests employing high-output power free-space lasers to achieve higher data rates and extend transmission distances beyond 10 meters.

References:

[1] Z. Wei et al., “Evolution of optical wireless communication for B5G/6G,” Progress in Quantum Electronics, vol. 83, p. 100398, 2022.

[2] Available at https://www.ericsson.com/en/mobility-report/future-mobiledata-usage-and-traffic-growth, May 2019.

[3] G.P.A.G.Bell, “Photophone transmitter,” USA Patent, 1880

[4] Cornwell, D. Space-Based Laser Communications Break Threshold. Opt. Photon. News, 27, 24–31, 2016.

[5] K. Greer, “Global-scale observations of the limb and disk (gold): Far-UV Imaging Spectrograph background at Geostationary Orbit,” 2020 IEEE Aerospace Conference, 2020. doi:10.1109/aero47225.2020.9172274

[6] IEEE standard for local and metropolitan area networks--part 15.7: Short-range optical wireless communications. doi:10.1109/ieeestd.2019.8697198

[7] “Infrared Data Association Releases IrDA Global Market Report 2007,” 2007.

[8] M. Leba, S. Riurean and A. Lonica, "LiFi — The path to a new way of communication," 2017 12th Iberian Conference on Information Systems and Technologies (CISTI), Lisbon, Portugal, 2017, pp. 1-6.

[9] S. D. H. Haas, “Principles of LED Light Communications”. 2015

[10] Wang, Yiguang, et al. "4.5-Gb/s RGB-LED based WDM visible light communication system employing CAP modulation and RLS based adaptive equalization." Optics express 23.10, pp. 13626-13633, 2015

[11] H. Chun et al., "LED Based Wavelength Division Multiplexed 10 Gb/s Visible Light Communications", Journal of Lightwave Technology, vol. 34, no. 13, pp. 3047-3052, 2016.

[12] S. Huang, C. Chen, R. Bian, H. Haas, and M. Safari, “5 Gbps Optical Wireless communication using commercial SPAD array receivers,” Optics Letters, vol. 47, no. 9, p. 2294, 2022. doi:10.1364/ol.454994.

[13] P. Pathak, X. Feng, P. Hu and P. Mohapatra, "Visible Light Communication, Networking, and Sensing: A Survey, Potential and Challenges", IEEE Communications Surveys & Tutorials, vol. 17, no. 4, pp. 2047-2077, 2015.

[14] D. R. Dhatchayeny, S. Arya and Y. H. Chung, "Infrared-based multiple-patient monitoring in indoor optical wireless healthcare systems", IEEE Sensors J., vol. 19, no. 14, pp. 5594-5599, Jul. 2019.

[15] X. Zhao, H. Chen and J. Sun, "On physical-layer security in multiuser visible light communication systems with non-orthogonal multiple access", IEEE Access, vol. 6, pp. 34004-34017, 2018.

[16] Z. Ghassemlooy, W. O. Popoola, and S. Rajbhandari, Optical Wireless Communications: System and Channel Modelling with MATLAB. Boca Raton ; London ; New York: CRC Press, 2018.

[17] K. Wang *et al*., "Evolution of Short-Range Optical Wireless Communications," in *Journal of Lightwave Technology*, vol. 41, no. 4, pp. 1019-1040, 15 Feb.15, 2023.

[18] G.A. Koepf, R.G. Marshalek, and D.L. Begley, Space laser communications: A review of major programs in the United States, International Journal of Electronics and Communications, 2002. 56: pp. 232–242.

[19] B. Furch, Z. Sodnik, and H. Lutz, Optical communications in space—A challenge for Europe, International Journal of Electronics and Communications, 2002. 56: pp. 223–231.

[20] B. Furch, Z. Sodnik, and H. Lutz, The ESA optical ground station—Ten years since first light, ESA Bulletin, 2007. 132: pp. 34–40.

[21] Available at http://esc.gsfc.nasa.gov/267/271.html. [Accessed on May 2019]

[22] 7V. Jungnickel, D. Schulz, J. Hilt, C. Alexakis, M. Schlosser, L. Grobe, A. Paraskevopoulos, R. Freund, B. Siessegger, and G. Kleinpeter, Optical wireless communication for backhaul and access, in European Conference on Optical Communications (ECOC), IEEE, pp. 1–3, 2015.

[23] Z. Zhao, Z. Zhang, J. Tan, Y. Liu, and J. Liu, 200 Gb/s FSO WDM communication system empowered by multiwavelength directly modulated TOSA for 5G wireless networks. IEEE Photonics Journal, 2018. 10(4): p. 7905908

[24] x Lawler, R. (2021) Alphabet's project Taara Laser Tech beamed 700TB of data across nearly 5km, The Verge. Available at: https://www.theverge.com/2021/9/16/22677015/project-taara-fsoc-wireless-internet-kinshasa-congo-fiber,25 August, 2023.

[25] R. Sharma, A. C. Kumari, M. Aggarwal and S. Ahuja, "Performance analysis of LED based indoor VLC system under receiver mobility," 2017 International Conference on Computing, Communication and Automation (ICCCA), Greater Noida, India, 2017, pp. 945-950

[26] C. Halim, B. Abdesselam, L. Abdelaziz, C. Ameur and Z. Xun, "3D Arrangement of LEDs for Indoor VLC Applications," *2020 IEEE International Symposium on Broadband Multimedia Systems and Broadcasting (BMSB)*, Paris, France, 2020.

[27] Z. Wei, M. Guan, Z. Zang and H. Y. Fu, "Utilization of 850 nm Near-infrared VCSEL for High-capacity Indoor Free Space Optical Communications," *2018 Asia Communications and Photonics Conference (ACP)*, Hangzhou, China, 2018,

[28] S. Almohanna *et al*., "Visible-NIR Laser Based Bi-directional Indoor Optical Wireless Communication," *2019 IEEE 10th GCC Conference & Exhibition (GCC)*, Kuwait, Kuwait, 2019.

[29] I.C. Lu, C.H. Lai, C.H. Yeh, and J. Chen, 6.36 Gbit/s RGB LED-based WDM MIMO Visible Light Communication System Employing OFDM Modulation, in Optical Fiber Communication Conference (OFC), Optical Society of America, Los Angeles, CA, pp. W2A–39, 2017.

[30] 42 K. Wang, A. Nirmalathas, C. Lim, and E. Skafidas, High-speed optical wireless communication system for indoor applications, IEEE Photonics Technology Letters, 2011.

[31] C.L. Schow, F.E. Doany, C.W. Baks, Y.H. Kwark, D.M. Kuchta, and J.A. Kash, A single-chip CMOS-based parallel optical transceiver capable of 240-Gb/s bidirectional data rates. Journal of Lightwave Technology, 2009.

[32] H. Elgala, R. Mesleh and H. Haas, "Indoor optical wireless communication: potential and state-of-the-art," in IEEE Communications Magazine, vol. 49, no. 9, pp. 56-62, September 2011.

[33] Ingham, JD and Penty, RV and White, IH and Cunningham, DG, 28 Gb/s unequalized PAM3 modulation of an 850 nm VCSEL for next-generation datacommunication links. CLEO: Science and Innovations, CLEO_SI, 2012.

[34] Qureshi, Z and Crisp, MJ and Ingham, JD and Penty, RV and White, IH and Ledentsov, NN and Lott, JA and Mutig, A and Bimberg, D, Monolithic "Electro-optically modulated VCSEL suitable for radio over fibre applications to 20 GHz". 2011 Optical Fiber Communication Conference and Exposition and the National Fiber Optic Engineers Conference, OFC/NFOEC, 2011.

[35] Ingham, JD and Penty, RV and White, IH and Westbergh, P and Gustavsson, JS and Haglund, A and Larsson, A, "32 Gb/s multilevel modulation of an 850 nm VCSEL for next-generation datacommunication standards". Optics InfoBase Conference Papers, 2012.

[36] Alsulami, A. Hussein, M. Alresheedi and J. Elmirghan, "Optical Wireless Communication Systems, A Survey", 2019.

[37] S. Rajbhandari et al., "A review of gallium nitride LEDs for multi-gigabit-per-second visible light data communications", Semiconductor Science and Technology, vol. 32, no. 2, p. 023001, 2017.

[38] D. Steigerwald et al., “Illumination with solid state lighting technology,” IEEE J. Sel. Topics Quantum Electron., vol. 8, no. 2, pp. 310–320, Mar./Apr. 2002

[39] A Yang, Y Wu, M Kavenhrad and G Ni, “Grouped Modulation Schemes for LED Array Module in a Visible Light Communication System”, IEEE Wireless Communication, vol. 22, issue 2, pp 24-28.

[40] K. Wang, Indoor Infrared Optical Wireless Communications: Systems and integration. Boca Raton, FL.: CRC Press, 2020.

[41] F. Xu, M. -A. Khalighi and S. Bourennane, "Impact of different noise sources on the performance of PIN- and APD-based FSO receivers," *Proceedings of the 11th International Conference on Telecommunications*, Graz, Austria, 2011.

[42] P. Brandl, R. Enne, T. Jukić and H. Zimmermann, "OWC Using a Fully Integrated Optical Receiver With Large-Diameter APD," in *IEEE Photonics Technology Letters*, vol. 27, no. 5, pp. 482-485, 1 March1, 2015.

[43] C. Piemonte, A. Ferri, A. Gola, T. Pro, N. Serra, A. Tarolli, N. Zorzi, Characterization of the First FBK High- Density Cell Silicon Photomultiplier Technology, in «IEEE TRANSACTIONS ON ELECTRON DEVICES», vol. 60, n. 8, 2013.

[44] Shenjie Huang, Yichen Li, Cheng Chen, Mohammad Dehghani Soltani, Robert Henderson, Majid Safari, and Harald Haas, "Performance analysis of SPAD-based optical wireless communication with OFDM," J. Opt. Commun. Netw. 15, 174-186, 2023.

[45] S. Zhang et al., “1.5 gbit/s multi-channel visible light communications using CMOS-controlled GaN-based LEDs,” J. Lightw. Technol., vol. 31, no. 8, pp. 1211–1216, Apr. 2013.

[46] A. M. Khalid, G. Cossu, R. Corsini, P. Choudhury and E. Ciaramella, “1-Gb/s transmission over a phosphorescent white LED by using rateadaptive discrete multitone modulation,” IEEE Photon. J., vol. 4, no. 5, pp. 1465–1473, Oct. 2012.

[47] Wang, Yiguang, et al. "4.5-Gb/s RGB-LED based WDM visible light communication system employing CAP modulation and RLS based adaptive equalization." Optics express 23.10, pp. 13626-13633, 2015.

[48] Wang, Yiguang, et al. "4.5-Gb/s RGB-LED based WDM visible light communication system employing CAP modulation and RLS based adaptive equalization." Optics express 23.10, pp. 13626-13633, 2015.

[49] I. -C. Lu, C. -H. Lai, C. -H. Yeh and J. Chen, "6.36 Gbit/s RGB LED-based WDM MIMO visible light communication system employing OFDM modulation," 2017

Optical Fiber Communications Conference and Exhibition (OFC), Los Angeles, CA, USA, 2017.

[50] H. Chun et al., "LED Based Wavelength Division Multiplexed 10 Gb/s Visible Light Communications", Journal of Lightwave Technology, vol. 34, no. 13, pp. 3047-3052, 2016.

[51] A Yang, Y Wu, M Kavenhrad and G Ni, “Grouped Modulation Schemes for LED Array Module in a Visible Light Communication System”, IEEE Wireless Communication, vol. 22, issue 2, pp 24-28.

[52] A. E. Ibhaze, P. E. Orukpe, and F. O. Edeko, “High-Capacity Data Rate System: Review of Visible Light Communications Technology,” Journal of Electronic Science and Technology, vol. 18, no. 3, p. 100055, 2020.

[53] L. Wei, C. Hsu, C. Chow and C. Yeh, "20.231 Gbit/s tricolour red/green/blue laser diode based bidirectional signal remodulation visible-light communication system", Photonics Research, vol. 6, no. 5, p. 422, 2018.

[54] D. Tsonev, S. Videv and H. Haas, "Towards a 100 Gb/s visible light wireless access network", Optics Express, vol. 23, no. 2, p. 1627, 2015.

[55] Y. Liu, W. Ali, R. Chen, N. Bamiedakis, M. Crisp, I. White, and R. Penty, “High-capacity optical wireless VCSEL ARRAY transmitter with uniform coverage,” Free-Space Laser Communications XXXV, vol. 12413, pp. 144-150, March 15, 2023.

[56] Ke Wang, "High-speed reconfigurable free-space optical interconnects with carrierless-amplitude-phase modulation and filter-enhanced spatial modulation," Opt. Lett. 45, 5476-5479 (2020

[57] Lu, Hai-Han et al. “10 m/25 Gbps LiFi transmission system based on a two-stage injection-locked 680 nm VCSEL transmitter.” Optics letters vol. 40, 2015.

[58] E. Sarbazi, H. Kazemi, M. Soltani, M. Safari and H. Haas, "A Tb/s Indoor Optical Wireless Backhaul System Using VCSEL Arrays", IEEE 31st Annual International Symposium on Personal, Indoor and Mobile Radio Communications, 2020.

[59] Katsuhisa Tada, Koichi Nitatori, Takashi Iwamoto, Takamitsu Miura, and Masahisa Sakai "VCSEL arrays for optical wireless systems", Proc. SPIE 4286, Vertical-Cavity Surface-Emitting Lasers V, 4 May, 2001.

[60] M. Yoshikawa, A. Murakami, J. Sakurai, H. Nakayama, T. Nakamura, High power VCSEL devices for free space optical communications, in: Proc. the 55th Electronic Components and Technology Conference, 2005.

[61] Zhang, L., Wei, Z., Wang, Z., Geng, Z., Wei, G., Cheng, J., Fu, H. and Dong, Y., 2021. High-speed multi-user optical wireless communication between VCSEL-integrated electronic devices. Optics Communications, 486, p.126774.

[62] Z. Wei, M. Guan, Z. Zang, H.Y. Fu, Utilization of 850 nm near-infrared VCSEL for high-capacity indoor free space optical communications, in: Proc. Asia Communications and Photonics Conference (ACP), 2018.

[63] S. Huang, C. Chen, R. Bian, H. Haas, and M. Safari. "5 Gbps optical wireless communication using commercial SPAD array receivers." Optics Letters, vol. 47, no. 9, pp. 2294-2297, 2022.

[64] Z. Chen and H. Haas, "Space division multiple access in visible light communications," 2015 IEEE International Conference on Communications (ICC), London, UK, 2015.

[65] Feng, F., Sangwongngam, P., Faulkner, G. and O'Brien, D. Wide field-of-view optical broadcasting for bi-directional indoor optical wireless communications employing PAM-4 modulation. Optics Letters, 44(24), p.6009. 2019.

[66] T. Koonen, F. Gomez-Agis et al., "High-Capacity Optical Wireless Communication Using Two-Dimensional IR Beam Steering," IEEE/OSA J. Lightw. Technol., vol. 36, no. 19, pp. 4486–4493, 2018.

[67] A. G. Al-Ghamdi and J. M. H. Elmirghani, "Line strip spot-diffusing transmitter configuration for optical wireless systems influenced by back-ground noise and multipath dispersion," IEEE Trans. Commun., vol. 52,no. 1, pp. 37–45, Jan. 2004.

[68] M. Karppinen, "Wireless Infrared Data Links: Ray-trace simulations of diffuse channels and demonstration of diffractive element for multibeam transmitters," Optical Engineering, vol. 41, no. 4, p. 899, 2002.

[69] Bouchet, O. (2007) Free-Space Optics: Propagation and Communication. London: ISTE.

[70] A. R. Henderson and K. Schulmeister, Laser Safety. London: Chapman & Hall, 2010.

[71] Z. Ghassemlooy, W. O. Popoola, and S. Rajbhandari, Optical Wireless Communications: System and channel modelling with MATLAB. Boca Raton ; London ; New York: CRC Press, 2018.

[72] K. Wang, Indoor Infrared Optical Wireless Communications: Systems and integration. Boca Raton, FL.: CRC Press, 2020.

[73] Safety of Laser Products - Part 1: Equipment Classification, Requirements and User's Guide, International Electrotechnical Commission (IEC) 60825-1:2014 Std., Aug. 2014.

[74] Safety of laser products - Part 12: Safety of Free Space Optical Communication Systems Used for Transmission of Information, International Electrotechnical Commission (IEC) 60825-12:2019 Std., Feb. 2019.

[75] M. Dehghani Soltani, E. Sarbazi, N. Bamiedakis, P. de Souza, H. Kazemi, J. M. Elmirghani, I. H. White, R. V. Penty, H. Haas, and M. Safari, "Safety analysis for laser-based optical wireless communications: A tutorial," Proceedings of the IEEE, vol. 110, no. 8, pp. 1045–1072, 2022.

[76] R. Kirrbach, M. Faulwaßer, M. Stephan, T. Schneider and F. Deicke, "High Power Eye-Safe Optical Wireless Gigabit Link Employing a Freeform Multipath Lens," in IEEE Communications Letters, vol. 26, no. 6, pp. 1343-1347, June 2022.

[77] A. G. Al-Ghamdi and J. M. H. Elmirghani, "Line strip spot-diffusing transmitter configuration for optical wireless systems influenced by back-ground noise and multipath dispersion," IEEE Trans. Commun., vol. 52,no. 1, pp. 37–45, Jan. 2004.

[78] Y. Tai and T. Miyamoto, "Experimental Characterization of High Tolerance to Beam Irradiation Conditions of Light Beam Power Receiving Module for Optical Wireless Power Transmission Equipped with a Fly-Eye Lens System," Energies, vol. 15, no. 19, p. 7388, Oct. 2022, doi: 10.3390/en15197388.

[79] Y. Liu, W. Ali, R. Chen, N. Bamiedakis, M. Crisp, I. White, and R. Penty, "High-capacity optical wireless VCSEL ARRAY transmitter with uniform coverage," Free-Space Laser Communications XXXV, vol. 12413, pp. 144-150, March 15, 2023

[80] H. Elgala, R. Mesleh, and H. Haas, "Indoor Optical Wireless Communication: Potential and State-of-the-Art," IEEE Commun. Mag., vol. 49, no. 9, pp. 56–62, Sep. 2011.

[81] D. Karunatilaka, F. Zafar, V. Kalavally and R. Parthiban, "LED Based Indoor Visible Light Communications: State of the Art", IEEE Communications Surveys & Tutorials, vol. 17, no. 3, pp. 1649-1678, 2015.

[82] M. Alresheedi, A. Hussein and J. Elmirghani, "Uplink design in VLC systems with IR sources and beam steering", IET Communications, vol. 11, no. 3, pp. 311-317, 2017.

[83] E. Sarbazi, H. Kazemi, M. Soltani, M. Safari and H. Haas, "A Tb/s Indoor Optical Wireless Backhaul System Using VCSEL Arrays", IEEE 31st Annual International Symposium on Personal, Indoor and Mobile Radio Communications, 2020.

[84] W. Yuan, L.-H. Li, W.-B. Lee, and C.-Y. Chan, “Fabrication of microlens array and its application: A review - chinese journal of mechanical engineering,” Springer, Aug. 29, 2023.

[85] R. Kirrbach, M. Faulwaßer, M. Stephan, T. Schneider and F. Deicke, "High Power Eye-Safe Optical Wireless Gigabit Link Employing a Freeform Multipath Lens," in IEEE Communications Letters, vol. 26, no. 6, pp. 1343-1347, June 2022.

[86] https://www.thorlabs.com/newgrouppage9.cfm?objectgroup_id=2861

[87] M. Karppinen, “Wireless Infrared Data Links: Ray-trace simulations of diffuse channels and demonstration of diffractive element for multibeam transmitters,” Optical Engineering, vol. 41, no. 4, p. 899, 2002.

[88] Y. Jin, A. Hassan and Y. Jiang, "Freeform microlens array homogenizer for excimer laser beam shaping", Optics Express, vol. 24, no. 22, p. 24846, 2016.

[89] Maik Zimmermann, Norbert Lindlein, Reinhard Voelkel, Kenneth J. Weible,"Microlens laser beam homogenizer: from theory to application," Proc. SPIE6663, Laser Beam Shaping VIII, 666302, 26 September 2007.

[90] X. Mu, Z. Wei, S. Wu, Z. Chen, Y. Dong, H. Y. Fu, "Homogenization of power intensity based on micro lens array in optical wireless communication systems," Proc. SPIE 11048, 17th International Conference on Optical Communications and Networks (ICOCN2018), 110481N, 2019.

[91] E. Sarbazi, H. Kazemi, M. Dehghani Soltani, M. Safari and H. Haas, "A Tb/s Indoor Optical Wireless Access System Using VCSEL Arrays," 2020 IEEE 31st Annual International Symposium on Personal, Indoor and Mobile Radio Communications, London, UK, 2020

[92] W. Matthews, Z. Ahmed, W. Ali and S. Collins, "A SiPM-based VLC Receiver for 3.45 Gigabits/s Communication Using OOK Modulation," 2020 IEEE Photonics Conference (IPC), Vancouver, BC, Canada, 2020.

[93] Kahn, Joseph M., and John R. Barry. "Wireless infrared communications." Proceedings of the IEEE 85.2 (1997): 265-298.

[94] Sarbazi, Elham, et al. "Design tradeoffs of non-imaging angle diversity receivers for 6G optical wireless access networks." GLOBECOM 2022-2022 IEEE Global Communications Conference. IEEE, 2022.

[95] Koonen, Ton, et al. "Bi-Directional All-Optical Wireless Gigabit Ethernet Communication System Using Automatic Self-Aligned Beam Steering." Journal of Lightwave Technology, 2022.

[96] H. Q. Ngo, A. Ashikhmin, H. Yang, E. G. Larsson and T. L. Marzetta, "Cell-Free Massive MIMO Versus Small Cells," in IEEE Transactions on Wireless Communications, vol. 16, no. 3, pp. 1834-1850, March 2017.

[97] T. Li, et al. "Novel digital radio over fibre for 4G-LTE," 2015 IEEE International Conference on Communication Workshop (ICCW), London, UK, 2015, pp. 312-317, doi: 10.1109/ICCW.2015.7247197.

[98] T. Li, et al. "Towards efficient and reconfigurable next-generation optical fronthaul networks for massive MIMO." Metro and Data Center Optical Networks and Short-Reach Links V. Vol. 12027. SPIE, 2022.

[99] Y. Tai and T. Miyamoto, “Experimental Characterization of High Tolerance to Beam Irradiation Conditions of Light Beam Power Receiving Module for Optical Wireless Power Transmission Equipped with a Fly-Eye Lens System,” Energies, vol. 15, no. 19, p. 7388, Oct. 2022.